Genetic and Morphological Evidence for Local Climate Adaptation in the Americas

by

Vincent M. Battista

A dissertation submitted in partial fulfillment
of the requirements for the degree of
Doctor of Philosophy
(Anthropology)
in the University of Michigan
2022

Doctoral Committee:

Associate Professor Abby Bigham, Co-Chair; University of California, Los Angeles
Associate Professor Milford Wolpoff, Co-Chair
Assistant Professor J. Brian Byrd, Michigan Medicine
Associate Professor Maureen Devlin
Assistant Professor Cara Ocobock, Notre Dame University

Vincent M. Battista

vmbatt@umich.edu

ORCID iD: 0000-0002-6507-1630

Dedication

This dissertation is dedicated to my grandfather, the late Don Vincenzo Battista, and to my father, Don Gianfranco Battista: "*Considerate la vostra semenza: fatti non foste a viver come bruti ma per seguir virtute e canoscenza*."

Acknowledgements

I would like to thank my co-advisors, Prof Abby Bigham (UCLA) and Prof Milford Wolpoff (UMich), for their constant support and encouragement throughout the writing of this dissertation. I also would like to thank the members of my committee -- Prof Cara Ocobock (ND), Prof Maureen Devlin (UMich), and Dr J. Brian Byrd (UMich Medicine) -- for their flexibility, their understanding, and guidance in helping me to shape the components of this research into a cohesive project. Additionally, I thank Prof John Speth (UMich), Dr Howard Tsai (UMich), and Prof Keolu Fox (UCSD) for challenging me to think outside the box -- and to recognize that the box is an arbitrary construct.

Several members of the Bigham Lab, both past and present, made significant contributions to this work. I extend my gratitude to Dr Obed Garcia, Dr Abagail Breidenstein, and Dr Ainash Childebayeva for their mentorship and friendship during my time at Michigan, as well as their many helpful pieces of advice. I also thank Kim Zhu, Paloma Contreras, Gene Estrada, Elliot Greiner, Benjamin Finkel, Marty Davidson III, Jim Torpy, Nick Trudeau, Marco Kamimura-Palacios, and the Nishimura-Schissler family for their camaraderie, thoughtful comments, and many enlightening conversations over the past many years. Finally, I appreciate the help of Prof Mark Shriver (Penn State) and Dr Tomás González Zarzar (Penn State)

I wholeheartedly thank Fran and Bill "Grey Ghost" Phillips for playing the role of stand-in parents even before lockdown took place; Steve "Z" Zawistowksi for his mentorship and for

reminding me of the importance of animal models; and Tom Migdalski, for teaching me the meaning of “less means more” when it comes to both bucktails and writing.

I thank Amy Persson for her unwavering, seemingly-limitless support; without it, I would not have accomplished much of anything. Additionally, I want to acknowledge the untold sacrifices made by my sisters, Arianna and Serena Battista; my parents, Deborah and Gianfranco Battista; my late nonna, Maria Izzo, who passed away during my preliminary exams; and my late grandmother, Linda Warburton, who died of COVID-19 during the writing of this dissertation. All of my family members, both genealogical and chosen, gave parts of themselves to this project.

Funding for this project came from the University of Michigan’s Department of Anthropology, Center for Latin American and Caribbean Studies (LACS), the School for Environment and Sustainability (SEAS), and the Population Studies Center. I also extend sincere thanks to Marshall Weinberg, who working with SEAS and the Population Studies Center funded an award for the Population, Development, and Climate Change Fellows Program of which I was a recipient. Without these funding sources, I would not have been able to complete this degree.

Finally, I would like to acknowledge that the majority of this research took place at the University of Michigan -- a university which exists due to concessions made to the state of Michigan under the Treaty of Fort Meigs (1817). In this treaty, Niswi-mishkodewinan (the Council of the Three Fires) exchanged land for the construction of a university *under the condition that Anishnaabek community-members and their descendants receive an education*: despite this legally-binding contract, and despite the fact that the skeletal remains of numerous

Indigenous ancestors passed through the halls of the institution, no self-identified Indigenous students matriculated at the University of Michigan until the end of the 20th Century.

Additionally, this dissertation was written in the ancestral homelands of Pawtucket, Massa-adchu-es-et (Massachusett), Wôpanâak (Wampanoag), and Ponkapoag communities. These Eastern Algonquian peoples are part of a deeply historical, geographically-widespread kinship network defined by similar language, shared traditions, common landscape management practices, and unique relationships with the natural world. As we will see in the subsequent pages of this dissertation, the mutualistic relationship of humans to the landscape is one that drives changes in our health, wellness, and longevity. I am humbled to have had the opportunity to sustain myself and my family – and to learn from human ancestors – in these places of profound cultural and spiritual importance.

Table of Contents

List of Tables

List of Figures

Abstract

This dissertation investigates environmental drivers of genetic and morphological variation in the American tropics. Using SNP data and spatially-dense 3D craniofacial landmarks, this project will test the hypotheses that: (1) Mesoamerican populations will show evidence of selection on genes that protect against heat stroke; (2) highland Andeans will show signals of selection on genes that protect against hypothermia, and (3) highland Andeans will exhibit craniofacial changes associated with enhanced conditioning of cold, dry air.

Over the past two million years, humans dispersed across the planet and managed to thrive in a variety of distinct ecological niches -- a process often facilitated by local adaptive evolution. Classic examples of this include high altitude (e.g., Andes) and circumpolar zones (e.g., Siberia), where humans have adapted to low oxygen availability and low ambient temperatures. Despite the extreme temperatures of high altitude (cold/arid) and lowland rainforest (hot/humid), there have been very few studies (if any at all) to examine the genetic substrate of local adaptation to these specific ecological niches.

To fill this void, this dissertation applies a population genetics framework to identify targets of selection in two Indigenous communities from Central and South America. To investigate putative adaptations to high heat and humidity, Chapter 1 interrogates SNP data from 65 Mexican Mayans from the Yucatán Peninsula. To identify putative adaptations to the tundra-like environment of high altitude, Chapter 2 reports selection scans on SNP data derived from 514 Peruvian Quechua. Chapter 3 reports a geometric morphometrics analysis on facial reconstructions from these two populations: using spatially-dense 3D point clouds, this project

investigates whether the Andean sample follows craniofacial patterns associated with cold climate that are exhibited in populations from high-latitude or circumpolar environments.

The results indicate that both populations underwent strong selective sweeps surrounding genes that might offset niche-specific thermal stress, supporting the first two hypotheses. In Mexican Mayans, there is evidence of selection in genes related to water/salt homeostasis (*AKAP11*), mitochondrial protein uncoupling (*ETFB*), vasodilation (*BDKRB2)*, and cellular responses to heat stress (*BAG6*). In Peruvian Quechua, there was significant evidence of selection in genes related to adaptive thermogenesis (*DYNC1H1*), brown fat cell differentiation (*ZNF52*), cellular responses to thermal stress (*FAF1*), and thyroid-mediated body temperature regulation (DUOX family). Geometric morphometrics analysis showed that midfacial protrusion and lengthened nasal aperture -- which are seen in cold-adapted populations from Tierra del Fuego, Siberia, and the Aleutian Islands -- are exhibited in the putatively cold-adapted Peruvian Quechua population. These results are consistent with the third hypothesis that Andean populations would exhibit craniofacial changes that facilitate the conditioning of cold, harsh mountain air.

This dissertation provides some of the first evidence of cold climate adaptation unique to high altitude as well as in the context of the global South. Additionally, this is likely some of the first explicit evidence of heat adaptation derived from a population genetics framework. These results cast light on how niche-specific adaptation may have contributed to broad evolutionary changes in human ancestors and their relatives. To this end, this research provides a case study of genetic adaptations to a novel ecological stress that can unfold over a relatively short interval (<13,000 years): broadly, local climate adaptation likely played a role in shaping variation for a myriad of critical biological processes ranging from metabolism to thyroid function.

Chapter 1 Introduction

1.1 Survival in Environmental Extremes

The human species has overcome numerous fitness-reducing stressors, such as cold or low oxygen availability, numerous times throughout its history. Evidence from the Dmanisi site in Georgia indicates that by about 1.7 million years ago, humans were able to disperse into relatively high latitude, relatively cold-climate regions of the planet (Lordkipanidze et al. 2013). By some 1.5 million years ago, human ancestors had settled the tropics of what is today Indonesia (Morwood et al. 2003). Some of the first occupational evidence of humans inhabiting environmental extremes comes from the Tibetan Plateau, where Denisovans survived in high altitude (> 3000 m above sea level), cold climate zones beginning roughly 160,000 years before present (Chen et al. 2019, Zhang et al. 2020). Within East Africa, there is a human presence at high altitude perhaps as early as 120,000 years ago, with clear occupational horizons being established as early as 47,000 years before present (Vogelsang et al. 2018, Ossendorf et al. 2019). The ability to exploit these novel ecological niches would not have been possible without a variety of biobehavioral adaptations to offset local stress (Aldenderfer 2011, Barton et al. 2011, Thompson et al. 2020). This process of dispersal, cultural innovation, and biological adaptation has allowed humans to thrive in even the harshest landscapes of the Ethiopian Highlands, the dry deserts of Southwest Asia, and remote mountains of Siberia (Boivin et al. 2016, Hershkovitz et al. 2018, Ossendorf et al. 2019, Douka et al. 2018).

Understanding the ways in which humankind adapts to such diverse environments is a significant focus across all subfields of anthropology (Fuentes 2017). The many cultural and

behavioral adaptations that offset environmental stress are central to understanding how humans not only became a cosmopolitan species, but how our ancestors survived drastic changes in both habitat and climate over varying timescales. One tool that has emerged to understand recent evolutionary adaptations is human genetics (Scheinfeldt and Tishkoff 2013). Generating and analyzing DNA sequence data from humans that inhabit distinct ecological regimes allows observers to identify population-specific patterns of change in genes implicated in adaptive responses to environmental stress (Marcus and Novembre 2016, Savolainen et al. 2013, Rees et al. 2020). This approach has identified local adaptive changes in groups that inhabit high altitude, that live in arsenic-rich environments, that subsist on high-fat food items, and that survive in the extreme cold (Bigham et al. 2010, Schlebusch et al. 2015, Fumagalli et al. 2015, Cardona et al. 2014).

Much of what is known about cold climate adaptation is from population genetics studies conducted with high latitude, circumpolar communities, or among broad geographic groups such as "Eurasians" (Fumagalli et al. 2015, Cardona et al. 2014, Igoshin et al. 2019, Hancock et al. 2011). While some historical research was conducted regarding cold habituation in the Andes (Baker 1963), there have been no subsequent population genetics studies to investigate potential adaptations to low ambient temperatures unique to altitude. Globally, some 82 million people live in excess of 2,500 meters above sea level, with one-quarter the population of Peru and over one half the population of Bolivia living above this threshold (Tremblay et al. 2021). On the opposite end of the spectrum, nearly 40% of the Earth's population lives in the tropics, a number that is expected to increase by 10% by the year 2050 (State of the Tropics Report, 2020). Despite this high number, there have been very few studies (if any at all) to examine the genetic substrate of adaptation to high heat and humidity. One population genetics study has identified adaptations to

high ambient temperatures -- achieved through thyroid-mediated temperature regulation -- and that was with Aboriginal Australians (Malaspinas et al. 2016). Even with this case study in mind, we are far from understanding evolutionary adaptations to thermal stress as they occur on a global scale. Expanding the studies of thermal stress to both extremes of temperature and humidity axes would cast considerable light on the multiple evolutionary pathways that contribute to thermal stasis, especially in populations from the Americas who have varying degrees of cold-adapted ancestry (Sellayah 2019). This would not only fill a significant gap in our understanding of local adaptation, but would elucidate the potential mechanisms through which human ancestors adapted to hot and cold extremes during dispersals in and out of the African tropics.

1.2 Cold Stress and Cold Exposure at High Altitude

In its mildest forms, cold stress presents thermal discomfort, impaired vigilance and decreased recall performance, and a host of other mental and physiological factors that increase the potential for task-related injury (Mäkinen 2007, Golant et al. 2008). Frequent or prolonged cold exposure ("CE") can trigger symptoms of chronic disease, highly-localized pain (e.g., in appendages), respiratory complications, and musculoskeletal duress; these are all amplified when blood oxygen saturation begins to decrease or when ambient temperature falls to around 14°F/-10°C (Raatikka et al. 2007, Schramm et al. 1997). Without insulative cultural buffers (e.g., clothing, shelter), human are susceptible to frostbite, hypothermia (i.e., core temperature lower than 95°F/35°C), pulmonary edema, dehydration via cold-induced diuresis, hypoglycemia, cardiac arrest, and mortality, especially in the elderly and hypothermic neonates (Näyhä et al. 2002, Mäkinen 2007, Wilson et al. 2007). In addition to periodic cold exposure, seasonality and

low ambient temperature have been reported to increase the prevalence of preterm birth, prenatal mortality, and aortic coarctation as well as to decrease birth weight of newborns (Strand et al. 2012; Bruckner et al. 2014; Van Zutphen et al. 2014). At a seasonal scale, prolonged CE has been associated with increases in BMI and waist circumference in Northern Europeans, caloric intake in individuals of European and Hispanic descent, and increased winter mortality from heart attack and stroke in Britain (Visscher and Seidell 2004, Ma et al. 2006, Wilkinson et al. 2004).

Similar to changes in temperature corresponding to latitude, temperatures decrease at a rate of about 6 degrees Celsius for every 1000 meters gained (Minder et al. 2010). This means that high-altitude regions, defined as being at least 2,500 meters above sea level (mASL), can be up to 15°C (~60°F) colder than at the same latitudinal position while at sea level. Individuals experiencing cold exposure undergo a suite of physiological changes including peripheral vasoconstriction, an increase in blood pressure, and increased energy expenditure related to thermoregulatory behaviors such as shivering; in extreme scenarios, cold exposure can lead to hypothermia and even death (Ocobock 2016, Granberg 1991, Hampton 1981). Furthermore, individuals experiencing altitude-induced hypoxia present reduced physiological responses to cold, which reduces their core body temperature and puts them at further risk for hypothermia (Kottke et al. 1948, Johnston et al. 1996).

1.3 Heat Stress and Human Evolution

In humans, air temperatures exceeding an individual's body temperature will trigger a sweat response, vasodilation, and elevated blood flow to the surface of the skin (Donaldson et al. 2003). Apart from excreting water through urine, humans lose a significant proportion of their

water in the form of sweat, which is a derived thermoregulatory response to heat stress (Lieberman, in Terjung 2011). Sweating pulls water to the skin's surface, which evaporates to remove heat; directing blood to superficial vessels allows heat to essentially radiate off the body (Gagnon and Crandall 2018). While losing water as sweat, the viscosity of blood increases, and red blood cell and platelet counts begin to rise (Keatinge et al. 1986). If a heat stimulus cannot be removed, an individual suffering from hyperthermia may experience respiratory alkalosis resulting from hyperventilation (Tsuji et al. 2016). At this stage, the human body is losing water, losing sodium, and undergoing an acid-base disequilibrium: changes in blood volume mean that the blood becomes more viscous, but at the same time is forced to the surface of the skin to cool (Chang et al. 2010, Holsworth et al. 2013). Additionally, blood osmolality increases, and localized swelling in the limbs (heat edema) begins to occur (Nichols 2014).

Electrolytes depleted through sweat and dehydration can cause muscle spasms and cramps, and if an individual cannot replenish liquids and reduce their body temperatures, they are at risk for heat exhaustion. In studies of outdoor workers, sweating can lead to up to a loss of 1.5L of water per hour, and over the course of a working day individuals can lose up to 6g of sodium (Brake and Bates 2003, Miller and Bates 2007, Bates and Miller 2008). High individual effort in high temperatures, especially without the ability to replenish liquids, is potentially lethal and can lead to exertional heat stroke (EHS); classic heatstroke (CHS) is defined as having body temperatures over 40.5°C and is most common in prepubertal or elderly individuals (Epstein and Yanovich 2019). Without intervention, individuals with CHS may present with nausea, vomiting, convulsions (i.e., seizures), and organ failure. Unlike CHS, the clinical features of EHS include common renal failure (> 30%) as well as marked to severe disseminated intravascular coagulation (i.e., blood clotting within vessels); furthermore, blood levels of creatine kinase and

potassium (hyperkalemia) are significantly increased, whereas calcium levels drop off (hypocalcemia) (Epstein and Yanovich 2019).

Even in mild forms, heat exposure can be dangerous for individuals with existing renal or cardiovascular diseases, or for those facing water insecurity (Donaldson et al. 2003, Rosinger 2018). For expectant mothers, heat exposure is associated with fetal neural tube defects, risk of stillbirth, and reduced gestation time (Milunsky et al. 1992, Auger et al. 2017, Dadvand et al. 2011, Schifano et al. 2016). Heat stress that leads to recurrent dehydration has many downstream effects impacting human health and longevity: in particular, this can be lethal for individuals forced to work in the heat for prolonged periods of time, and has been implicated in the epidemic of chronic kidney disease in outdoor laborers from the American tropics (Brooks et al. 2012).

1.4 Human Heat Adaptation and Regional Continuity in Mesoamerica

The ability to regulate body temperature and hydration levels has long been a focus in the study of hominin evolution, specifically for Pleistocene humans living in tropical climates and contemporary descendants that participate in traditional hunting-and-foraging activities (Schreider 1964, Zihlman and Cohn 1988, Ruff 1993, Lieberman in Terjung 2011, Pontzer et al. 2021). Despite this highly-regional focus and emphasis on “deep time”, little is known about heat adaptation from the purview of population genetics. Speculatively, this lack of knowledge could be the result of a perception that humans derive entirely from a single recent branch of hominids that was uniformly adapted to the tropics of East Africa (Rito et al. 2019). However, given: (1) the frequency of human dispersal into novel ecological regimes, even within Africa (Ossendorf et al. 2019); (2) the high selective coefficient on metabolism as it relates to body temperature regulation (Racimo et al. 2015); and (3) near-constant population reticulation in global archaic

hominid lineages, as well as within and among recent human ancestors (Slatkin and Racimo 2016); there is no reason to suspect that a suite of "tropical" adaptations were necessarily ever fixed among early humans. Additionally, rapid and drastic fluctuations in global climates over the last 40,000 years drove a number of demographic shifts in ancestral human populations, especially for those living in marginal environments in Eurasia (Eriksson et al. 2012, Seersholm et al. 2020). These changes in local climate drove dispersals, bottlenecks, and isolation among the ancestors of modern Indigenous populations of the Americas (Bourgeon et al. 2017, Fagundes et al. 2019). As a result, the earliest peoples of Central America, who arrived in the region some 13,400 years before present, were closely related to the ancestors of modern Siberians and thus were a cold-adapted population from Eurasia (Amorim et al. 2017, Prufer et al. 2019, Stinnesbeck et al. 2020). These early Americans radiated into a low-latitude coastal environment, which at the time consisted of dry, hot savannah: today, daily maximum temperatures routinely surpass 35°C, and the high levels of relative humidity often drive daily heat indices of over 50°C for several weeks on end (Harris et al. 2020, Bauer-Gottwein et al. 2011). Temperatures in this range are incredibly harmful to the human body, especially if an individual becomes dehydrated: in studies of heat stress in Mesoamerican sugarcane farmers working in temperatures exceeding 40°C, the experience of dehydration and high ambient temperatures was shown to be particularly harmful to the kidneys (Brooks et al. 2012). For outdoor workers in Central America, dehydration resulting from heat exposure is implicated in significant increases in urinary osmolality and specific gravity, eventually causing long-term kidney damage (García-Trabanino et al. 2015). Across this region, chronic kidney disease (CKD) is reaching the status of an epidemic, leading to thousands of preventable deaths -- particularly

among men whose jobs force them into excessive hyperthermia and dehydration for several days on end (Brooks et al. 2012).

Yet despite the effect of high ambient temperatures and water instability, Indigenous communities throughout this region created incredibly complex state-level societies that sustained substantial population sizes (Prufer et al. 2019, Stinnesbeck et al. 2020). Evidence from evolutionary genomics indicates that over this interval, Indigenous Mesoamericans adapted to high-starch diets, pathogens, and even increased solar irradiation (Ávila-Arcos et al. 2019, Reyes et al. 2021, Zhou et al. 2016). However, it is unknown whether these populations have evolved to offset the cost of heat exposure. It is possible that Indigenous communities from Central America have genetic adaptations to provide efficient water transport, protect against impaired renal function (e.g., urinary osmolality), and offset various inflammatory pathways (fever, edema) associated with heat stress.

1.5 Thermal Stress and Signatures of Selection in the Human Genome

Because of the many fitness-reducing effects of prolonged cold exposure, cold climate adaptation is often invoked to describe numerous evolutionary changes observed in anatomical and genetic data alike (Bramble and Lieberman 2004, Racimo et al. 2017, Steegmann 2007). Much of what is known about past adaptation to climate stress is gleaned from fossil crania, which reveal a number of changes in facial architecture, size, and proportionality that are associated with local climate variables (Laitman et al. 1996, Franciscus 1999, Rae et al. 2006). In the postcranial skeleton of tropical human populations, there was a tendency towards gracile body proportions; yet Pleistocene Eurasian hominins retained a relatively thick trunk compared to their counterparts inhabiting the tropics of east Africa (McHenry 1992, Churchill 2014). Like many later populations

from high latitude, these early Eurasians appear to have benefitted from trunk and limb proportions that facilitate body temperature homeostasis during cold exposure, such as a broader trunk and arctic body proportions (Holliday et al. 1997, Trinkaus et al. 1998, Katzmarzyk and Leonard 1998, Steegmann et al. 2002, Steegmann 2007). Populations such as the Neanderthals, who thrived in Eurasia for the latter half of the Pleistocene, exhibit a series of craniofacial traits including large nasal apertures, swept zygomatics, and projecting midface that are associated with warming, moistening and conditioning of inspired air (Yokley 2009, Noback et al. 2011, Wroe et al. 2018).

While it is likely that all Out of Africa populations are relatively cold adapted based on having ancestry that survived frequent glacial cycles, the best evidence of recent selection for efficient thermogenesis is demonstrated by the clinal increase of adaptive variants in association with latitude (Schaefer et al. 2021, Hancock et al. 2011, Sellayah et al. 2014, Key et al. 2018). Selection scans, where multiple statistical tests are deployed across swaths of a genome, have revealed that the most extreme examples of cold climate adaptations are found in the populations that inhabit the northern edges of the human range; for example, in peoples like Greenlandic Inuit, Alaskan Eskimos, and indigenous Siberians, there is a pattern of selection for loci implicated in thermogenesis through fatty acid metabolism (Hsieh et al. 2017, Fumagalli et al. 2015); Greenlandic Inuit carry an adaptively-introgressed variant spanning *TBX15*, which in addition to mediating trunk proportionality has been implicated in the formation of a heat-generating form of fat called brown adipose tissue (BAT) (Racimo et al. 2017). While the association of this region with changes in trunk proportionality suggests evolutionary conformation to Bergmann's and Allen's rules (Steegmann 2007), the implication of *TBX15* in BAT thermogenesis is of particular importance given that a unit of BAT can generate significant amounts of heat relative to that produced by resting muscle alone (Steegmann et al. 2002, Steegmann 2007, Muzik et al. 2013). In

particular, genes encoding energetically-efficient thermoregulatory responses (especially genes whose activity are inducible by cold exposure) are potential candidates for recent selection in humans occupying cold climate extremes.

To knowledge, only one study has identified regions of the genome undergoing selection that are implicated in physiological responses to heat stress. Research into thyroid function by Qi et al. (2014) investigated the temperature-dependent release of thyroxine from thyroxine binding globulin (TBG). When body temperatures rise to around 39°C, the concentration of free thyroxine in blood increases by some ~23%, which then drives an increase in thermoregulatory output. Qi et al. (2014) showed that among Aboriginal Australians, two mutations in the TBG pathway reduce the surge of thyroxine and reduce metabolic output during heat stress. This is potentially adaptive to high ambient temperatures in that it simultaneously prevents the body from overheating while reducing the energetic budget required for body temperature homeostasis. Similarly, evolutionary genomics research with Aboriginal Australian communities detected evidence of selection on *NETO1* and *KCNJ2*, two genes influencing thyroid function, and a region of the genome that mediate serum urate levels, protecting against dehydration (Malaspinas et al. 2016)

Given the lack of comparative studies, one can only speculate as to which genes might be under selection within a putatively heat-adapted population such as Mesoamericans. Similar to what was seen in Aboriginal Australians, it is possible that genes related to thyroid function and known thermoregulatory pathways might be under selection in other populations inhabiting the tropics. Additionally, given the effects of chronic dehydration on health and survival, there might be evidence of selection on genes related to renal function and water homeostasis. Finally, genes contributing to heat adaptation might be related to: (1) heat shock proteins' cellular responses to

heat stress (Schlesinger 1990); (2) muscle contraction and vasodilatory responses (Charkoudian et al. 1985), and (3) whole-body metabolism (Périard et al. 2015).

1.6 Detecting Recent Evolutionary Change in Indigenous American Groups

The burden of cold exposure is known have influenced genetic variation and components of body proportionality in several circumpolar, high-latitude communities (Voruganti et al. 2012, Cardona et al. 2014, Clemente et al. 2014, Fumagalli et al. 2015, Hsieh et al. 2017). Evidence from population genetics indicates that Indigenous populations of the Americas have undergone selection for genes related to hypoxia, diet, local pathogens, and solar exposure (Bigham 2010, Ávila-Arcos et al. 2019, Zhou et al. 2016). However, little focus has been directed to studying how populations from Central and South America offset thermal stress.

Like much of Mesoamerica, the Mexican state of Chiapas consists of hot, humid tropical forests (González-Espinoza et al. 2004, Torrescano-Valle and Islebe 2015). Recent climate data reveal that coastal sites such as Tapachula receive some 2,076mm of precipitation per year (Wootton et al. 2021). In similar environments across Central America, midday temperatures can surpass 40°C during the hottest months of the year: and coupled with high humidity, this can create a heat index of over 55°C, which can enhance the likelihood of exertional harm and dehydration (Brooks et al. 2012, Harris et al. 2020). On the other side of the spectrum are the Andes. Populations such as the Peruvian Quechua live in an environment with low oxygen availability and are known to be adapted to hypoxic stress (Bigham and Lee 2014). High-altitude settlements such as Cerro de Pasco and La Rinconada of Peru are located in habitats that are considered cold-steppe or tundra, and can experience snow cover for the entire year (Brush 1982). At these high

elevations, the additive effects of cold climate and hypoxia can take a significant toll on the human body (Kottke et al. 1947, Johnston et al. 1996, Simmons et al. 2010).

These populations inhabit the ecological extremes of the American tropics and have done so for perhaps as long as 12,000 years (Rademaker et al. 2014, Hubbe et al. 2020). Over this interval, these populations evolved to offset the stress of hypoxia and infectious diseases which are two well-described environmental stressors (Bigham et al. 2020, Hollenbach et al. 2001, Barquera et al. 2020). However, it is unclear whether these populations have adapted to unique, regional forms of thermal stress: the tundra-like environment of the high Andes, and the tropical rainforest of southeast Mexico.

In the first and second chapters of this dissertation, I perform selection scans on genetic data derived from Mexican Mayans and Peruvian Quechua populations. In Chapter 1, I test the hypothesis that Mexican Mayans have undergone selection on genes that prevent bodily overheating and facilitate water/salt balance -- two components of body temperature homeostasis that are critical to survival in hot, humid environments. In Chapter 2, I test the hypothesis that Peruvian Quechua have undergone selection on genes that help protect against the fitness-reducing effects of cold. The statistical tests I use are: (1) locus-specific branch length (LSBL), a frequency-based test that can detect highly-differentiated mutations between three related groups (Mexican Mayans, Peruvian Quechua, and Han Chinese), and (2) XP-nSL, a test that scores haplotypes given the number of segregating loci across populations. High-ranking SNPs (i.e., polymorphic sites) or genomic regions identified through LSBL indicate a statistically-significant difference in the frequency of a given variant in one population relative to others. Top-scoring haplotypes detected in XP-nSL are embedded within sweep regions, or spans of the genome with high levels of homogeneity surrounding an adaptive mutation. Together, LSBL and XP-nSL provide an

orthogonal approach to recognizing high-frequency variants embedded within genomic regions that are maintained by selection. The top scoring variants are used to create candidate gene lists, which are then queried in gene ontology datasets, which inform about gene function, biological pathways, protein/gene interactions, and corresponding cellular functions. In Chapter 3, I apply a geometric morphometrics framework to investigate how changes in midfacial anatomy correspond to climate variables. Using digital 3D facial reconstructions from Mexican Mayans and Peruvian Quechua, I test the hypothesis that the putatively cold-adapted Peruvian sample shows increased midfacial protrusion and lengthened nasal aperture, along with other traits that are associated with the conditioning of cold, inspired air (Noback et al. 2011).

This study highlights a series of anatomical and genetic changes in Indigenous populations inhabiting distinct environments in the American tropics. These results inform us of how local adaptation, even over relatively short evolutionary timescales, can drive significant divergence in components of human biology (genes, anatomy, etc). Finally, this study casts light on the adaptive processes that shape genetic variation in populations from fairly extreme ecological contexts.

Chapter 2 Heat Adaptation in Mexican Mayans

2.1 Heat Adaptation and Human Evolution

Early members of the genus *Homo*, who first appeared in the African fossil record around 2 million years ago, embarked on broad geographic dispersals and settled remote corners of the planet (Dubois 1896, Leakey 1973, Bar-Yosef 1994, Wood and Collard 1999, Bar-Yosef and Belfer-Cohen 2001). During this time, climatological shifts drove remarkable ecological and environmental changes across the African subtropics (Potts 2012, Patterson et al. 2017). These ancient hominins were fairly large-bodied endotherms that seemingly thrived in hot environments, a feature that resulted from a variety of biological and behavioral innovations (Bramble and Lieberman 2004, Tilkens et al. 2007, Potts 2012, Pontzer 2012). In particular, the ability to offset heat stress during foraging and hunting behaviors (e.g., endurance hunting) garners a central focus in the study of human evolution (Schreider 1964, Zihlman and Cohn 1988, Lieberman in Terjung 2011, Hora et al. 2020, Pontzer et al. 2021).

Much of what is known about heat adaptation in early humans derives from morphological studies on fossil remains (Ruff 1993, 1994). Perhaps the primary evidence for heat adaptation among hominids is exhibited in changes in body shape and size (Ruff 1994). Compared to populations inhabiting cold climates, the bodies of tropically-adapted populations tend to have a greater surface area to volume ratio, which enhances heat dissipation and thus contributes to bodily cooling (Ruff 1993, Patterson et al. 2017). There are several lines of evidence suggesting that an upright posture is itself an adaptation to heat: during the heat of midday, a bipedal posture reduces the surface area of the body that is exposed to solar radiation

(Wheeler 1984). Furthermore, by elevating the center of mass away from the earth's surface, the human body is spared from heat radiation emanating upward from the earth's surface: this also exposes the trunk to higher airflow and lower relative humidity, which accelerate convective cooling (Wheeler 1991). Despite these anatomical adaptations, the human body is mechanically inefficient in that around 90% of energy is transformed to heat during exercise (Gagge and Gonzalez 2011). This puts us at risk of overheating during a period of exertion, especially when ambient temperatures hover around 36 degrees Celsius (Belval and Morrisey 2019).

Unlike other primates, humans have a high density of eccrine sweat glands -- a trait that allows humans to produce large amounts of sweat (Lieberman, in Terjung 2011). During heat exposure, aquaporin channels permit fluid to pass into a sweat gland and ultimately to the skin's surface where water (sweat) droplets are then vaporized (Belval and Morrisey 2019). This process of vaporization cools the site at which sweat evaporates, which in turn cools the surface of the skin and underlying blood vessels, and cooled blood is transported back to the body's core where it contributes to lowered body temperature (Best et al. 2019). Considering the lethality of dehydration during extreme heat stress, sweating is somewhat of an evolutionary trade-off: on the one hand, sweating contributes to water loss, but at the same time it is a critical thermoregulatory mechanism given how readily it can cool the human body (Best et al. 2019). Assuming that water can be replenished, this unique thermoregulatory adaptation would have conferred a significant evolutionary advantage to ancient humans experiencing unavoidable heat and aridity.

In settings where heat stress is driven by both high temperatures and high humidity, atmospheric saturation significantly reduces the efficiency of sweating (Wendt et al. 2007). In these situations, bodily water might be depleted more quickly than it can be replenished, putting

individuals at risk for dehydration and even heat stroke (Beker et al. 2018). Dehydration experienced during childhood can have long-term health implications, and it is associated with elevated blood pressure and increased risk of haemorrhagic stroke later in life (Smith et al. 2006). Severe dehydration experienced during adulthood, such as that which is experienced by outdoor laborers in the tropics, is closely linked with chronic kidney disease and ultimately death (Brooks et al. 2012).

Today, populations inhabiting hot climates exhibit a variety of physiological traits believed to offset heat stress: these include reduced basal metabolic rates, a reduced threshold for cutaneous vasodilation, and increased sensitivity to thermal stimulus (Taylor 2006). However, it is uncertain whether these phenotypes are the result of acclimatization or local evolutionary adaptation.

While populations that live in regions with high ambient temperatures show somewhat distinct physiological responses to heat stress, the environmental and genetic contributions to these responses are not particularly clear. There is some incidental evidence that populations inhabiting warm climates have undergone selection on genes that influence energy expenditure, basal metabolic rate, and thus body temperature (Sellayah 2019). For example, the Akimel O'odham (Pima) community of what is today called Arizona may have undergone selection on variants that suppress an individual's metabolic rate: in this community, there are relatively high frequencies of energy-wasting variants in genes such as *ADRB3* (e.g., rs4994; global MAF ~ 11%; Akimel O'odham MAF = 31% (Fairley et al. 2020, Walston et al. 1995). This might indicate that when a thermoregulatory pathway undergoes selection, cold climate-adapted populations might show evidence of selection on metabolism-boosting variants, whereas

putatively heat-adapted populations might undergo selection on a haplotype that reduces basal metabolism and helps with energy "shedding" [sic] (Sellayah et al. 2019).

While there is ample evidence of cold climate adaptation in northern human populations, there is little explicit evidence of recent, population-specific evolutionary adaptation to heat stress. To knowledge, only one study has applied a comparative genetics approach to identify how a putatively heat-adapted population offsets the burden of high ambient temperatures: in working with Aboriginal Australian populations, Malaspinas et al. (2016) identified evidence of selection on two genes that might be adaptive to hot, dry environments. These were: *NETO1*, which mediates body temperature regulation through the thyroid system, and *KCNJ2*, which is associated with serum urate levels and thus might be protective against dehydration (Malaspinas et al. 2016). This study validates an earlier finding by Qi et al. (2014) whose research with Aboriginal Australian communities identified unique thermal triggers for thyroid that offset the stress of high ambient temperatures. Unfortunately, additional evidence of heat adaptation in human populations is lacking.

In contrast, animal studies contain a wealth of information about the genetic and anatomical changes associated with heat adaptation. Genomic scans in heritage breeds of pigs, cattle, and ovicaprids show evidence of selective sweeps surrounding known genes related to kidney function, water absorption, and adaptive cooling (Ai et al. 2015); the encoding of heat shock proteins and oxidative stress responses (Li et al. 2019, Freitas et al. 2021); thyroid stimulating hormones, and interleukin receptor genes (Eydivandi et al. 2021). Perhaps the most extreme example of heat adaptation in animals pertains to domestic camelids. In a study of bactrian camels (*Camelus bactrianus*), dromedary camels (*Camelus dromedarius*), and alpaca (*Vicugna pacos*), there was directional selection on genes related to oxidative stress response,

salt metabolism and sodium reabsorption, water homeostasis with aquaporins, and genes encoding heat shock factors (Wu et al. 2014). While it remains true that domestic animals are developed, line-bred, and improved by human agents, it is possible that these signals of selection result in part from local climate adaptation as opposed to artificial selection alone. Regardless of the selective mechanism, there is a clear overrepresentation of genes related to cellular responses to heat stress (via heat shock proteins), body temperature regulation, and salt/water balance among domesticates inhabiting regions with high ambient temperatures. It is possible that human populations inhabiting these same environmental extremes exhibit similar evolutionary adaptations that help offset the stress of heat exposure.

One environment where evolutionary adaptations to heat stress are expected to take place is the American tropics. In this region, even relatively-low humidity levels for tropics (~40%) can compound on the effect of high ambient temperatures to create dangerously-high heat indexes: in lowland forests of Southern Mexico and Central America, where midday temperatures often surpass 40°C (104°F), individuals routinely face a heat index of over 55°C (131°F) (Harris et al. 2020). For the earliest human settlement of this region, such high temperatures would have provided significant affronts to health and longevity; this is especially the case considering that the founding lineage of the Americas was a relatively small population migrating southward from colder, circumpolar zones (Amorim et al. 2017). Despite these stressors, ancient migration waves into the American tropics were ultimately a success, thus providing biological anthropologists with a unique case study regarding timing and spatial scale of local evolutionary adaptations to heat stress. This study has the potential to fill this gap in knowledge, and inform us of how humans adapt to thermal stress at a genomic level. Additionally, this provides a glimpse into how humans can adapt to significant changes in local

climate variables over relatively short intervals. The physiological impact of dispersal into the American tropics by ancient humans in many ways mirrors the predicted increase in global temperatures (Tabari 2020, Fischer et al. 2021). In both scenarios, we see populations traditionally inhabiting cold or mild climates and a significant shift in ecological stressors such as higher temperature maxima and significant increases in humidity (Afrane et al. 2012, Equihua et al. 2017, Franklinos et al. 2019).

To determine whether populations from this region are adapted to their relatively unique tropical environment (defined by high ambient temperatures and high humidity), we performed selection scans on SNP data from 65 Mexican Mayans recruited in and around the city of Palenque, Chiapas, Mexico. These data were used to test whether Mexican Mayans have undergone recent evolutionary changes that facilitate body temperature regulation during exposure to high ambient temperatures.. We hypothesized that considering Mexican Mayans inhabit a tropical lowland environment with a particularly high heat index, natural selection might act on pathways that facilitate body temperature regulation and that would help prevent dehydration. Specifically, we predicted evolutionary changes in functional loci implicated in salt regulation and water homeostasis, which are two components of osmotic balance that might protect against dehydration from sweating. Additionally, given the pattern seen in animal models, selection would favor haplotypes that contribute to enhanced cellular responses to heat stimulus or thermal stress, vasodilation (which contributes to thermal cooling), and hormonal regulators of body temperature (Li et al. 2019, Freitas et al. 2021, Wu et al. 2014).

2.2 Materials and Methods

2.2.1 Participant Recruitment

Participants in this study were Tzeltal, Tzotil, or Ch'ol-speaking Mayans recruited from Palenque, Chiapas, Mexico (N = 100). All study participants provided written informed consent in Spanish at the time of recruitment. The study was approved by the institutional review boards at the University of Michigan and Centro de Investigación y Docencia Económicas (CIDE Mexico City, Mexico). Participants provided three mLs of blood at the time of recruitment. Blood was field stabilized in cell lysis buffer. Stabilized blood samples were then hand-carried to the University of Michigan where DNA extraction was performed using the Puregene Protocol (Qiagen, Valencia, CA) in the Bigham Lab for Anthropological Genomics.

2.2.2 Genome-Wide SNP Data

Genome-wide SNP array data was generated for each study participant using the Affymetrix (Santa Clara, CA) Axiom Biobank Array. This array detects roughly 606,000 known variants (either SNP or indels) across the genome. Quality control analysis was performed on the full dataset in Plink 1.9 (Chang et al. 2015). We removed variants failing Affy Best Practices, with a genotype missingness rate greater than 5%, or with a minor allele frequency of less than 2.5%. Participants with greater than 4th degree of relatedness were filtered out of the dataset following the method of Manichaikul et al. (2010), which allowed us to retain whichever individual had the higher genotyping rate. The remaining dataset consisted of genotype data for 313,533 autosomal variants in 73 individuals.

2.2.3 Population Affinity and Admixture Mapping

To analyze population structure and identify admixture, the Mexican Mayan genotype data were merged with data derived from 514 Peruvian Quechua participants as well as publicly available data from 60 Yoruban, 45 Han Chinese from Beijing, 45 Japanese from Tokyo, and 60 individuals of north-central European ancestry from the Centre d'Etude du Polymorphisme Humain (CEPH). These populations were selected in order to detect high levels of non-Indigenous ancestry resulting from transatlantic gene flow occurring within the last 500 years. With this expanded dataset, I conducted PCA in Plink and used the program ADMIXTURE to model different numbers of ancestral groups (K = 1 through 9). Any individual with European ancestry > 20% was filtered out of the dataset. The final dataset consisted of 65 unrelated Mexican Mayan individuals. Participants were 49.23% (N = 32) female, and had low to undetectable levels of recent European ancestry.

2.3 Identifying Signatures of Selection

2.3.1 Number of Segregating Sites

Two tests were used to detect evolutionary changes in Mexican Mayans: cross population number of segregating sites by length (XP-nSL) and the locus specific branch length (LSBL). XP-nSL is a method of identifying variation among haplotypes caused by past selective sweeps that is robust to variation in recombination rates (Ferrer-Admetlla et al. 2014, Szpiech et al. 2021).

Consider a locus k, with either haplotypes that are ancestral in nature ($A(k)$) or that are derived ($D(k)$), and let the value $n_A(k) = |A(k)|$ and the value $n_D(k) = |D(k)|$. The number of sites at which the haplotypes i and j are identical-by-state (IBS) can be defined as $L_{ij}(k)$ for a given

genomic region *k*. The number of segregating sites per locus (nSL proper) for a given site *k* can is calculated as:

$$nS_L(k) = log\frac{SL_A(k)}{SL_D(k)}$$

Where:

$$SL_A(k) = \left(n_{A\ \ 2}(k)\ \right)^{-1}\Sigma_{i<J\in A(k)}L_{ij}(k),$$

and:

$$SL_D(k) = \left(n_{D_2}(k)\ \right)^{-1}\Sigma_{i<J\in D(k)}L_{ij}(k)$$

From this, $SL_A(k)$ and $SL_D(k)$ refer to the mean value of $L_{ij}(k)$ over all possible haplotype combinations, each of which represents conformation to the ancestral or derived variant for a locus *k* within a particular population. XP-nSL (cross-population nSL) expands this test to population dyads: instead of interrogating pairwise ancestral/derived allele sets, XP-nSL compares sets of haplotypes between a "reference" and "target" population (Szpiech et al. 2021).

If $P_1(k)$ and $P_2(k)$ represent haplotype pairs about site *k* in populations P1 and P2 respectively, let $n_{P1}(k) = |P_1(k)|$ and the value $n_{P2}(k) = |P_2(k)|$.

Then:

$$XPnS_L\ (k) = log\frac{SL_{P1}(k)}{SL_{P2}(k)},$$

and:

$$SL_{P1}(k) = \left(n_{P1}(k)\ \right)^{-1}\Sigma_{i<J\in P1(k)}L_{ij}(k),$$

and:

$$SL_{P2}(k) = \left(n_{P2}(k)\ \right)^{-1}\Sigma_{i<J\in P2(k)}L_{ij}(k).$$

This means that SL_{P1} and SL_{P2} represent the averages for $Lij(k)$, or the number of consecutive positions containing identical haplotypes *i* and *j* across all possible haplotype dyads within each population. Positive XP-nSL values represent a selective sweep in the "target" population (here, Mexican Mayans), whereas negative XP-nSL values represent selection in the reference population. Here, we use genotype data from 514 Peruvian Quechua as the comparative sample. Sweep regions can be identified as a series of neighboring XP-nSL values that form a peak above the putatively-selective locus. A high peak is indicative of strong selection in a particular locus; a "plateau" of many high-scoring variants indicates an exceptionally strong selective sweep that creates a long-range haplotype.

Calculating XP-nSL in the program Selscan requires complete observations in phased genotype data (i.e., 100% of individuals are represented at a given locus) (Szpiech et al. 2021). Incomplete observations were removed using Plink 1.9 (Chang et al. 2015), and genotype data were phased using SHAPEIT 4.2 (Delaneau et al. 2018). XP-nSL scores were calculated for each variant and were normalized across 100kb windows using SelScan's ancillary program called Norm. The resulting data files (one per chromosome) were concatenated in Python 3.9.5 and then analyzed in R 4.1.0 (Van Rossum and Drake 1995, R Core Team 2021). I used the *quantile*() function in R to identify and extract the top 1%, 0.5%, and 0.25% of all variants and windows. Variants were considered to be statistically significant if they fell within the top 0.5% of the empirical distribution of XP-nSL scores (Szpiech et al. 2021).

2.3.2 Locus-Specific Branch Length Estimates

LSBL is a test to detect statistical differences in SNP fixation between three population dyads (Shriver et al. 2004, Mattiangeli et al. 2006). Highly-differentiated SNPs, represented as long branches at a given locus, indicate evolutionary divergence of one population from the others. LSBL is derived from Wright's *F* statistics, which were developed to describe the level of heterozygosity expected at a particular locus for a given population (Wright 1950).

If the symbol $\bar{p}$ represents the average frequency for a given allele in a total population; σ^2_S represents the variance in the frequency of that between subpopulations (*S*) weighted by their respective sizes; and σ^2_T refers to the variance of in the total population (*T*), F_{ST} can be defined as:

$$F_{ST} = \frac{\sigma_S^2}{\sigma_T^2} = \frac{\sigma_S^2}{\bar{p}(1-\bar{p})}$$

Given the size of human populations, exact frequencies for a given SNP often cannot be measured. In such instances, estimators like that of Weir and Cockerham are used (Weir and Cockerham 1984). Weir and Cockerham's estimator θ calculates F_{ST} for population pairs and then weights these according to ratio of population sizes, denoted by the symbol *M*. Where $F_{ST:A}$ represents the F_{ST} value for a given population *A;* and $F_{ST:B}$ represents the value of F_{ST} calculated for population *B*; Weir and Cockerham's θ for the population pair A:B can be calculated as:

$$\theta_{A:B} = \frac{(F_{ST:A} + F_{ST:B})}{\left(F_{ST:A} + F_{ST:B} + 2\frac{1}{(M+1)}[M(1-F_{ST:A}) + (1-F_{ST:B})]\right)}$$

Calculating Weir and Cockerham's θ three population dyads (i.e., $\theta_{A:B}$, $\theta_{B:C}$, and $\theta_{A:C}$) for loci across the genome, LSBL estimates can be produced as follows:

$$LSBL_A = \frac{\theta_{A:B} + \theta_{A:C} - \theta_{B:C}}{2}$$

The resulting values thus represent the amount of differentiation for a target population relative to two outgroups. These LSBL values can then be placed into an empirical distribution in order to identify the SNPs with the greatest estimated branch lengths (i.e., greatest statistical distances) that exceed a predetermined genome-wide significance level.

To calculate LSBL for Mexican Mayans, I merged the genotype data with data derived from Peruvian Quechua and Han Chinese individuals (N = 45). For each population pair (Mexican:Peruvian, Chinese:Mexican, Peruvian:Chinese), Weir and Cockerham's θ was calculated in VCFTools for each SNP (Danecek et al. 2011). The resulting pairwise weighted θ estimates were then normalized over 100kb sliding windows with a 50kb overlap (Danecek et al. 2011).

After concatenating the resulting 22 chromosome-specific files in Python (version 3.9.5), I exported the results to R (version 4.1.0) (Van Rossum and Drake 1995, R Core Team 2021). LSBL was calculated using the pairwise estimates of θ in R using scripts written for this dataset. I used the *quantile*() function in R to identify and extract any window or SNP falling in the top 1%, 0.5%, and 0.25% of their respective distributions. To avoid biases resulting from sampling error, windows were omitted if the mean number of observations between three sample dyads was fewer than four SNPs. SNPs were considered to be statistically significant if they fell within the top 0.5% of the empirical distribution of LSBL scores.

2.3.3 Pathway Analysis

SNPs distributed at the "shoulders" of sweep regions may have relatively high-ranking (yet statistically insignificant) SNP scores for one or both tests. In order to capture variation at the peripheries of such haplotypes, SNPs falling within the top 1% of distributions for SNP scores were retained and annotated in gene ontology datasets. Individual identifiers for SNPs or genomic regions that surpassed the statistical significance cutoffs for their respective tests were queried in Affymetrix's NetAffx analysis center (https://www.affymetrix.com). This provided the names and symbols for each gene, or a list of genes falling within a particular window. These gene lists were uploaded to Reactome (www.reactome.org) and Gene Ontology databases (http://geneontology.org/), providing relevant information about pathways, interactions, and relevant biological functions. The Gene Ontology (GO) database was queried for search terms related to body temperature regulation, thyroid function, water homeostasis, and heat shock protein binding. Pathway results in Reactome were considered to be significant at the level of $\alpha = 0.025$.

2.4 Results

2.4.1 Population Structure

Analysis of population structure is important to identify signals of admixture and to remove individuals with high European or African ancestry that might influence results. To analyze population structure and identify admixture, the Mexican Mayan dataset was merged with SNP data from 514 Peruvian Quechua, 60 Yorubans, 45 Han Chinese from Beijing, 45 Japanese from Tokyo, and 60 individuals of north-central European ancestry from the Centre d'Etude du Polymorphisme Humain (CEPH). To ensure that linked SNPs did not bias the results of the principal component analysis, a total of 29,495 SNPs with high LD ($r^2 > 0.8$) were pruned

out of the dataset. ADMIXTURE analysis using the remaining 284,038 variants (Supplementary Figure 1A) demonstrated that the model with the lowest cross-validation error was K = 5 groups. This best-fit model groups Han Chinese and Japanese from Tokyo as a single East Asian population to the exclusion of CEPH Europeans, Yorubans, Mexican Maya, and Peruvian Quechua.

To estimate the total "local" ancestry private to the Americas, a pooled ancestry component was produced for each participant. This was calculated as the sum of Mexican Mayan-like and Peruvian Quechua-like ancestry components. After removing related individuals and participants with high levels of European ancestry, 65 individuals remained in the dataset. PCA was conducted to identify any other cryptic relatedness, admixture, or additional population structure (Supplementary Figure 1B). This analysis showed that Mexican Mayans and Peruvians have a partial overlap, and cluster to the exclusion of other global populations. An estimated 57.92% of variation in ancestry is captured by the first PC, whereas the second PC accounts for 24.67%. Plotting the first and third PCs segregates the Mexican Mayan and Peruvian Quechua sample (PC3 = 18.73% of variance), yet preserves the tight cluster of the East Asian samples.

2.4.2 Genetic Evidence for Local Adaptation in Mexican Mayans

Selection scans were performed on SNP data generated for 65 individuals. From the dataset of 313,533 SNPs, a subset of 93,369 SNPs were removed from the dataset for not having complete observations between the three populations: this either arose from low-confidence calls or not being present in the CHB dataset. The remaining 216,636 variants were used to calculate locus-specific branch lengths (Supplementary Figure 2). These ranged from being weakly-negative (indicating disparity in observed gene diversity and expected heterozygosity) to a

maximum branch length of 0.661. SNPs with branch lengths of least 0.228 were considered statistically significant at the 99.5% level. A total of 1,084 SNPs, overlapping with the coding regions of 478 genes, exceeded this threshold. The longest branch length detected was that of rs6693069 (LSBL = 0.6611), a missense variant in *HMCN1,* a gene involved in the cell-division cycle*,* that results in an alanine to threonine change in the 91st exon of the gene.

LSBL values were calculated for a total of 43,095 windows (Table 2). Windows with fewer than four SNPs were omitted to avoid the effect of small sample sizes in driving up the mean value of LSBL. Windowed branch lengths ranged from -0.139 to 0.342, and were considered significant at the 99.5% level if branch lengths surpassed 0.155. A total of 216 windows had weighted LSBL scores surpassing this threshold. The top-scoring region was located on Chromosome 1 spanning positions 186,050,001 to 186,150,001 with a windowed LSBL of 0.342. This window overlapped with two genes: *HMCN1*, and *MIR548F1*, a non-protein coding gene that encodes microRNAs (miRNAs).

XP-nSL values were calculated for 306,079 autosomal variants. A total of 1,537 variants had XP-nSL scores greater than the 99.5% significance cutoff of 0.219. The variant with the highest-scoring haplotype was rs14182775 (XP-nSL = 0.445), a SNP in *PSORS1C1* (aka *SEEK1*), a gene associated with susceptibility to psoriasis (OMIM: 613525). At this locus, the B variant is fixed in the Mexican Mayan sample, but is at a somewhat lower frequency in the Peruvian Quechua sample (0.647/0.353). This variant is at very high frequencies in most populations from 1000 Genomes (MXL = 0.984/0.016, CHB = 1/0, CEU = 1/0, YRI = 1/0).

A total of 28,663 normalized XP-nSL windows were calculated; the resulting haplotype scores ranged from -4.446 to 4.844. XP-nSL windows were considered significant at the 99.5% level if their scores exceeded 3.208 (Table 3). The three highest-scoring XP-nSL windows were

clustered in a one megabase region on Chromosome six. The top window (Chr6:31,100,001-31,200,001) had a score of 4.844 and included the genes *CCHCR1, TCF19, POU5F1, HCG27,* and *HLA-C,* as well as three genes in the psoriasis-susceptibility family (*PSORS1C1, PSORS1C2,* and *PSORS1C3*).

Twenty-six variants within coding regions of 19 genes were statistically significant for both XP-nSL and LSBL (Figure 1). Variants that are in high-scoring haplotypes and that are highly-differentiated between populations provide compelling evidence of evolutionary divergence between samples (Supplementary Table 1). These high scoring SNPs overlapped with: eight genes related to various metabolic functions (*PPARG, TH, TSEN2, MYT1L, NRG1, STK19, MKRN2, ITPK1*); three genes in the HLA family (*HLA-DOB, HLA-DPB1, HLA-DQA2*), which are critical for immune responses; *C3*, a gene related to *Leishmania* infection; *PSORS1C1*, which is related to psoriasis susceptibility; *APCDD1L*, a gene implicated in amelogenesis imperfecta which is a heritable disease leading to malformation of dental enamel; one gene involved in keratinization and protein binding (*KAZN*); and one gene related to actin binding and structural molecule activity (*SNTG2*). Of note, two genes had several SNPs located in the intersection of the top LSBL and XP-nSL values. These were: *PSORS1C1,* which contained five SNPs (rs3815087, rs3095301, rs3095302, rs3131003, rs3130558); and *NRG1*, which contained three SNPs (rs10092307, rs17717485, rs4733325).

2.4.3 Gene Interactions and Pathway Analysis

A tiered approach was used in order to identify interactions between genes under selection and the most relevant pathways with which they were associated. Candidate lists submitted to Reactome (https://reactome.org/) were curated for: (1) genes overlapped by the top

150-ranked SNPs for LSBL; (2) genes overlapped by the top 150-ranked SNPs for XP-nSL; (3) genes encompassed by the top 25 LSBL window scores; (4) genes encompassed by the top 25 XP-nSL window scores; and (5) a master list of all genes contained in the above. SNP and gene lists submitted to Gene Ontology were created for SNPs falling in the top 1% of the distribution of scores for either test, and genes encompassed by the top 25 windows for both XP-nSL and LSBL.

Genes identified in SNP-based LSBL were included in eighteen Reactome pathways surpassing the significance threshold ($\alpha = 0.025$). Of these, three genes (*NRG1, YES1, WWOX*) were involved in 11 different pathways related to ERBB signaling. Overall, the most significant pathway ($p = 0.0006$) was "GRB7 events in ERBB2 signaling" (R-HSA-1306955), which is mediated by the gene *NRG1.* Genes detected through the windowed LSBL analysis were included in eight Reactome pathways that achieved statistical significance. Among these were proton-coupled neutral amino acid transport facilitated by *SLC36A1* (R-HSA-428559), transport of fatty acids via *SLC27A6* (R-HSA-804914), and genetic defect related to biotin metabolism (R-HSA-3323169).

Fifteen Reactome pathways were significant for genes identified by SNP XP-nSL. The gene *TJP1* is implicated in "RUNX1 regulates expression of components of tight junctions" (R-HSA-8935964), the top pathway ($p < 0.0002$) for genes identified by SNP-based XP-nSL.
For genes identified in windowed XP-nSL, 23 had significant pathway associations in Reactome. The top-ranking pathway was "Translocation of ZAP-70 to Immunological synapse" (R-HSA-202430; $p = 1.11 \times 10^{-16}$) related to several genes in the HLA-D family: *HLA-DRB5, HLA-DRA, HLA-DQA1, HLA-DQB2, HLA-DRB1,* and *HLA-DQB1.* Genes in the HLA family were significantly overrepresented among the top-scoring pathways: of the 23 significant pathways, 21

contained at least one gene in HLA, and 14 contained multiple genes in HLA-D.

2.4.4 Genetic Adaptations to Heat Stress

The combined list of LSBL and XP-nSL SNP scores overlapped with 27 genes with putative adaptations to heat stress that were listed in Gene Ontology (GO) and Reactome databases (Table 1). Only two genes from the top 25 window regions of both statistics matched with adaptive pathways listed in GO: *YWHAE* and *BAG6*, which were associated with cellular responses to heat (GO:1900034).

Selection scans detected several genes involved in the pathway entitled "cellular responses to heat stress" (R-HSA-3371556) and "Regulation of HSF1-mediated heat shock response" (R-HSA-3371453). These genes include *RPTOR*, *NUP88*, *HSPA12A*, and *NUPL1*. Two genes contained branch lengths that reached statistical significance, *RPTOR* (rs12939557, LSBL = 0.566) and *NUPL1* (rs11556093, LSBL = 0.231). *NUP88* contained one SNP situated in a high-scoring haplotype (rs150994660, XP-nSL = 0.229). The gene *HSPA12A,* contained two intronic variants (rs10787720, LSBL = 0.225; rs7086870, LSBL = 0.232) that fell in high-scoring haplotypes as well as a high scoring upstream variant (rs4752011, XP-nSL = 0.255; Figure 2).

Evidence of selection in genes related to heat homeostasis was found in the large proline-rich protein BAG6 (*BAG6*) gene (Figure 3). Gene ontology databases indicate that *BAG6* plays a role in heat shock protein binding (GO:0030544) indicating that it is necessary for cellular responses to heat stress. The entirety of *BAG6* falls above the 99.5% significance threshold for XP-nSL scores with the mean SNP score being 0.293, corresponding with the second highest-scoring window (XP-nSL = 4.731). Both *BAG6* and *YWHAE*, a gene implicated in cellular

responses to heat (GO:1900034), were detected within outlying windows from XP-nSL. However, the inclusion of *YWHAE* in this window is solely a result of its proximity to the high-scoring *BAG6* gene, evidenced by the fact that *YWHAE* contained no individual SNPs that neared statistical significance.

NRG1 contained several statistically-significant SNPs: three fell within the top 0.5%ile of scores for both LSBL and XP-nSL (rs10092307, rs17717485, rs4733325); one was significant only for XP-nSL (rs13254149); four remaining SNPs were significant for LSBL with one variant falling within the top 0.1% of scores (rs10954820, LSBL = 0.588). *NRG1* is involved in MAPK signalling (R-HSA-5683057), which is known to contribute to temperature homeostasis and hyperosmotic responses during heat stress in model organisms (Dunayevich et al. 2018). Finally, *RB1*, a gene contributing to temperature homeostasis (GO:0120163) contained a SNP with a deeply-divergent branch (AX-11489736, LSBL = 0.411).

Several genes related to thyroid hormone generation and metabolic processes were detected through XP-nSL SNPs. The Dual Oxidase family of genes (DUOX) had several variants falling within the top 0.25% of XP-nSL scores, including *DUOX2* (rs269866; XP-nSL = 0.304), *DUOXA1* (rs61751061, max = 0.291), and *DUOXA2* (rs61733394; XP-nSL = 0.276; and rs2576090; XP-nSL = 0.276) (Figure 4, Supplementary Figure 3). *TPO,* which also plays a role in thyroid hormone production, contained one highly-differentiated variant (rs13431646, LSBL = 0.238).

Selection scans identified several genes related to heat production via mitochondrial uncoupling protein (R-HSA-163200). Genes involved in this pathway included: *ETFB*, which had six SNPs within the top 0.5%ile of XP-nSL scores, the top scoring of which was rs10410947 (XP-nSL = 0.258); *NDUFAF6,* which had five variants with significant haplotype scores

centered about rs2044035 (XP-nSL = 0.244); and *NUBPL*, which had one significant SNP identified for LSBL (rs17379852 LSBL = 0.239).

The metabolism of long chain fatty acids is a process that mediates heat production in brown adipose tissue (Heeren and Scheja 2018, Xiang et al. 2018). Five genes responsible for regulating lipid metabolism by PPARalpha (R-HSA-400206) were statistically significant: *ABCA1, ABCB4, AHRR, PPARG*, and *MED13L*. Additional evidence of selection was seen in genes within the ATP-binding cassette (ABC) family and within *PPARG*. *ABCA1* contained one highly-differentiated SNP (rs12003756:,LSBL = 0.424). The gene *ABCB4* also harbored a high-ranking LSBL value (rs6657239, LSBL = 0.509), and had a peak XP-nSL value of 0.225 (rs1149222) with three other SNPs reaching statistical significance for haplotype scores. *PPARG* contained six SNPs that reached statistical significance for XP-nSL alone. The highest-scoring SNP overall was rs1175541 (XP-nSL = 0.245). One SNP was significant for LSBL (rs10510419, LSBL = 0.307). One variant was significant for both XP-nSL and LSBL (rs62243565, LSBL = 0.281, XP-nSL = 0.227). *MED13L* contained one SNP with a high XP-nSL value (rs11067898, XP-nSL = 0.230). In addition to *PPARG* and *MED13L*, *LPL* was another gene detected in the selection scan that is implicated in white adipocyte differentiation (R-HSA-381340). *LPL* contained one very long branch at rs28424158 (LSBL = 0.567).

Several genes related to the balance of bodily salt and water content were detected in selection scans. *TPK1* is implicated in both aquaporin-mediated transport (R-HSA-445717) and renal water homeostasis mediated by vasopressin (R-HSA-432040). *TPK1* contained one extremely long branch, indicating evolutionary divergence in Mexican Mayans at this locus (rs28692603: LSBL = 0.513). There were four genes related to water homeostasis (GO:0003091, GO:0070295, GO:0030104) that each contained one high-scoring variant: *AKAP11*

(rs200595109: XP-nSL = 0.230), *FLG* (rs12728605: LSBL = 0.314), *HYAL2* (rs709210: XP-nSL = 0.229), and *NEDD4L* (rs79039291: XP-nSL = 0.307). The gene *HSD17B4* is implicated in acid and bile salt metabolism (R-HSA-194068) and contains eight SNPs that surpassed the significance threshold for XP-nSL, the highest of which was rs162196 (XP-nSL = 0.230).

2.5 Discussion

The ability to offset thermal stress is critical to human survival, yet genetic adaptations to high heat index are not well described. This study conducted a selection scan to compare patterns of genetic variation between a putatively heat-adapted Mexican Mayan sample, and a related population (Peruvian Quechua) that inhabit a cold, high-altitude environment in South America. By leveraging a frequency-based test of selection (LSBL) against a haplotype-based scoring system (XP-nSL), we detected evidence of past selective sweeps at genes associated with cellular responses to heat stress (*HSPA12A*), water/salt homeostasis (*NEDD4L*), and body temperature regulation (DUOX family). This provides potential evidence of local evolutionary adaptation to the environmental variables found in the tropical lowland forests of southeast Mexico.

We identified 27 genes that may have undergone selection to high ambient temperatures or the interactive effects of high heat and humidity. The highest-scoring variants (top 0.1% of scores) of our selection scan overlapped with *BAG cochaperone 6, BAG6*, a gene involved in heat shock protein binding (GO:0030544). *BAG6* is an ATP-independent molecular chaperone; the role of *BAG6* is to guide against hydrophobic and misfolded protein aggregation (Tanaka et al. 2006). It plays an important role not only in ubiquitination, offsetting stress in the endoplasmic reticulum (ER) and ER associated degradation (ERAD), and indirectly influences

the insulin-like growth factor receptor (IGFR) signaling pathway (Wang et al. 2011, Osorio et al. 2016). Processes that mediate cellular responses to heat stress, such as those encoded by heat shock protein (HSP) binding genes and their cofactors, would likely confer adaptive benefits to populations living in the tropics (Freitas et al. 2021).

In the absence of HSP induction, normal heat shock resistance also can be achieved through the overexpression of ubiquitin (Schlesinger 1990, Friant et al. 2003). Proteins are marked for proteolysis with ubiquitin (ubiquitin-dependent proteolysis) (Schrader et al. 2009). It is possible that a number of ubiquitin-dependent proteolysis genes facilitate the transport of heat denatured proteins out of the body. Apart from *BAG6*, two other genes involved in ubiquitination and deubiquitination showed evidence of recent positive selection in Mexican Mayans: *NRG1* and *TPK1*. *NRG1* is involved in MAPK signaling (R-HSA-5683057), which is known to contribute to temperature homeostasis and hyperosmotic responses during heat stress (Dunayevich et al. 2018). Other pathways that contribute to thermal stasis involve thyroid hormone function, vasodilation, and inflammatory responses. This study found evidence of selection on *Dual Oxidase 2*, *DUOX2,* a gene involved in thyroid hormone synthesis, which helps mediate body temperature (GO:0006590). In populations from cold climate, there is a well-reported association between thyroid levels and basal metabolic rate (Leonard et al. 2005). In the context of adaptation to hot tropical environments, it is possible that selection against variants that increase body temperature could be protective against heat stroke. *Bradykinin Receptor 2*, *BDKRB2,* is a gene implicated in vasodilatory responses (GO:0042311); *Neuregulin*, *NRG1,* is a gene related to MAPK signalling which in turn plays roles in inflammatory and fever responses (R-HSA-5683057). Additionally, the ability to maintain bodily water during heat exposure (and sweating) might be adaptive to hot climates. This study detected selection on the gene *NEDD4-*

Like Ubiquitin Ligase, *NEDD4L,* which facilitates water/salt balance through the process of water homeostasis (GO:0030104).

2.5.1 Evidence of Selection on Thermoregulatory Loci

Gene Ontology queries allow an observer to create a dataset of genes or proteins that have previously been described as contributing to putatively-adaptive responses to heat stress. While it is possible that single genes (e.g., *UCP1*) are significant contributors to thermoregulatory responses to heat stress, it is likely that thermal adaptation is highly polygenic and thus might shape variation across a number of seemingly-unrelated genes or pathways. In the absence of functional validation, it is uncertain whether or not (or which of) these candidate genes contain fitness-increasing changes that result in enhanced thermoregulatory behaviors under the condition of high heat stress. As such, one should take caution in that our candidate genes were identified on the basis of exhibiting one of two hallmarks of recent selection: either a high-frequency, long-ranging haplotype, or significant asymmetry in evolutionary divergence between population dyads.

This study identified 21 significant SNPs spanning five genes related to body temperature homeostasis. Within these selection-nominated genes, there was strong evidence of nonrandom genetic change acting upon *Peroxisome Proliferator Activated Receptor Gamma*, *PPARG*, a lipid metabolism-regulating gene (R-HSA-400206), which was detected by both LSBL and XP-nSL. This gene, along with three nearby genes, *NUBPL*, *ETFB*, and *NDUFAF6*, are suggested to be adaptive to cold climate (Hancock et al. 2008). Given the high number of statistically-significant SNPs identified by XP-nSL for *PPARG, ETFB,* and *NDUFAF6,* there are clear evolutionary changes affecting the structure and maintenance of haplotypes around these genes. Additionally,

selection scans identified four genes related to the body's ability to reabsorb water and process salts. These include genes within water homeostasis pathways *AKAP11, FLG, HYAL2*, and *NEDD4L* (GO:0030104, GO:0003091), as well as *TPK1*, which is related to vasopressin-mediated renal water homeostasis (R-HSA-432040). Similar results were reported in Aboriginal Australians, where *SLC2A12*, a gene related to serum urate levels, was detected in selection scans (Malaspinas et al. 2016). Selection in these pathways indicate that the ability to regulate the balance of bodily water and salts, perhaps in a manner that prevents dehydration, could be adaptive in regions with high heat index.

We detected evidence of natural selection in five genes related to thyroid function, the *Thyroid Peroxidase*, *TPO,* gene and four genes within the DUOX family, *DUOX1, DUOXA1, DUOX2,* and *DUOXA2*. These genes, which mediate thyroxine secretion, are hypothesized to contribute to body temperature regulation (Warner et al. 2013). Thyroxine (also known as T4) is a thyroid hormone that is stored in thyroxine-binding globulin (TBG). TBG releases T4 in a temperature-dependent manner: in situations such as fever, where there are increases in body temperature, this change will trigger a cascade of T4 production and increase metabolic output (Qi et al. 2014).

In regions of the planet where ambient temperatures remain fairly low, such as at high altitude or high latitude, T4-mediated increases in body temperature might confer a selective advantage (Leonard et al. 2005, Snodgrass et al. 2005). Evidence from high altitude shows that the thyroid axis is activated during ascent (von Wolff et al. 2018). Two studies in Nepal showed an association of increased free T4 levels with elevation (Nepal et al. 2013, von Wolff et al. 2018). One study of high altitude natives and acclimatized lowlanders showed an increase in both T4 and T3 with altitude which trended towards baseline during descent to sea level (Basu et

al. 2003). In Indigenous circumpolar communities such as the Yakut (Sakha) and Evenki of Siberia, individuals show elevated T4 levels and basal metabolism compared to Russian counterparts (Leonard et al. 2005, Snodgrass et al. 2005). Similarly, Indigenous Nenet communities from Svalbard and Arkangelsk, Russia show elevated T4 during the winter months, and exhibit significantly higher T4 levels compared to Russians (Tkachev et al. 1991, Bojko 1997). In high-latitude men from northern Finland, serum free T3 levels were lower in winter than in summer, and TSH levels were higher in December than in any other month; additionally, urinary free T3 levels were significantly higher in winter than in summer (Hassi et al. 2001). This indicates that there is an increase in T3 disposal during cold periods, which in turn might imply that short-term thyroid responses are crucial in the context of cold climate (Leonard et al. 2005).

In hot environments, one might expect to see selection that attenuates thyroid production or sensitivity, thus decreasing basal metabolic rate. Selection on genes involved in thyroid function (*NETO1* and *KCNJ2*) has previously been reported in another putatively-heat adapted population, Aboriginal Australians (Malaspinas et al. 2016). In this population, it appears that thyroid hormone levels are modulated in response to ambient temperature such that they prevent an individual's body temperature from reaching dangerously high levels (Qi et al. 2014).

Further evidence of the adaptive significance of thyroid hormone is seen in putatively cold-adapted populations from the Peruvian Andes. Between chronic mountain sickness-afflicted Andeans and a comparative sample of individuals of Mexican Ancestry from Los Angeles (MXL), Zhou et al. (2013) revealed a high level of F_{ST} spanning the same DUOX sweep region reported here. Results of later selection scan projects identified DUOX as a region undergoing recent selection in Andeans (Jacovas et al. 2018, Borda et al. 2020). Using the population branch

statistic (PBS), a test that is similar to LSBL, Jacovas et al. (2018) identified one SNP within *DUOX2* (rs269866) that is highly differentiated between lowland Mesoamericans (MAF = 0.068) and Andean highlanders (MAF = 0.42).

In our study, the variant rs269866 is at similarly low frequency in Mexican Mayans (MAF = 0.0154), and at relatively high frequency in Peruvian Quechua (MAF = 0.4944). Homozygotes for the G mutation of this SNP exhibited increased DUOX2 protein expression; if this leads to an increase in body temperatures, it holds that a heat-adapted population might show selection against the G allele in favor of the derived A allele, reducing the frequency of the former in favor of the latter and thus protecting against exertional heat stress. In a later study, Borda et al. (2020) reported that *DUOX2* is under selection in Andeans relative to Indigenous communities from the Amazon, and that mutations within this gene are associated with hypothyroidism. The authors speculate that selection in this pathway might be related to innate immunity or might protect against iodine deficiency. Interestingly, both the results of this study and those of Borda et al. (2020) identified selection operating on the same variants yet did so through different statistical methods -- a frequency based test (Borda et al. 2010) versus a haplotype-based test (this study). Given the high number of statistically significant XP-nSL scores but the relatively short LSBL branches across this gene family, it is likely that the shared haplotype is under selection and not necessarily a specific SNP. However, there are seven SNPs within the DUOX family that have high pairwise frequency differences between Mexican Mayans and Peruvian Quechua (Supplementary Table 2, Supplementary Figure 3).

2.5.2 Limitations and Alternate Approaches

One limitation of relying solely on selection scan approaches to human evolution is that pairwise haplotype-based tests cannot account for shared genetic drift: while we were able to leverage an out-group statistic (LSBL) against a haplotype-based test (XP-nSL) to identify relatively local evolutionary changes, this approach lacks somewhat of a historical depth. Additionally, since our scans used SNP data alone (i.e., without further validation with sequence-based tests of selection), we were only observing how variation is shaped among known variable sites in the human genome. This is perhaps the reason why several peaks identified in XP-nSL neared the significance cutoff, yet showed an asymmetrical decay with distance from a putatively-adaptive peak (i.e., SNP under selection) that was not included in the SNP panel.

This project would benefit from functional validation of candidate SNPs as well as from sequence-based tests that can detect evolutionary departures between populations. One limitation to this study is that fluctuations in allele frequencies can be caused by a variety of selective or demographic forces. To this end, common null models used in population genetics frameworks are: (1) that mutations will primarily accrue in a neutral manner (Tajima 1989), (2) that there will be no difference in the ratio of nonsynonymous to synonymous changes between populations (McDonald and Kreitman 1991), and (3) that evolutionary equidistance indicates no population-specific divergence (Yi et al. 2010). In essence, most selection scans are burdened with testing against neutrality; while this is a valid null hypothesis, neutral evolution and directional selection are distinct evolutionary scenarios that can resemble one another, a factor that can mask or mimic signatures of local adaptation (Tiffin and Ross-Ibarra 2014, Rees et al. 2020). This signal is obscured in instances of selection that are highly polygenic in nature; in scenarios where background selection enhances the signal of drift in driving population differentiation; and in cases where soft sweeps increase the frequency of neutrally-evolving variants merely due to their

proximity to beneficial alleles. To this end, it is crucial to combine frequency-, haplotype-, or sequence-based approaches to distinguish instances of natural selection from drift and other demographic factors.

One issue presented in this study is that the limited geographic scope of our Mexican Mayan dataset fails to indicate how heat adaptation works in the broader regional context. For example, operating within only a few degrees of latitude an individual trekking across Mexico would encounter a variety of different habitats that are uniformly warm but with a vast gradient in humidity (e.g., savannah and desertic environments in central southern Mexico). To fully address how humans adapt to heat regardless of heat index, it would be helpful to expand the dataset to include additional Indigenous communities inhabiting other regions of Central and South America. This pooled genomic dataset would have increased power to detect genomic changes that span the humidity spectrum in relatively low-latitude zones and would point towards selection occurring on the leading edge of the migration wave into Mesoamerica some ~13,000 years before present (González González et al. 2008, Sellayah et al. 2014): this ancestral Paleoindian population would have faced a shared evolutionary burden of high heat before differentiating into distinct environments at opposite ends of a humidity continuum. Expanding the scope of our selection scans would be of particular interest to the study of thermal adaptations considering that despite high daytime temperatures, inland deserts often have night time lows that can fall well below freezing during the colder months of the year (Weiss and Overpeck 2005). As such, this aspect of the project could reveal how adaptation to arid environments with extreme temperature swings might differ from adaptation to tropical lowland environments with a relatively stable (and absolutely higher) level of humidity.

This study identified severaal sweep regions surrounding genes related to dermatological health and immune response, renal function, and temperature homeostasis. To investigate how genes involved in body temperature regulation and water reabsorption might manifest in periods of heat stress, an association study can be performed to identify genetic contribution to traits such skin surface temperature and serum osmolality. This would strengthen the assertion that Mexican Mayans have undergone selective changes that protect against local environmental stress.

One such factor that might influence our results is the strong population bottleneck on the founding lineage of Indigenous Americans (Fagundes et al. 2018). Due to random sampling error, populations descending from these First Peoples of the Americas exhibit reduced genetic diversity (i.e. compared to populations in Asia) that in some ways mimics selection. A frequency-based test used in this study, LSBL, compared variation within and between Maya, Quechua, and Han Chinese: with these three populations, differentiation resulting only from shared drift between the Indigenous samples would result in a long branch directed towards the Han Chinese subsample. Indeed, the empirical distribution of LSBL revealed that the shape of the distribution for the Han Chinese sample was skewed to longer branch values relative to the Mayan and Quechua subsamples. While a high number of long LSBL estimates unique to one population might result from either selection or drift, we do not expect this fact to detract from our results given that we leveraged within-continent variation (Mexican Mayans vs Peruvian Quechua) against between-continent variation (Mexican Mayans vs Han Chinese, Peruvian Quechua vs Han Chinese).

Additional instances of drift were counteracted by using haplotype-based tests of selection. XP-nSL scores a haplotype based on the decay of homozygosity as it relates to

recombination distance. The underlying rationale of XP-nSL is that a variant under selection will have a relatively high frequency and will have exceptionally long-range linkage disequilibrium (LD) (Szpiech et al. 2021). Due to LD, consecutive XP-nSL values create peaks for high-scoring haplotypes and valleys for low-scoring haplotypes, the latter of which indicates selection in the reference population. Unlike LSBL, XP-nSL scores that fall in the top 0.5% extreme of the distribution of XP-nSL scores are generally embedded within or alongside other high-scoring SNPs. Our strategy of adopting a conservative genome-wide significance threshold (0.5% false-positive rate), and considering that XP-nSL scores essentially prioritize homogeneity (i.e., reduced genetic variation resulting from sweeps), provides a high-confidence method of detecting extremely differentiated haplotypes that indicate evolution by natural selection.

2.5.3 Conclusions

Prolonged exposure to temperature extremes is a known reducer of fitness, specifically in the form of hypothermia in cold climates and hyperthermia achieved either through overexertion or environmental heat stress. While there is compelling evidence of cold climate adaptation in circumpolar populations, the same cannot be said for evolutionary adaptations to heat stress in equatorial or low-latitude populations. We hypothesized that in tropical lowland environments, selection might act on pathways that would help prevent dehydration: this study detected strong selective sweeps in genes related to salt regulation (*HSD17B4*) and water homeostasis (*NEDD4L*), which are two components of osmotic balance that might protect against excessive water loss through sweating. We also hypothesized that selection might act on pathways related to cellular responses to heat stimulus, vasodilation (a process that brings blood to the skin's surface to facilitate cooling), and metabolic or hormonal regulators of body temperature.

Selection scans identified long-range haplotypes centered on heat shock protein-encoding genes (*HSPA12A*), as well as genes involved in lipid metabolism (*PPARG),* vasodilation (*BDKRB2),* and thyroid function (DUOX family). In addition, genes related to antigen response (*HLA-DRB*) and wound healing (*PSORS1C1*) showed signatures of recent selective sweeps, highlighting the evolutionary importance of disease adaptation in recent human evolution.

Our results point towards a scenario in which adaptations to heat stress span a variety of different cellular, vascular, and metabolic pathways that likely all contribute in some manner to thermal adaptation to high ambient temperature. This is central not only to the study of how humans adapted to our shared tropical home range some 2 million years ago, but also for understanding the timing and strength of selection operating on a myriad of adaptive pathways that hitherto may not have been appreciated in the study of human evolution. In particular, there is an overwhelming amount of research conducted on fossil ancestors, and alongside cold-adapted populations, as well as in regards to physiological responses to heat: this study represents a departure from these regional or temporal matters of interest, and provides some of the first genetic evidence of natural selection to high ambient temperatures in living humans. This in turn contributes to our collective knowledge regarding putatively-adaptive responses to environmental stress at varying scales, and is thus informative for our understanding of critical biological functions (e.g., water/salt homeostasis) in environmental extremes.

2.6 Tables and Figures

Table 2.1: Thermoregulatory genes identified in selection scans.

Response	Gene	Pathway
Heat Response	*NUP88*	Response to heat (GO:1900034)
Heat Response	*RPTOR*	Response to heat (GO:1900034)
Heat Response	*BAG6*	Heat shock protein binding (GO:0030544)
Heat Response	*FAF1*	Heat shock protein binding (GO:0031072)
Heat Response	*HSPA12A*	Protein binding (GO:0005515)
Heat Response	*NUPL1*	Cellular response to heat stress (R-HSA-3371556)
Heat Response	*YWHAE*	Response to heat (GO:0034605)
Lipid Metabolism	*ABCA1*	Regulation lipid metabolism by PPARalpha (R-HSA-400206)
Lipid Metabolism	*ABCA4*	Regulation lipid metabolism by PPARalpha (R-HSA-400206)
Lipid Metabolism	*PPARG*	Regulation of lipid metabolism (R-HSA-400206)
MAPK Signalling	*NRG1*	MAPK signalling (R-HSA-5683057)
Protein Uncoupling	*ETFB*	Mitochondrial protein uncoupling (R-HSA-163200)
Protein Uncoupling	*NDUFAF6*	Mitochondrial protein uncoupling (R-HSA-163200)
Protein Uncoupling	*NUBPL*	Mitochondrial protein uncoupling (R-HSA-163200)
Temperature Homeostasis	*RB1*	Temperature homeostasis (GO:0120163)
Thyroid Regulation/Generation	*DUOX1*	Thyroid hormone generation (GO:0006590)
Thyroid Regulation/Generation	*DUOX2*	Thyroid hormone generation (GO:0006590)
Thyroid Regulation/Generation	*DUOXA1*	Regulation of thyroid hormone generation (GO:2000609)
Thyroid Regulation/Generation	*DUOXA2*	Regulation of thyroid hormone generation (GO:2000609)
Thyroid Regulation/Generation	*TPO*	Thyroid hormone generation (GO:0006590)
Vasodilation	*BDKRB2*	Vasodilation (GO:0042311)

Table 2.2: Top 25 Windows Identified in LSBL

Chromosome	Window Start	Window End	Window LSBL	Genes in Window
1	186050001	186150000	0.3417351	*MIR548F1, HMCN1*
11	49700001	49800000	0.30838869	*LOC440040*
10	38300001	38400000	0.28588161	*ZNF33A*
8	146250001	146350000	0.28057352	
2	48400001	48500000	0.27486715	
16	20850001	20950000	0.274222	*DCUN1D3*
13	25850001	25950000	0.2735926	*NUPL1*
17	37100001	37200000	0.2651515	*LRRC37A11P*
5	108900001	109000000	0.26487735	
5	150800001	150900000	0.2643895	*SLC36A1, FAT2*
5	108950001	109050000	0.25349415	
5	109900001	110000000	0.25336695	*TMEM232*
15	54850001	54950000	0.25189535	*UNC13C*
1	196550001	196650000	0.24551427	*KCNT2, CFH*
2	61250001	61350000	0.24009751	*PEX13, KIAA1841*
18	9100001	9200000	0.2398365	*NDUFV2, ANKRD12*
5	79650001	79750000	0.2374105	*ZFYVE16*
9	108550001	108650000	0.2330175	
5	43100001	43200000	0.2311006	*NIM1K*
1	11950001	12050000	0.22621315	*PLOD1, MFN2*
1	6650001	6750000	0.226003	*KLHL21, PHF13, THAP3*
14	49000001	49100000	0.2258048	
1	118450001	118550000	0.22519	*WDR3, SPAG17*
20	35250001	35350000	0.2250355	*NDRG3*
1	39800001	39900000	0.22217695	*MACF1*

Table 2.3: Top windows identified in XP-nSL.

Chrom	Start	End	Score	Genes in Window
6	31100001	31200001	4.84365	*PSORS1C1, PSORS1C2, CCHCR1, TCF19, POU5F1, PSORS1C3, HCG27, HLA-C*
6	31600001	31700001	4.73096	*ABHD16A, APOM, BAG6, C6orf25, C6orf47, CLIC1, CSNK2B, DDAH2, GPANK1, LY6G5B, LY6G5C, LY6G6C, LY6G6D, LY6G6E, LY6G6F, PRRC2A*
6	32700001	32800001	4.55939	*HLA-DOB, HLA-DQB1, TAP2, HLA-DQB2, HLA-DQBA2, MIR3135B*
1	167600001	167700001	4.52777	*RCSD1, MPZL1*
15	36800001	36900001	4.24381	*C15orf41, MIR4510*
17	14100001	14200001	4.22943	*COX10, CDRT15, HS3ST3B*
9	135300001	135400001	4.20053	*C9orf171*
6	32100001	32200001	4.19692	*GPSM3, FKBPL, NOTCH4, PPT2, LOC100507547, AGPAT1, RNF5, AGER, PRRT1, EGFL8, PBX2, PPT2-EGFL8, C6orf10, RNF5P1*
14	33700001	33800001	4.19607	*NPAS3*
11	2300001	2400001	4.16304	*ASCL2, C11orf21, TSPAN32, CD81-AS1*
22	44700001	44800001	4.15783	*KIAA1644, LOC101927526*
20	16700001	16800001	4.15236	*PCSK2, OTOR, KIF16B, SNRPB2,*
5	176000001	176100001	4.07706	*CDHR2, EIF4E1B, GPRIN1, SNCB, TSPAN17, LOC102577424*
6	32200001	32300001	4.01502	*C6orf10, NOTCH4*
16	79000001	79100001	4.00968	*WWOX*
6	31000001	31100001	3.93041	*HCG22, MUC22, C6orf15, PSORS1C1, CDSN*
6	32300001	32400001	3.92154	*C6orf10, HCG23, BTNL2, HLA-DRA*
2	800001	900001	3.88501	*LINC01115, LOC101060385.*
1	15300001	15400001	3.86271	*KAZN*
8	28100001	28200001	3.85515	*PNOC, ELP3*
11	2200001	2300001	3.84415	*MIR4686, ASCL2*
11	6500001	6600001	3.84202	*DNHD1, ARFIP2, TIMM10B*
18	77100001	77200001	3.83102	*ATP9B, NFATC1*
17	1300001	1400001	3.77107	*CRK, YWHAE, MYO1C, INPP5K*
6	32500001	32600001	3.76159	*HLA-DRB1, HLA-DRB5, HLA-DRB6, HLA-DQA1*

Figure 2.1: Top SNPs for XP-nSL and LSBL.

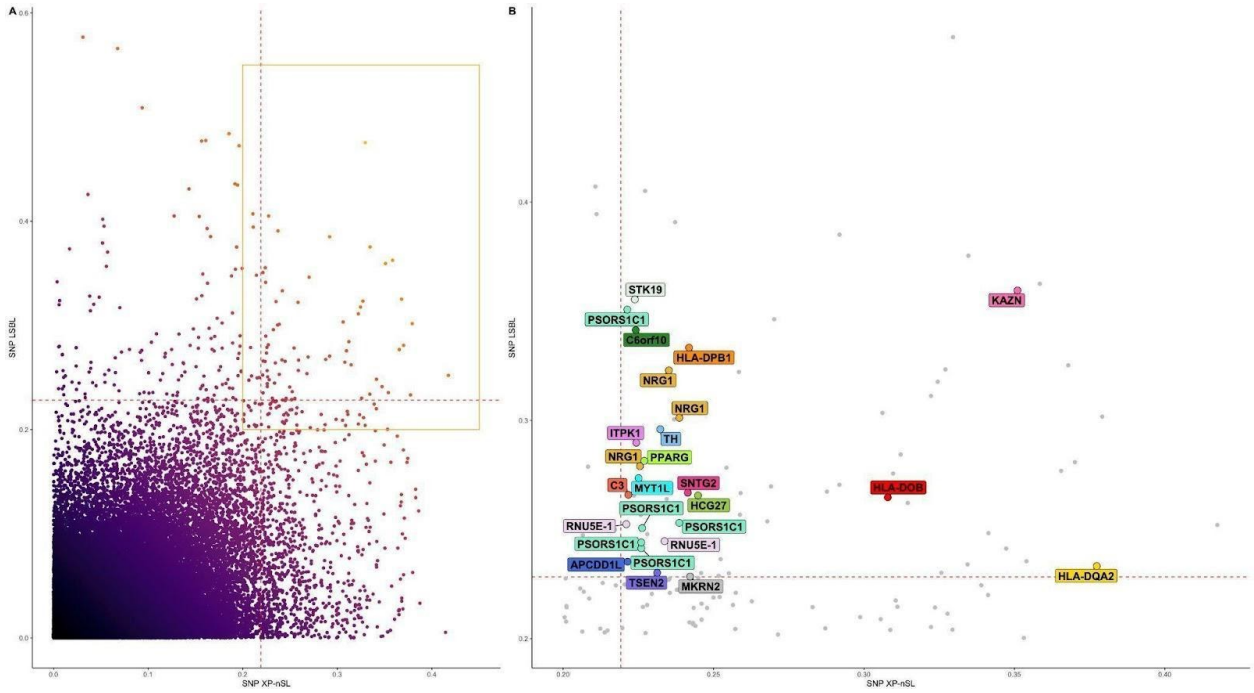

This study detected 26 SNPs that were statistical outliers for both XP-nSL and LSBL. Both graphs represent the relationship of haplotype scores (XP-nSL, X-axis) and branch lengths (LSBL, Y-axis). Dashed lines represent the 0.995 significance cutoff for respective tests. Each dot represents a SNP. In Panel A, the color of each dot represents the mean of branch length estimate and haplotype score at that locus. Panel A represents the LSBL:XP-nSL ratio for all positive scoring SNPs, and the orange box corresponds to the top SNPs illustrated in Panel B. Panel B represents statistically significant SNPs for both tests that overlap with protein-coding regions of genes. Colors of SNPs in Panel B correspond to gene symbols, with which the SNPs are labeled. SNPs that are unlabeled were intergenic variants.

Figure 2.2: Sweep region around the HSPA12A locus

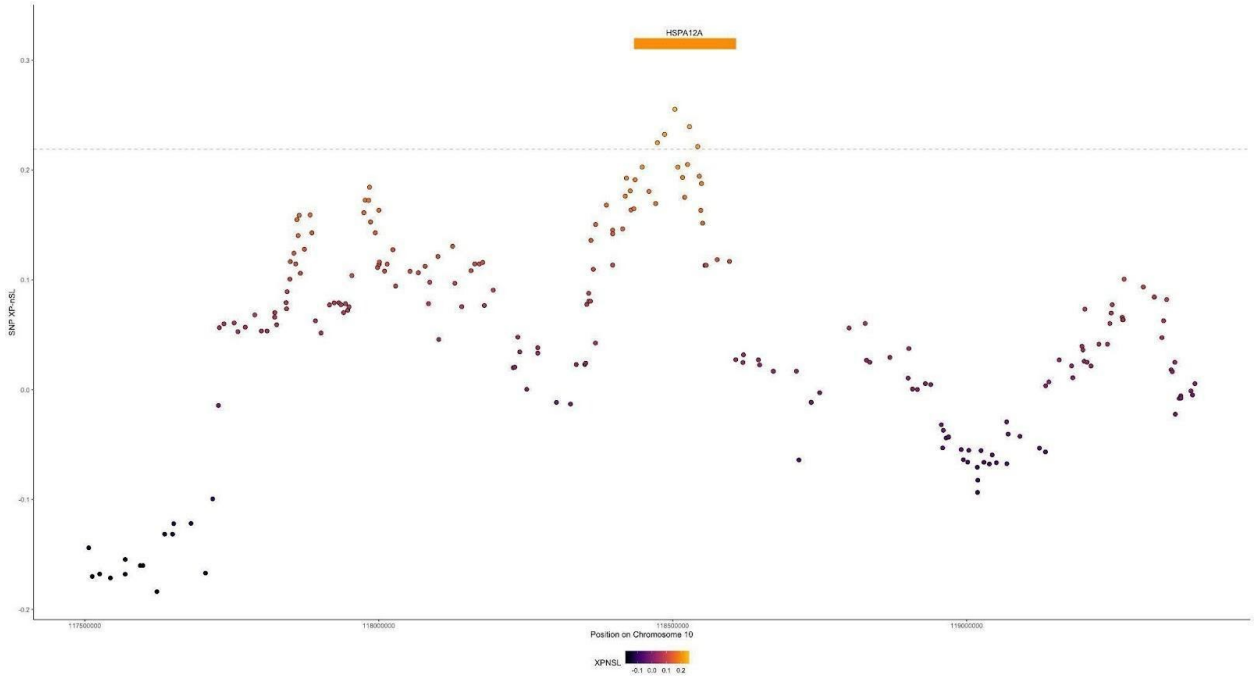

Each dot represents a SNP. Position on the X axis corresponds to chromosomal position, and position along the Y axis represents SNP-based XP-nSL. Dashed line indicates genome-wide significance cutoff for XP-nSL values at the 99.5% level. Horizontal bar represents the location of *HSP12A* within the genomic window.

Figure 2.3: Sweep region centered on BAG6

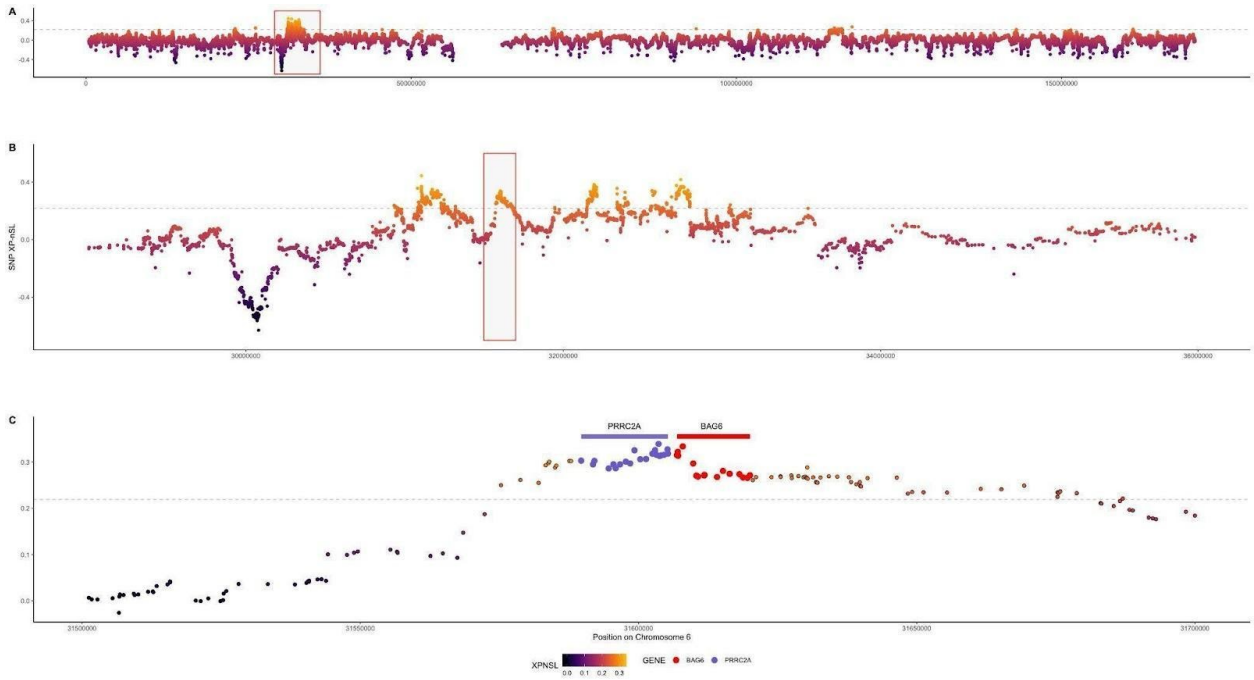

Each dot represents a SNP. The color of each dot corresponds to adjusted XP-nSL values for their window. Position on the X axis corresponds to chromosomal position, and position along the Y axis represents SNP-based XP-nSL. Dashed grey line indicates genome-wide significance cutoff for XP-nSL at the 99.5% level. Red boxes indicate "zoom" regions for subsequent panels. Panel A represents the exceptionally high XP-nSL values in the sweep region of Chromosome 6. Panel B represents the location of BAG6 within the larger sweep region. Panel C represents the XP-nSL scores for protein-coding variants within *BAG6*.

Figure 2.4: Sweep region encompassing the DUOX gene family.

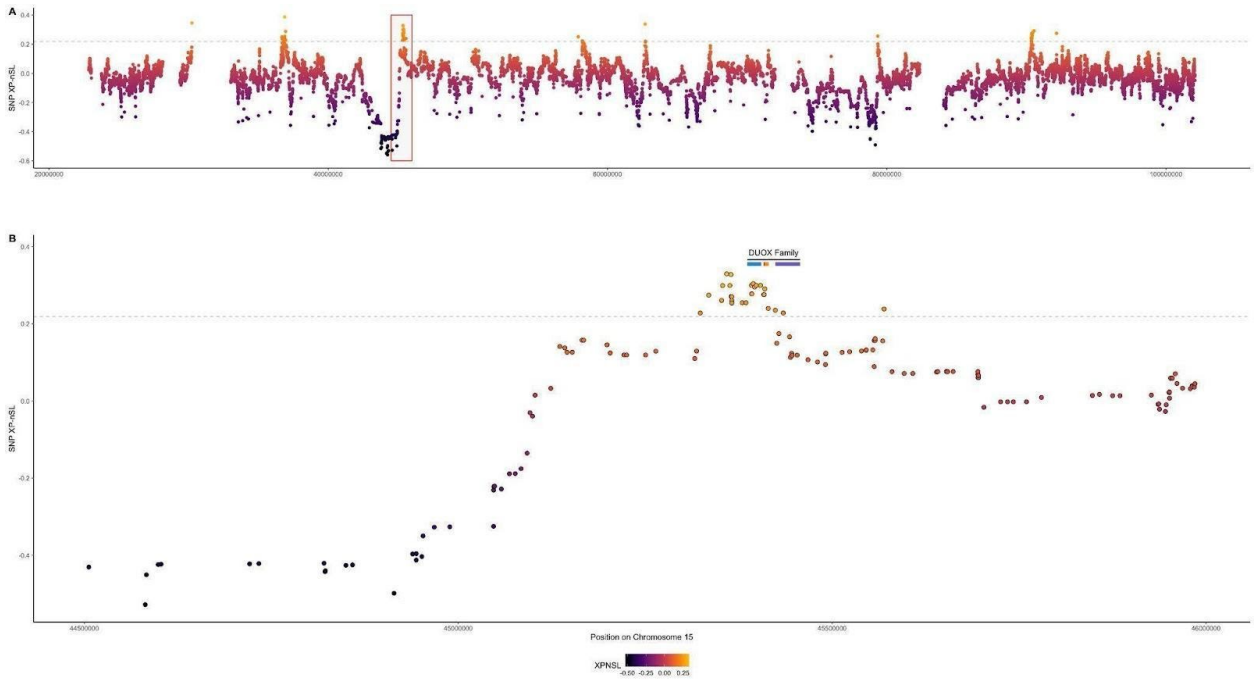

Sweep region encompassing the DUOX family of genes. Each dot represents a SNP. The color of each dot corresponds to XP-nSL values scaled for SNPs represented in the plot. Position on the X axis corresponds to chromosomal position, and position along the Y axis represents SNP-based XP-nSL. Dashed grey line indicates genome-wide significance cutoff for XP-nSL at the 99.5% level. Red boxes indicate "zoom" regions for subsequent panels. Panel A represents the exceptionally high XP-nSL values in the sweep region of Chromosome 15. Panel B represents the location of the DUOX family of genes within the sweep region, represented by a horizontal bar above the XP-nSL plateau.

Figure 2.5: Pairwise differences in SNP frequencies with DUOX.

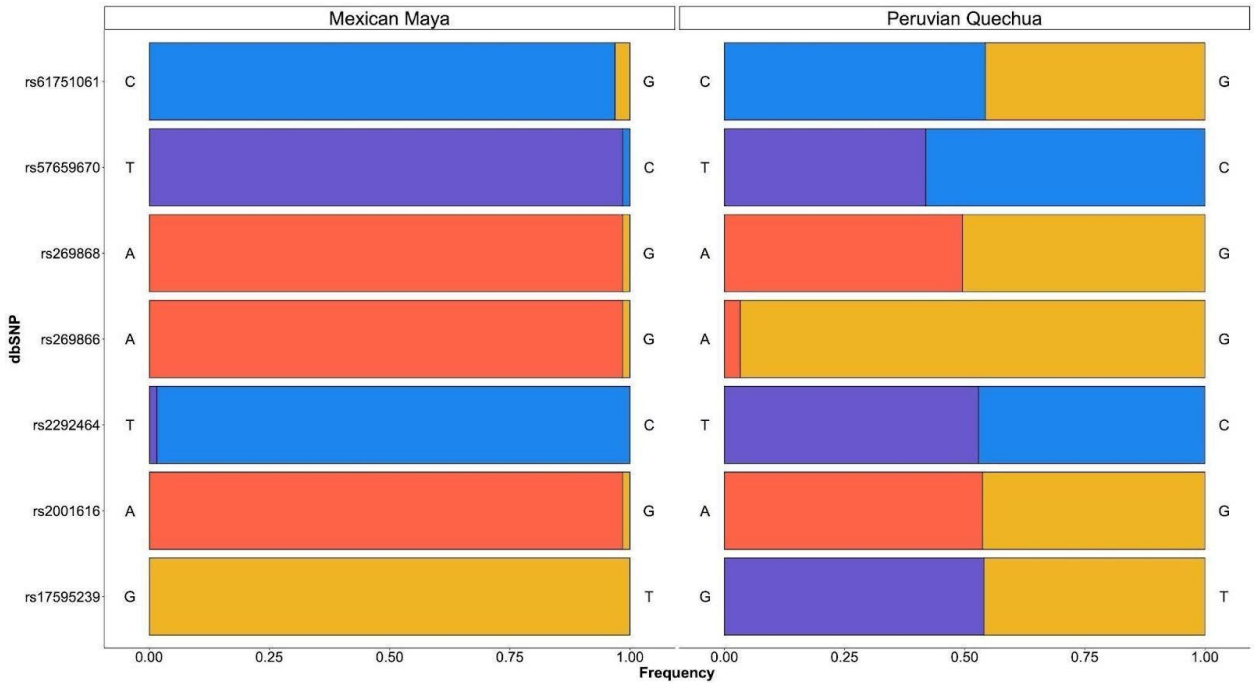

Each row represents the frequency of one of two variants for each SNP; colors and letters correspond to bases at a given position. X axis indicates frequency. Y axis represents each SNP. See Supplementary Figure 3 for global distribution of SNP frequencies.

Table 2.4: (Supplemental Table 1) Putatively adaptive genes found in the top 0.1% of scores.

Test(s)	Gene	Adaptation	Response	Pathway
SNP XP-nSL, Window XP-nSL	*BAG6*	Thermoregulation	Heat Response	Heat shock protein binding (GO:0030544)
SNP XP-nSL	*DUOX2*	Thermoregulation	Thyroid Regulation/Generation	Thyroid hormone generation (GO:0006590)
SNP LSBL	*BDKRB2*	Thermoregulation	Vasodilation	Vasodilation (GO:0042311)
SNP LSBL	*NRG1*	Thermoregulation	MAPK Signaling	MAPK Signaling (R-HSA-5683057)
SNP XP-nSL	*NEDD4L*	Water/Salt Balance	Water Homeostasis	Water homeostasis (GO:0030104)
SNP XP-nSL	*PSORS1C1*	Pathogens/Parasites	Superficial wound healing?	--
SNP XP-nSL	*PSORS1C2*	Pathogens/Parasites	Superficial wound healing?	--
SNP XP-nSL	*HLA-DOB*	Pathogens	Antigen response	MHC class II antigen presentation (R-HSA-2132295)
SNP XP-nSL	*HLA-DQA2*	Pathogens	Antigen response	MHC class II antigen presentation (R-HSA-2132295)
SNP XP-nSL	*HLA-DQB2*	Pathogens	Antigen response	MHC class II antigen presentation (R-HSA-2132295)

Table 2.5: (Supplemental Table 2): DUOX-family SNPs under selection in Mexican Mayans

Gene	dbSNP	Previous Studies	Mexico XP-nSL	Mexico LSBL	Freq Mexico	Freq Peru
DUOX2	rs269868	Jacovas et al. 2018	0.29947	0.0329	0.0154	0.4473
DUOX2	rs269866	Jacovas et al. 2018	0.30423	0.0789	0.0154	0.4944
DUOX2	rs57659670	Jacovas et al. 2018; Borda et al. 2020	0.29939	0.0221	0.0154	0.4384
DUOX2	rs2001616	Borda et al. 2020	0.29951	0.0933	0.0154	0.4426
DUOXA1	rs61751061	Borda et al. 2020	0.29069	0.0004	0.0308	0.4528

Figure 2.6 (Supplemental Figure 1A): Results of Population Structure Analysis

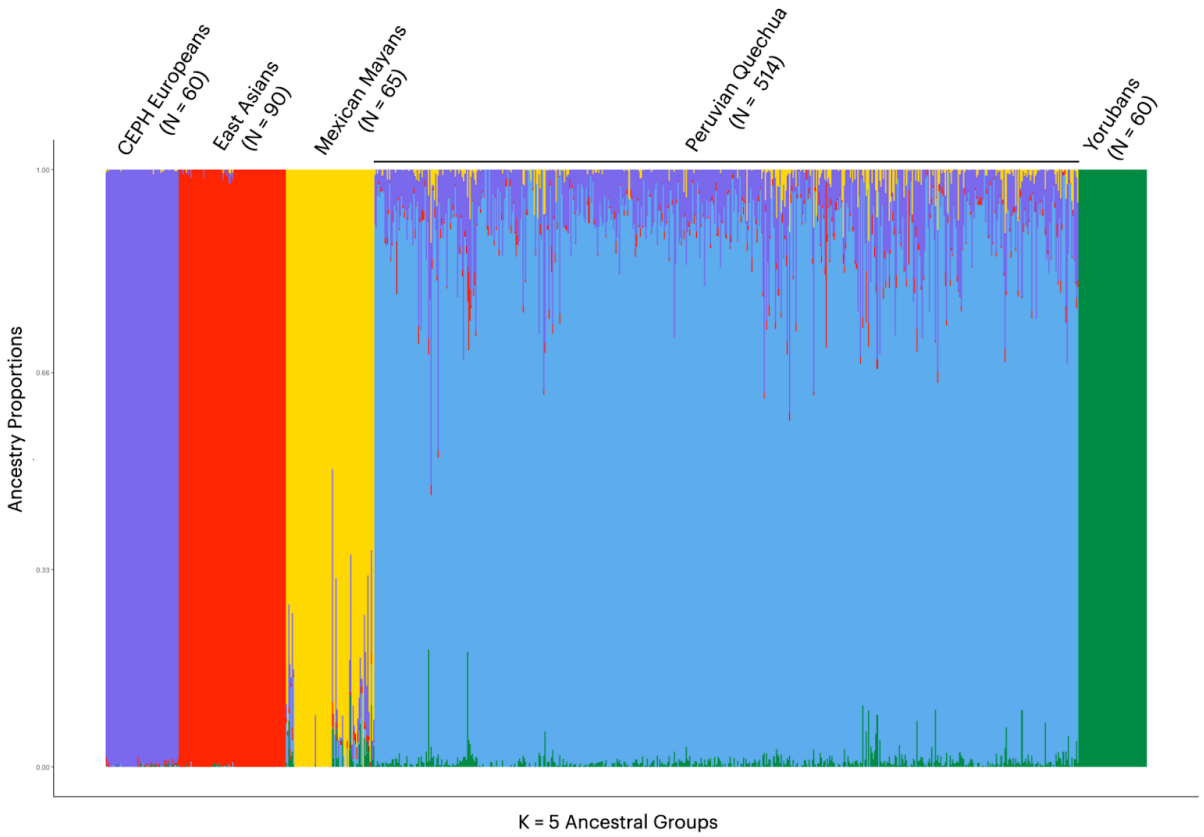

Results of ADMIXTURE analysis. Each vertical bar represents one individual, and the proportions of colors within bars correspond to the amount of ancestry (ancestry proportions) for K = 5 ancestral groups. Purple indicates ancestry similar to CEPH Europeans. Red corresponds with inferred East Asian ancestry. Gold indicates Mexican Mayan ancestry. Blue indicates Peruvian Quechua ancestry. Green indicates ancestry similar to Yoruban Africans.

Figure 2.7 (Supplemental Figure 1B): Results of Population Structure Analysis

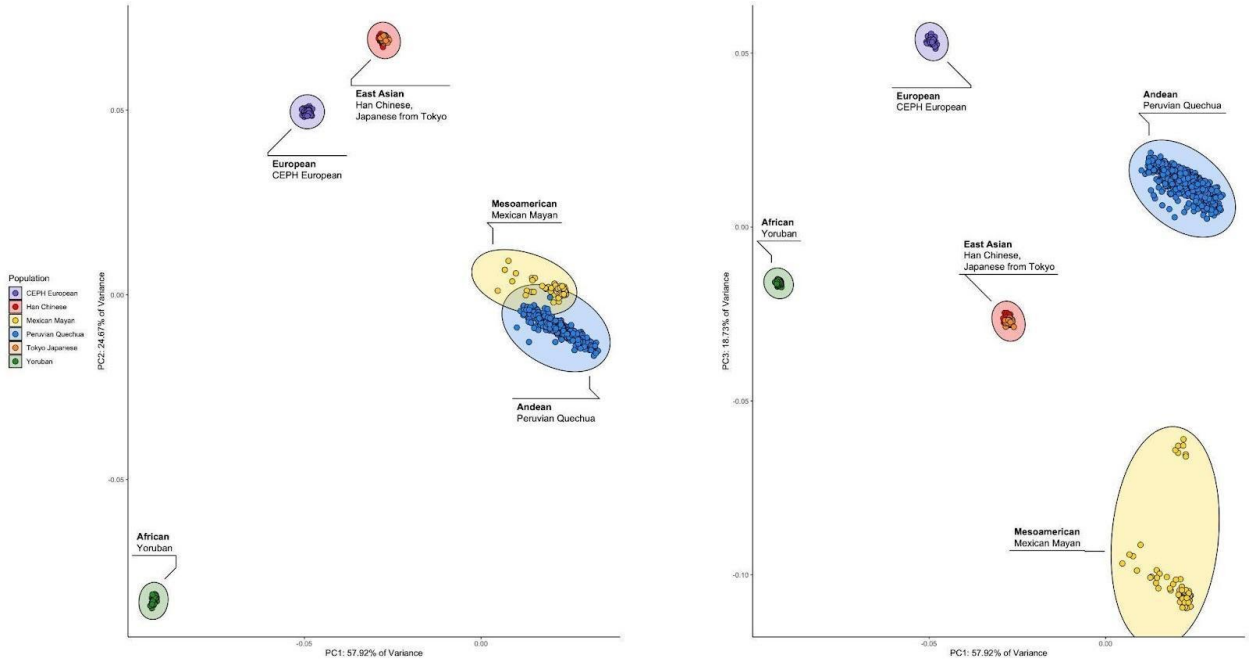

PCA was used to detect population structure and individuals with high levels of admixed ancestry. Each dot represents an individual. Ellipses indicate 95% CI for population clusters. Colors correspond to populations. The X axis of each graph represents the PC1 score, which accounted for 57.92% of variance. Left Panel: PC1 plotted against PC2, which accounted for 24.67% of variance. Right Panel: PC1 plotted against PC2, which account for 18.73% of variance.

Figure 2.8 (Supplemental Figure 2): Histogram showing empirical distribution of locus-specific branch length values

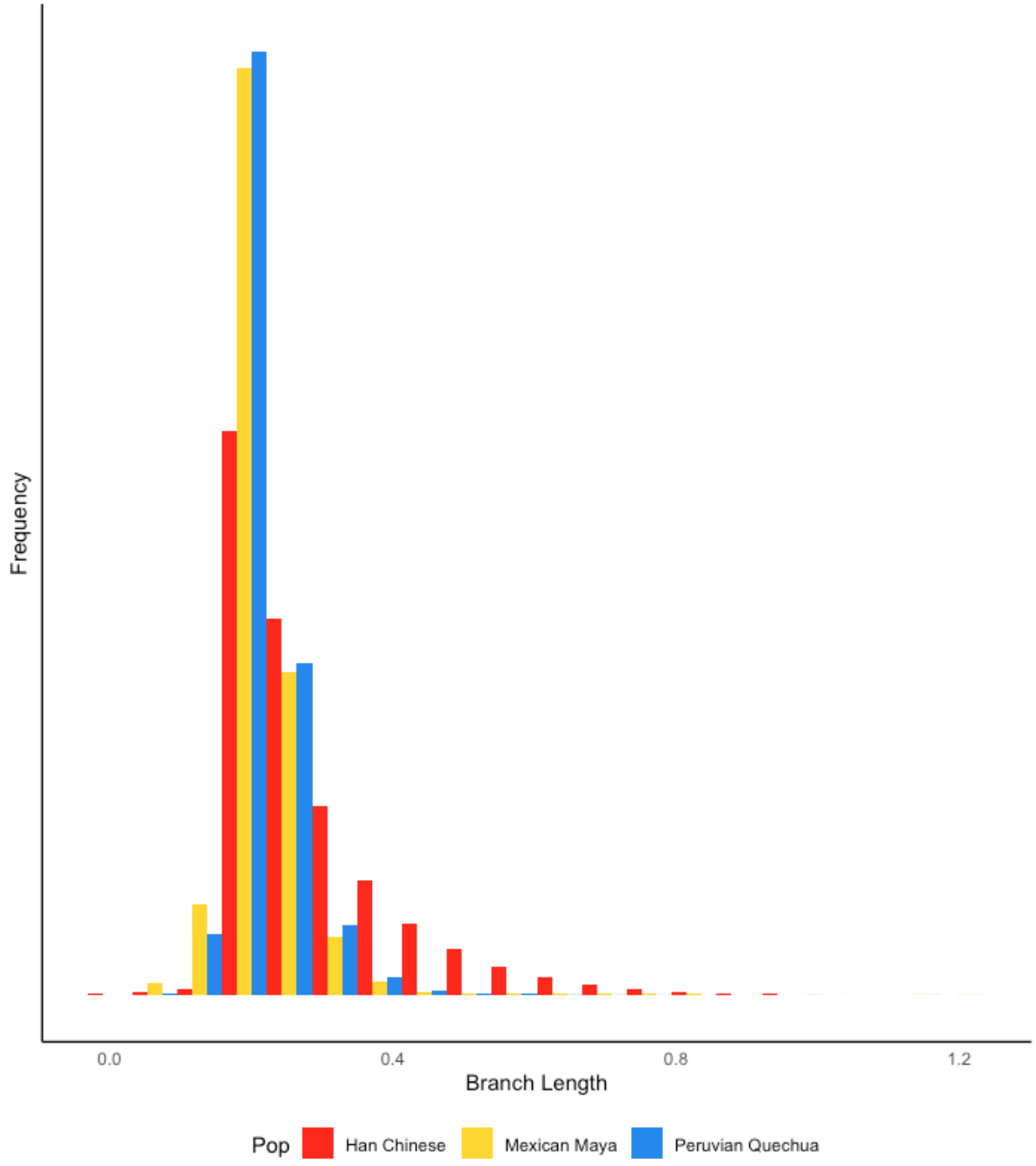

Frequency distribution of SNP-based LSBL scores for Han Chinese (red), Mexican Mayans (yellow), and Peruvian Quechua (blue). For graphical purposes, branch length estimates were rescaled to positive integers following Shriver et al. (2004).

Figure 2.9 (Supplemental Figure 3): Global SNP frequencies for variants within the DUOX family

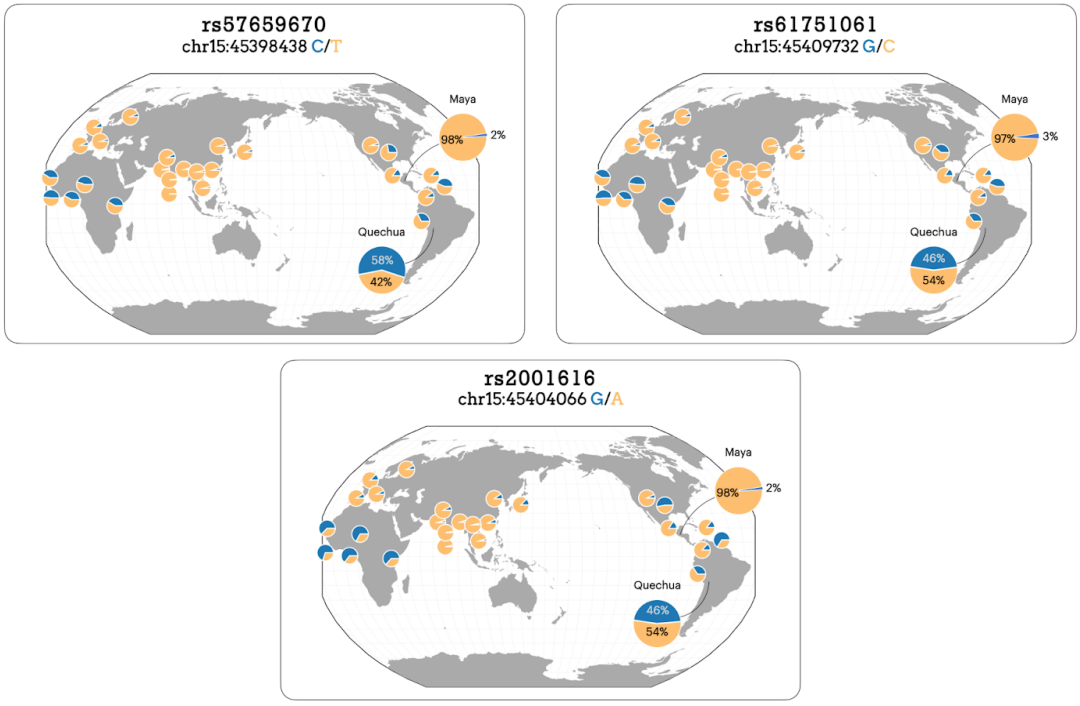

Base maps generated using GGV (Marcus and Novembre 2016).

Chapter 3 Genetic Evidence of Cold Climate Adaptation in High-Altitude Peruvian Quechua

3.1 Cold Adaptation and Human Evolution

Throughout human history, the processes of migration and dispersal have brought human populations into contact with unfamiliar and often hostile landscapes (Jeong and DiRienzo 2014). One of the leading drivers of local adaptation is the burden of thermal stress, and evidence of niche-specific evolution can be gleaned from genome data derived from humans inhabiting cold climate extremes (Fumagalli et al. 2015, Hsieh et al. 2017, Racimo et al. 2017). However, little attention has been paid to putative cold climate adaptations among populations of high altitude and in the context of the global south.

High altitude is one of the most hostile environments to human survival (Gallagher and Hackett 2004, Wickens et al. 2015). The thin atmosphere of elevation has low oxygen availability relative to sea level and freezing night time temperatures, which together create a significant physiological burden: for every 1000m gained in altitude, temperature will plummet roughly 6.5° Celsius; over this interval, the proportion of available oxygen relative to sea level decreases at a rate of ~5% (Minder et al. 2010, Fehren-Schmitz et al. 2017; Supplementary Figure 1). This makes high altitude environments substantially colder, and more harsh, than lowland habitats found at similar latitudes. Despite these clear obstacles to reproductive fitness, some 82 million people live at altitudes exceeding 2500 meters above sea level (Tremblay and Ainslie 2021). In particular, there are three regions of the planet with exceptionally long occupation histories in which humans have adapted to high-altitude (Figure 1): the Ethiopian

Highlands, the Qinghai-Tibetan Plateau, and the Andean Altiplano, the latter of which has been inhabited for some 10,000 years (Beall et al. 1998; 2002; Rademaker et al. 2014). Like other high altitude populations, Andean highlanders show evidence of particularly strong selection on genes that offset the effects of hypoxia (Bigham et al. 2009, 2010; Brutsaert et al. 2019). While evolutionary responses to low oxygen availability retain much of the focus in discussions about altitude adaptation, there are other environmental stressors that similarly correspond to increases in elevation.

The interactive effects of cold exposure and hypoxia are potentially a significant driver of natural selection. During cold exposure, humans undergo a series of physiological changes including peripheral vasoconstriction, increases in blood pressure, shivering, and increased total energy expenditure (Granberg 1990, Gordon et al. 2009, Ouellet et al. 2012, Ocobock 2016). Interestingly, hypoxia is known to inhibit shivering responses during cold exposure, increase respiratory heat loss during hyperventilation, accelerate the rate of core cooling, and lead to an overall reduction body core temperature compared to normoxic conditions (Kottke et al. 1947, Johnston et al. 1996, Simmons et al. 2010). Additively, the effects of low ambient temperature and low oxygen availability are a significant burden to humans living in high altitude (Beall 2006, 2014).

Given the reduced concentrations of vapors and aerosols at extreme elevations, high altitude environments in the Andes also have the highest levels of ultraviolet radiation (UVR) detected on the planet (Cabrol et al. 2014). Increased UVR exposure leads to DNA damage and is a risk factor for skin cancer, yet the human body's ability to synthesize vitamin D_3 is driven largely by UV stimulus (D'Orazio et al. 2013). In humans, natural selection has shaped variation in skin color phenotypes corresponding with UVR levels at the earth's surface: in particular,

populations experiencing high levels of UV have relatively higher melanin production whereas populations from regions with low UV have evolved depigmented skin (Jablonski and Chaplin 2010, 2017).

Despite the combined environmental stressors of low oxygen availability, extreme levels of UV radiation, and year-round nighttime temperatures below freezing, the high Andes have been occupied since the late Pleistocene (Åkesson et al. 2019, Fehren-Schmitz et al. 2017). While there is ample evidence that Andeans have undergone selection to offset altitude-induced hypoxia, it is unclear whether or not they have evolutionary adaptations to the cold (Bigham et al. 2010, Crawford et al. 2017, Brutsaert et al. 2019). Historical studies of cold acclimatization among Andean highlanders suggest that they offset the stress of low ambient temperature by increasing their metabolic output and warming their peripheries; however, it is unclear whether these physiological responses are the result of phenotypic plasticity, epigenetics, or recent selection (Baker 1963, Mazess and Larson 1972). Similarly, while there is apparent selection on genes that respond to UV and cold stress, it is unclear whether selective sweeps have acted upon photoprotective phenotypes in these altitude-adapted populations.

It is likely that Andean populations have adapted to this entire set of environmental challenges of high altitude. Given the energetic cost of surviving in low ambient temperatures, and considering that hypoxia inhibits thermoregulatory responses, it is possible that selection acts on genes regulating body temperature homeostasis, as seen in cold adapted populations from the far north (Cardona et al. 2014, Fumagalli et al. 2015). One might expect to find evidence of recent selective sweeps in genomic regions associated with vasoconstrictive/vasodilatory responses to low temperature, or cold-induced thermogenesis mediated by brown fat (Devlin 2015).

In high latitude or high altitude environments, humans wear protective coverings over much of their bodies as a way of protecting against cold and high winds. Given that the face traditionally is the only uncovered (i.e., solar-exposed) part of the body, it is possible that UVR would disproportionately damage the eyes (van Kujik 1991). Over an individual's lifetime, this could cause cataracts, macular degeneration, and acute photokeratitis (i.e., snow blindness) (Taylor 1989). The poor growing environment (e.g., low temperature, freezing soil) at extreme altitude of Tibet, along with wearing skin coverings year-round, led to selection on the *VDR* gene (Hu et al. 2017). *VDR* is a gene related to vitamin D protein binding, but it is uncertain whether this changes vitamin D levels in Tibetans. However, variants with *VDR* show a strong cline in variant frequency with distance from Africa (e.g., rs10946808) suggesting that it might be related to lowered vitamin D found at distance from the tropics (Ramagopalan et al. 2010). Considering the low levels of vitamin D observed in some Andean children, it is possible that natural selection on genes related to vitamin D binding helps to offset the effects of hypovitaminosis D (Terán et al. 2018).

To test the hypothesis that Andean populations have adapted to the suite of ecological stressors of high altitude (a cold, dry, hypoxic environment with high UV), SNP data for a cohort of 514 Indigenous Peruvian Quechua participants were examined for signals of recent evolutionary change. These results cast light on how humans successfully adapt to novel, local environments over relatively short timescales, which in turn is informative for the broader story of how human ancestors were able to disperse from temperate lowlands in Africa into ecologically-diverse environments across Eurasia and beyond. Furthermore, this represents an interesting case study into human evolutionary change in that observers have a high degree of certainty regarding the chronology for human settlement in Central and South America: this

means that results can be anchored in relatively broad population divergence dates (e.g., Eurasians versus Indigenous Americans), informing us about the speed of diversification and adaptation among related groups. In the context of high altitude, these results would be critical for understanding how humans can protect against cold exposure, the burden of which is significantly enhanced by low oxygen availability (Johnston et al. 1996, Simmons et al. 2010). Furthermore, as climate change leads to significant ozone depletion and an increase in UVR levels reaching the earth's surface, it will be important to understand how the human body responds to ultraviolet stress at both cellular and genomic levels (Barnes et al. 2019).

3.2 Materials and Methods

3.2.1 Participant Recruitment

This study's participants consisted of 603 self-identified individuals of Indigenous Quechua ancestry. Of these, 301 individuals were born at high altitude and were recruited in Cerro de Pasco, a town located 4,338 meters above sea level (mASL). The remaining participants were recruited at sea level (i.e., 0 mASL) in Lima, Peru. One subset of participants recruited at 0 mASL consisted of 152 individuals born at high altitude, but who migrated permanently to sea level; the remaining 150 individuals consisted of self-identified Quechua born at sea level. The final dataset was 36% female, and consisted of healthy, unrelated adults between the ages of 18 and 35 (mean age of 24.57 ± 5). At the time of recruitment, all study participants provided written informed consent. This was approved by the Institutional Review Boards of the University of Michigan and Universidad Peruana Cayetano Heredia.

Given their genetic proximity to populations from the Andes, Mexican Mayans were used as a comparative sample for haplotype-based tests of selection (i.e., XP-nSL). The Mexican

Mayan dataset consisted of 65 individuals from the Tzeltal, Tzotil, or Ch'ol-speaking communities in Palenque, Chiapas, Mexico, who were sequenced by the Bigham Laboratory at the University of Michigan. Using SNP data derived from Indigenous Central Americans offsets the strong founder effect experienced during the settlement of the Western Hemisphere (Amorim et al. 2017).

For locus-specific branch lengths estimates, SNP frequencies were calculated for Peruvian Quechua, Mexican Mayans, and 45 Han Chinese from Beijing. Han Chinese individuals were chosen as an outgroup for this study because they represent an East Asian outgroup that models recent common ancestry for Indigenous American populations. For ADMIXTURE analysis, the Peruvian Quechua and Mexican Mayan datasets were merged with SNP data from 60 Yorubans, 45 Han Chinese from Beijing, 45 Japanese from Tokyo, and 60 individuals of north-central European ancestry from the Centre d'Etude du Polymorphisme Humain (CEPH): these SNP data come from the HapMap dataset and are used to detect recent gene flow and to filter individuals with an excess of recent European or African ancestry.

3.2.2 Haplotype-Based Test of Selection with XP-nSL

Calculating the number of segregating loci across populations (XP-nSL) is a method of detecting genetic variation among haplotypes determined by past evolutionary change in the form of selective sweeps (Ferrer-Admetlla et al. 2014, Szpiech et al. 2021).

Consider a locus k with either an ancestral ($A(k)$) or derived ($D(k)$) set of haplotypes, and let the value $n_A(k) = |A(k)|$ and the value $n_D(k) = |D(k)|$. The number of consecutive, uninterrupted sites at which a haplotypes i and j are identical-by-state (IBS) can be defined as

$L_{ij}(k)$ for a given genomic region or locus about k. The number of segregating sites per locus (nSL proper) for site k can be calculated as:

$$nS_L(k) = log\frac{SL_A(k)}{SL_D(k)}$$

Where:

$$SL_A(k) = \left(n_{A\ \ 2}(k)\ \right)^{-1}\Sigma_{i<J\in A(k)}L_{ij}(k), \text{ and}$$

$$SL_D(k) = \left(n_{D_2}(k)\ \right)^{-1}\Sigma_{i<J\in D(k)}L_{ij}(k)$$

From this, $SL_A(k)$ and $SL_D(k)$ represent the mean value of $L_{ij}(k)$ over all possible haplotype dyads, each of which represents either the derived or ancestral condition for a given locus k within a particular population. XP-nSL (cross-population nSL) expands this test to population pairs: instead of investigating pairwise ancestral/derived allele sets, XP-nSL compares sets of haplotypes between a "reference" and "target" population (Szpiech et al. 2021).

If $P_1(k)$ and $P_2(k)$ represent haplotype pairs about site k in populations P1 and P2 respectively, let $n_{P1}(k) = |P_1(k)|$ and the value $n_{P2}(k) = |P_2(k)|$. Then:

$$XPnS_L\ (k) = log\frac{SL_{P1}(k)}{SL_{P2}(k)}$$

$$SL_{P1}(k) = \left(n_{P1}(k)\ \right)^{-1}\Sigma_{i<J\in P1(k)}L_{ij}(k), \text{ and}$$

$$SL_{P2}(k) = \left(n_{P2}(k)\ \right)^{-1}\Sigma_{i<J\in P2(k)}L_{ij}(k).$$

This means that SL_{P1} and SL_{P2} represent their respective averages for $Lij(k)$, or the number of consecutive loci along a genomic region in which the haplotypes i and j are identical over all possible haplotype pairs within each population. Positive XP-nSL values represent a selective sweep in the "target" population (here, Peruvian Quechua), and negative XP-nSL values

represent selection in the reference population. Here we used data from 65 Mexican Maya as the reference population. Sweep regions can be identified as a span of XP-nSL values increasing in frequency such that they create a peak above the putative selected locus, and a high number of consecutive peaks indicate particularly strong selection over a given haplotype.

XP-nSL requires phased genotype data with no missingness (i.e., only using SNPs at which 100% of individuals are represented). Genotype data were phased using SHAPEIT 4.2 (Delaneau et al. 2019). Any site with missingness was removed using Plink 1.9. The phased genotype data were used to calculate XP-nSL in SelScan (Szpiech and Hernandez 2014). XP-nSL values were calculated for each SNP, and then normalized in non-overlapping 100kb windows using SelScan's ancillary program, Norm (Szpiech et al. 2021). SNPs with negative XP-nSL values were removed from the analysis as they indicated selection occurring in the reference population (here, Mexican Maya). The resulting data files were merged in Python. SNP-based and windowed XP-nSL scores were calculated in R using the *quantile*() function, which generates sample quantiles for a given probability. Windows and SNPs were considered significant if they fell within the top 0.5% of their respective distributions.

3.2.3 Population Divergence with Locus-Specific Branch Length Estimates

Locus-Specific Branch Length (LSBL) is a test that identifies statistical differences in SNP frequencies between three population dyads (Shriver et al. 2004, Mattiangeli et al. 2006). The utility of LSBL is that it allows an observer to identify SNPs that are highly-differentiated between three related populations. Highly-differentiated SNPs, represented as long branches at a given locus, indicate evolutionary divergence of one population from the others (Figure 2).

LSBL is derived from F_{ST} , a measure of population differentiation, which was developed by Wright, to describe the level of heterozygosity expected for a population at a given locus

(Wright 1950). If the symbol $\underline{p}$ represents the mean frequency of a given allele p for a total population; σ^2_S represents the variance in allele frequency between subpopulations (*S*) weighted by their respective sizes; and σ^2_T denotes the variance of in the total population (*T*), F_{ST} can be defined as:

$$F_{ST} = \frac{\sigma_S^2}{\sigma_T^2} = \frac{\sigma_S^2}{\bar{p}\,(1 - \bar{p}\,)}$$

Given the size of human populations, exact allele (or SNP) frequencies often cannot be measured and thus estimators such as that of Weir and Cockerham are used (Weir and Cockerham 1984) . Weir and Cockerham's estimator θ calculates F_{ST} for population dyads and weighs these by the ratio of population sizes denoted by the symbol *M*. Where $F_{ST:A}$ represents the F_{ST} value for population *A;* and $F_{ST:B}$ represents the value for population *B*; Weir and Cockerham's θ for the population dyad A:B can be calculated as:

$$\theta_{A:B} = \frac{(F_{ST:A} + F_{ST:B})}{\left(F_{ST:A} + F_{ST:B} + 2\frac{1}{(M+1)}[M(1 - F_{ST:A}) + (1 - F_{ST:B})]\right)}$$

Once Weir and Cockerham's θ has been calculated for three population pairs (i.e., $\theta_{A:B}$, $\theta_{B:C}$, and $\theta_{A:C}$) for loci across the genome, LSBL estimates can be produced as follows.

$$LSBL_A = \frac{\theta_{A:B} + \theta_{A:C} - \theta_{B:C}}{2}$$

The resulting values thus represent the amount of differentiation for a target population relative to two outgroups. These LSBL values can then be placed into an empirical distribution in

order to identify the SNPs with the greatest estimated branch lengths (i.e., greatest statistical distances) that exceed a predetermined genome-wide significance level.

Using SNP data from unrelated individuals with minimal recent Eurasian ancestry, I generated LSBL estimates for Quechua, Maya, and Han Chinese. For each population dyad (Maya:Quechua, Han:Maya, Han:Quechua), Weir and Cockerham's θ (WCθ) was calculated using the *--weir-pop-fst* function in VCFTools (Danecek et al. 2011). WCθ was produced for each SNP and again for 100kb sliding window with 50kb steps. The resulting pairwise WCθ values were merged in Python. The final step for LSBL ($i.e.,\ (\theta_{A:B}\ +\ \theta_{A:C}\ -\theta_{B:C})/2$) was calculated in R.

Significance levels for windowed and SNP-based LSBL were calculated in R using the *quantile*() function (R Core Team 2021). LSBL values were identified as statistical outliers if they surpassed α = 0.005.

3.2.4 Gene Ontology, Protein Interactions, and Pathway Analysis

SNPs surpassing the significance threshold for XP-nSL and LSBL (both SNP-based and window-based) were filtered in R, and exported for annotation using Affymetrix's NetAffx database (https://www.affymetrix.com). SNP and gene lists were compiled and used to identify functional variants under selection.

Gene Ontology (GO) Knowledgebase is an online database of gene functions spanning a variety of taxa and biological processes (http://geneontology.org/). GO was queried using keywords "cold", "thermogenesis", "UV radiation", "pigmentation", "heat", and "hypoxia". The resulting gene list was downloaded and merged in Python. This dataset was then cross-referenced with the candidates detected in the selection scan.

To identify potential interactions between genes and proteins, candidate lists were submitted to Reactome (www.reactome.org), an online pathway browser, and the Interactome Atlas, a product of the Human Reference Protein Interactome (HuRI) Mapping Project (http://www.interactome-atlas.org).

3.3 Quality Control and Population Structure

SNP data were generated for 603 individuals of Quechua ancestry. To ensure that relatedness did not skew the results of selection scans, King analysis was performed in Plink to filter any individuals with high levels of relatedness. If two individuals were closer than the 4th degree of relatedness, or with the proportion of genome that is identical by descent (IBD) greater than or equal to 0.0442, the individual with a lower genotyping rate was removed. After removing related participants, a total of 579 Quechua individuals remained. These individuals had SNP data across 628,679 SNPs passing Affy's Best Practices. Plink was used to remove 19,096 variants with genotyping rates lower than 95%, and 376,199 that did not meet the minimum threshold for minor allele frequency of 2.5%.

To analyze population structure and identify admixture, the Peruvian Quechua dataset was merged with SNP data from 65 Mexican Mayans, as well as publicly available data from 60 Yorubans, 45 Han Chinese from Beijing, 45 Japanese from Tokyo, and 60 individuals of north-central European ancestry from the Centre d'Etude du Polymorphisme Humain (CEPH). A total of 29,495 linked SNPs ($r^2 > 0.8$) were pruned out of the dataset in Plink 1.9. Ancestry proportions were calculated in ADMIXTURE using the remaining 352,833 variants (Figure 3A). Different numbers of ancestral groups (K = 1 through 9) were calculated, and the model with the lowest cross-validation error was K = 5 groups. Given the close genetic affinity between

Indigenous American populations, a pooled Indigenous American ancestry component was produced for each individual: this was calculated as the sum of Mexican Mayan-like and Peruvian Quechua-like ancestry components. Sixty-five individuals had less than 80% pooled Indigenous American ancestry and high amounts of either European or African ancestry, and thus were filtered out of the dataset (Figure 3A). With the resulting 514 individuals, PCA was conducted to identify additional admixture and population structure (Figure 3B). PCA revealed that Mexican Mayans and Peruvians plot alongside one another, creating a pan-Indigenous American cluster to the exclusion of other global populations. The first PC accounts for 57.92% of the variation in ancestry, whereas the second PC accounts for 24.67%.

3.4 Results of Selection Scan in Peruvian Quechua

Our selection scan was performed on 514 Peruvian Quechua study participants using two tests of natural selection: LSBL and XP-nSL. LSBL, an allele frequency based test, and XP-nSL, a haplotype-based test of selection, allowed us to leverage orthogonal data types to identify putatively-selected regions of the genome. The LSBL analysis was performed on 220,175 variants. Peruvian Quechua LSBL values ranged from weakly-negative values (indicating differences in observed gene diversity and expected heterozygosity) to branch lengths of 0.8492. Positive branch lengths indicate local evolutionary divergence, and these were considered significant at the 0.5% level if they were greater than or equal to 0.2094. Windows were considered significant if their LSBL values were greater than or equal to 0.1596. There were 1,085 variants with scores greater than 0.2094. Of these, 632 overlapped with genes known to the NetAffx database. There were 193 windows encompassing 167 genes falling in the 0.5% tail. The SNP with the highest-scoring branch length (0.8492) was rs61732502, a missense variant in

the *HLCS* gene. The top LSBL window, with a branch length of 0.5557, was located on chromosome 12 (Chr12:99450001-99550000) and encompassed the *ANKS1B* gene. The highest SNPs within this region were intergenic, and no SNPs within this gene window had LSBL values of statistical significance.

XP-nSL analysis considered 306,079 autosomal SNPs. A total of 1,532 individual variants passed the significance 0.5% threshold of 0.3296, of which 1,239 were within coding regions of 571 genes. There were 72 XP-nSL windows with normalized scores greater than the significance cutoff of 4.0751. These windows spanned 167 genes and included a total of 1,303 variants. For the individual variant scores analysis, 396 of these 1,303 variants were significant at the 0.5% level. The variant with the highest haplotype score was rs150705013, with an XP-nSL value of 0.6535. The SNP rs150705013 was a missense variant in *LRGUK*, a gene implicated in kinase activity (GO:0016301). The top-scoring XP-nSL window (Chr20: 44500001- 44600001) had a normalized score of 5.8818 and spanned eight genes (*ZSWIM3, ZSWIM1, SPATA25, NEURL2, CTSA, PLTP, PCIF1, ZNF335*) that are implicated in a variety of processes such as protein metabolism (R-HSA-1911457) and hindbrain development during early embryogenesis (R-HSA-6810129).

By merging the list of SNPs and genomic regions that were statistically significant for both tests, we have the power to identify regions that are not only highly-differentiated between groups, but also that show evidence of undergoing selective sweeps. Several genes that are putatively adaptive to arid, high-altitude environments contained SNPs that exceeded the significance threshold for both LSBL and XP-nSL. These were: *CLN3* (rs151181; LSBL = 0.2402, XP-nSL = 0.4066), a gene implicated in water homeostasis (GO:0030104); and two pigment-mediating genes, *MITF* (rs56386221; LSBL = 0.2288, XP-nSL = 0.3504) and *BBS5*

(rs16856972; LSBL = 0.2267, XP-nSL = 0.3083). The high level of differentiation and placement within a high-scoring haplotype offer two threads of evidence suggesting that UV radiation and aridity might shape genetic variation in the high Andes.

3.4.1 Adaptation to Cold Climate

Our selection scan identified significant variants in several genes related to cold adaptation (Table 1). Out of the 1142 genes bearing evidence of selection, 24 genes encode proteins that are associated with physiological or cellular responses to cold. Analysis of candidate genes in the Human Reference Protein Interactome (HuRi) Mapping Project identified interactions between 11 protein-coding genes and putatively cold- or altitude-adaptive candidates that are not extensively described in population genetics literature.

One of the strongest signals of selection related to thermal responses is in the gene *CLPB* (Figure 4). A sweep region on chromosome 11 contained six SNPs in *CLPB* that were of statistical significance: five SNPs (rs76126651, rs57669200, rs7940062, rs80338635, rs76324022) landed in the top 0.5% percentile of SNP scores (XP-nSL > 0.3296), and one fell within the top 0.25% (rs144942416: XP-nSL = 0.4887). Interestingly, *CLPB* is implicated in "response to heat" (GO:0009408). *CLPB* shows a high similarity to the ClpB protein, which in bacterial models acts alongside heat shock proteins to recover or repair cells that are damaged during heat exposure (Wortmann et al. 2015). The human CLPB includes ankyrin repeats instead of the two ATPase domains found in bacterial homologs, and CLPB is localized in the mitochondria where depletion of CLPB triggers a stress response (Mróz et al. 2020). Interestingly, aberrant mutations in the *CLPB* gene lead to significant increases in ATPase activity (Wortmann et al. 2015). Evidence from single-celled organisms indicates that ClPb plays

different roles in the context of low temperatures: in *Pseudomonas*, there is over a six-fold increase in ClpB expression during cold (Kumar et al. 2020); in *Synechococcus*, ClpB renatures and solubilizes aggregated proteins when exposed to low temperatures, possibly facilitating acclimatization to cold (Porankiewicz and Clarke 1997).The gene *LPL*, which encodes enzymes found in cells lining muscular capillaries and adipose tissue, is implicated in response to cold (GO:0009409): *LPL* contained four SNPs that surpassed the genome-wide significance threshold. Two of these SNPs, rs270 and rs145657341, were significant at the 99.75% level. This haplotype has a tall, narrow peak, indicating that the selective sweep around *LPL* has occurred (Figure 5). A single SNP in *CDH8* (rs17379848), another gene in the cold response pathway, had a high XP-nSL score of 0.3715.

Evidence for selection was detected in nine genes related to the process of cold-induced thermogenesis (GO:0106106). These genes included *ABHD6, ARRDC3, DYNC1H1*, *ESRRG, IL18R1, NR1D1, PCTP*, *RB1,* and *ZNF516*. Five of these genes contained SNPs surpassing the significance threshold for LSBL. These were: *ESRRG* (rs1856521; LSBL = 0.2304), *NR1D1* (rs141144358; LSBL = 0.3932), *PCTP* (rs79436929; LSBL = 0.3389), *RB1* (rs406098; LSBL = 0.3456), and *ZNF516 (*rs77998951; LSBL = 0.4004). *AARDC3* and *ABHD6* each contained one SNP that was significant for XP-nSL (rs566525954: SNP XP-nSL= 0.3553 and AX-83055620: SNP XP-nSL = 0.3329, respectively). *DYNC1H1* was located in the middle of a one megabase sweep region on chromosome 14 (Chr14:102250000-103250000). This window spanned seven high-scoring SNPs within *DYNC1H1* with a mean XP-nSL value of 0.3689 (Figure 6), including one peak centered around the variant rs142883042 (SNP XP-nSL = 0.4108). In addition to being related to cold-induced thermogenesis, gene ontology databases indicate that *DYNC1H1* is

related to adaptive thermogenesis (GO:1990845), temperature homeostasis (GO:0001659), and regulation of cold-induced thermogenesis (GO:0120161).

The heat shock protein (HSP) family of genes is known to respond to both high and low temperatures. Three genes that relate to heat shock protein binding (GO:0031072) were detected in the selection scan, *DNAJC18, DNAJC12,* and *FAF1*. *DNAJC18*, which is a member of the heat shock protein 40 family, was identified through an LSBL window (Chr5:138750001-138850000; Window LSBL = 0.1634). The gene *DNAJC12* was identified through a high-scoring XP-nSL variant (rs74142901: SNP XP-nSL = 0.3433). One SNP in *FAF1*, implicated in HSP binding, contained an LSBL branch that surpassed the significance threshold (rs12065210: SNP LSBL = 0.391).

One pathway of achieving body temperature homeostasis is mediated by thyroid hormone (Qi et al. 2014, Ocobock 2016). Three genes related to thyroid function were detected in selection scans: *DUOX2, DUOXA1*, and *THADA.* Interestingly, *DUOX2* and *DUOXA1* contained five SNPs that were outliers for LSBL and also fell in the negative extreme of XP-nSL scores, indicating a hard sweep on the reference population (Mexican Mayans). These genes play a role in thyroxine secretion and contribute to body temperature regulation (Warner et al. 2013). The thyroid hormone thyroxine (also known as T4) is stored in thyroxine-binding globulin (TBG), and is released in a temperature-dependent manner: increases in body temperature (e.g., fever) will trigger a cascade of T4 production and increase metabolic output (Qi et al. 2014). In cold climate regions, T4-mediated increases in body temperature might confer a selective advantage (Leonard et al. 2005, Snodgrass et al. 2005). Several studies have shown that thyroid hormone production is activated during ascent to high altitude: two studies in Nepal showed an association of increased free T4 levels with elevation (Nepal et al. 2013, von Wolff et al. 2018). One study

of high altitude-adapted natives and altitude acclimatized lowlanders showed a positive relationship between T4 and T3 and elevation, which reverted to baseline upon return to sea level (Basu et al. 2003).

Indigenous circumpolar populations such as the Evenki, Yakut, and Nenet show elevated T4 levels and higher basal metabolism when compared to their Russian counterparts (Leonard et al. 2005, Snodgrass et al. 2005, Tkachev et al. 1991, Bojko 1997). In northern Finnish males, serum free T3 levels were lower in winter than in summer, and thyroid stimulating hormone levels were highest in December; additionally, urinary free T3 levels were significantly higher in winter months than in summer (Hassi et al. 2001). This indicates that there is an increase in T3 disposal during cold periods, which in turn might imply that short-term thyroid responses are crucial in the context of cold climate (Leonard et al. 2005). DUOX was previously described as having high fixation indices between chronic mountain sickness patients from the Peruvian Andes and individuals of Mexican ancestry from Los Angeles (MXL) (Zhou et al. 2013). A study by Jacovas et al. (2018) identified DUOX as undergoing selection in Andeans relative to lowland Amazonians and Mesoamericans. More recently, Borda et al. (2020) reported that *DUOX2* is under selection in Andeans relative to Indigenous communities from the Amazon, and that mutations within this gene are associated with hypothyroidism. In our study, a number of variants within the DUOX family are highly differentiated between Mexican Mayans and Peruvian Quechua (Supplementary Figure 2). Relative to what was reported by Jacovas et al. (2018), rs269866 (*DUOX2*) is at lower frequency in our Central American sample (Mexican Mayans: G = 0.0154; Mesoamericans: G = 0.068), and at a higher frequency in the Andean Highlander sample (Peruvian Quechua: G = 0.4994; Andeans: G = 0.42). Homozygotes for the G mutation of this SNP exhibited increased DUOX2 protein expression (Borda et al. 2020). If this

upregulation of DUOX2 corresponds to an increase in body temperatures, it holds that a cold-adapted population would show selection for the G allele and against the derived A allele. In such a scenario, a relative increase in the frequency of the G allele might correspond to protective effects against cold stress. Six SNPs in *THADA*, a gene known to contribute to the process of nonshivering thermogenesis, were detected by an LSBL window (W:LSBL = 0.2308) and contained one SNP with a high-scoring individual LSBL (rs10179648; SNP LSBL = 0.3293) with a correspondingly high but insignificant XP-nSL score (SNP XP-nSL = 0.267).

The selection scan identified several additional significant results for genes in other GO categories related to cold adaptation. These included brown adipocytes (GO:0050873), nonshivering thermogenesis (GO:0090336), bodily response to cold (GO:0009409), brown fat cell differentiation (GO:0050873), and regulation of brown fat cell differentiation (GO:0090335) (Table 1).

3.4.2 Genes Adaptive to both Cold and High Altitude

The Hypoxia Inducible Factor 1 Subunit Alpha (*HIF1A*) gene has been well described in the population genetics literature as being one of the primary targets of natural selection for humans inhabiting high altitude (Bigham et al. 2010, Pagani et al. 2012, Crawford et al. 2017). *HIF1A* is related not only to cellular responses to hypoxia (GO:0071456), but also to heat shock protein binding (GO:0031072). *HIF1A* contained one high-scoring SNP in XP-nSL (rs149348765; XP-nSL = 0.3536) (Figure 7). *HYPK* has been associated with lowered hemoglobin levels (Alkorta-Aranburu et al. 2012) in Ethiopian highlanders and is within a top-ten XP-nSL window (Chr15:43800001 - 43900001; W:XP-nSL = 4.86036). This window encompasses *SERINC4, HYPK,* and *SERF2* and contains four SNPs with XP-nSL scores falling

within the top 0.01% of the distribution. Three of these SNPs, including one in *HYPK* (rs12702), were statistical outliers for LSBL (Table 3).

Many of the genes under selection in altitude-adapted Peruvians are linked within a complex series of protein interactions that facilitate thermoregulatory responses to cold as well as physiological responses to hypoxia (Figure 8). Vasodilation (GO:0042311), a process that facilitates blood circulation by relaxing smooth muscle cells and increasing the internal diameter of blood vessels, is adaptive both to high altitude as well as thermoregulation (Charkoudian 2016). In the context of cold, cyclical vasodilation and vasoconstriction allows extremities such as fingers (i.e., the Hunting reaction) to be re-warmed and avoid long term damage such as frostbite (Daanen 2003). In high altitude environments, hypoxic vasodilation overrides sympathetic vasoconstriction which can slightly decrease blood pressure (Bärtsch and Gibbs 2007).

Three genes identified in the selection scan fell in this GO category: *ATG5*, *BDKRB2*, and *PRKG1*. The *ATG5* gene contained one highly-differentiated SNP, rs478310, with an LSBL SNP score of 0.6317. *BDKRB2* contained one high-scoring SNP (rs1046248: XP-nSL = 0.3344). *PRKG1* contained two SNPs that were statistical outliers for XP-nSL (rs73341244: XP-nSL = 0.3547; rs61849212: XP-nSL = 0.366437), and two significant for LSBL (rs11000060: LSBL = 0.2398; rs12571679: LSBL = 0.2153). Related to these genes was *CTNNA3*, implicated in the regulation of heart rate by cardiac conduction (GO:0086091). One intron variant in this gene, rs10997077, was highly differentiated between Peruvian Quechua, Han Chinese, and Mexican Maya, and had an exceptionally long branch length (LSBL = 0.4030) indicating evolutionary divergence. *CTNNA3* is associated with various cardiovascular phenotypes such as diastolic and

systolic blood pressure measurements, forced vital capacity, and subcutaneous adipose tissue (Liang et al. 2017, Gao et al. 2013, Ong et al. 2013).

3.4.3 Putative Adaptation to High UV Radiation

Several genes contained significant variants or showed significant windows for LSBL and XP-nSL that were related to skin and eye pigmentation. In fact, the top candidate from the windowed XP-nSL analysis, located on Chromosome 20 (Chr20:44,500,001-44,600,001; W:XP-nSL = 5.88182), was flanked by two other windows that reached statistical significance. One of these neighboring windows (Chr20:44,600,001-44,700,001; W:XP-nSL = 4.13824) contained five SNPs in the *MMP9* gene, related to pigmentation (GO:0043473) and which is perhaps protective against the penetration of UV into skin and the cellular response to UV (GO: 0034644). These five SNPs within *MMP9* were detected as statistical outliers in the SNP-based XP-nSL analysis, creating a peak clustered about one variant, rs17576 (SNP XP-nSL 0.3975). In addition to the results from chromosome 20, our XP-nSL analyses identified significant SNPs in *DDB2* (rs144989465, XP-nSL = 0.3627), *ADAMTS20* (rs367649909, XP-nSL = 0.3465), *AP3B1* (rs150651515, XP-nSL = 0.3422), and *VDR. VDR* contained eight variants with statistically significant XP-nSL scores, seven of which fell within the top 99.75% of the distribution of SNP scores (Figure 9). Our LSBL analyses detected long Andean Quechua branch lengths for SNP rs16856972 in *BBS5* (LSBL = 0.2267) and SNP rs56386221 in *MITF* (LSBL = 0.2288). Both of these SNPs also had correspondingly high-scoring haplotypes. *BBS5* SNP rs16856972 was included in a high scoring XP-nSL window (window XP-nSL = 0.3083), and *MITF* SNP rs56386221 displayed a high scoring SNP XP-nSL score (SNP XP-nSL = 0.3504).

3.4.4 Additional Evidence for Adaptation to High-Altitude Hypoxia

The selection scan detected a number of genes that were related to response to hypoxia (GO:0001666) (Table 2). A statistically-significant haplotype window spanning *MIEF1* contained two SNPs, one of which was significant at the 0.5% cutoff for SNP-based XP-nSL (rs150822596: XP-nSL = 0.3616). The genes *MIEF1* and *PSMA4* were both detected by XP-nSL windows, and *MIEF1* contained one SNP within a high scoring haplotype (rs150822596: XP-nSL = 0.3616). *PSMA4* had a relatively high-scoring but insignificant SNP for XP-nSL, but was overlapped in a high-scoring window (4.2878). *NOS2* contained one variant with a high-scoring branch length (rs6505483: LSBL = 0.2251).

EGLN3P1, which belongs to a family of genes (*EGLN*) that regulate HIF, was overlapped by an XP-nSL window with a score of 4.86201 (Chr21:15900001-16000001). *CHRNB2* is included in the response to hypoxia pathway and contains one high-ranking SNP (AX-86548950; XP-nSL = 0.3597) that clustered around two neighboring SNPs with high XP-nSL values to create an outlying peak on chromosome 1. Finally, several genes contained a low number of SNPs that reached statistical significance for XP-nSL (*ROCK2*, rs41264193: XP-nSL = 0.3615; *RYR2*, rs16834779: XP-nSL = 0.3487), or that were highly differentiated between populations (e.g., *LOXL2*).

Two genes identified in selection scans, *SH2B1* and *SH2B3*, are known to contribute to blood coagulation, platelet aggregation, and thrombopoietin-mediated signaling (GO:0007596, GO:0090331, GO:0038163). *SH2B1* contained two SNPs that were outliers for LSBL (rs7201929, rs7498665), and *SH2B3* had three SNPs that were outliers for XP-nSL (rs11065898, rs3184504, rs148791142), one of which was significant at the 99.95% level (rs148791142; XP-nSL = 0.4708).

3.4.5 Genes Adaptive to Pathogen and Parasite Stress

From the top 25 genomic windows identified through XP-nSL, six overlapped with genes that are implicated in immune responses. The top-scoring window overall is located on Chromosome 20 spanning positions 44500001 to 44600001, with an adjusted XP-nSL score of 5.8818. This window overlaps eight genes: *ZSWIM3, ZSWIM1, SPATA25, NEURL2, PLTP, PCIF1, ZNF335,* and the putatively-adaptive gene *CTSA. CTSA* is related to both adaptive and innate immune responses (R-HSA-1280218, R-HSA-168249). Other genes located in high-scoring windows include *DERA,* a gene related to innate immune system*; IFNB1, IL27*, and *INPPL1*, which are related to Cytokine signaling in the immune system (R-HSA-1280215); and *DVL2*, which is implicated in WNT5:FZD7-mediated leishmania damping and *Leishmania* infection (R-HSA-9673324; R-HSA-9658195).

The TRIM family of major histocompatibility complex (MHC) proteins are implicated in both adaptive and innate immunity, and protect against pathogens such as viruses and bacterial infections (Ozato et al. 2008). The role of *TRIM31,* an E3 ubiquitin ligase, is to regulate mitochondrial antiviral signaling after viral infection (Liu et al. 2017). *TRIM31* contained two of the highest scoring SNPs in the study: rs3734838 (XP-nSL = 0.6294) and rs1116221(XP-nSL = 0.5628) are located at the center of a plateau of XP-nSL scores, spanning 26 of the 50 highest-scoring SNPs overall. This long, intact haplotype encompasses positions 29970000 to 30140000 on chromosome 6 and contains the genes *ZNRD1-ASP, ZNRD1, PPP1R11, RNF39, TRIM31, TRIM31-AS1, TRIM40*, and *TRIM15*. The 136 variants falling in this window region have a mean SNP XP-nSL score of 0.4315, well above the genome-wide significance level of 0.3647 (top 0.25%). Additionally, the normalized XP-nSL score for the window spanning Chr6:30000001 to

Chr6:30100001 is 5.6131, the second highest window score overall, falling at the high end of the distribution of windowed XP-nSL scores (Top 0.01% = 5.5411). *RNF39*, another gene implicated in innate immunity (GO:0045087), contained 11 SNPs that were statistical outliers for XP-nSL, with a mean haplotype score of 0.4576; rs2074479, the top SNP in this gene, had an XP-nSL score of 0.479713, and one SNP (rs2074479) had a high-scoring haplotype (XP-nSL = 0.4733) and was highly differentiated (LSBL = 0.2836).

ATG16L1, a gene implicated in GTP-ase binding and defense responses to gram-negative bacteria (GO:0051020, GO:0050829), contained a SNP that was an outlier for both LSBL and XP-nSL. The intron variant rs6431586 was significantly differentiated between the three study populations (LSBL = 0.4285) and had the highest haplotype score within the gene window (XP-nSL = 0.3607).

Several genes that are associated with protective responses against Leishmaniasis, a disease caused by the high-altitude surviving *Leishmania* parasite, were identified as statistical outliers indicating recent selection. These genes were: *LMLN* (Chr3:197650001 - 197750000; W:LSBL = 0.4623), *DVL2* (Chr17:7134129, rs222835: SNP:LSBL = 0.2371), and *GPR25* (Chr1:200800001 - 200900001; W:XP-nSL = 4.4293). *GPR25* contains three SNPs with outlying XP-nSL scores (rs6704302: XP-nSL = 0.3253; rs12565385: XP-nSL = 0.3451; rs7531238: XP-nSL = 0.3503), yet none of these had outlying branches from LSBL.

Ten SNPs in the overlapping *APOBR*/*IL27* region contain statistically-significant XP-nSL scores (Figure X). The tall peak in this region is indicative of a selective sweep centered on one variant in *APOBR* (rs13306186) with an extremely high XP-nSL score of 0.5272. *APOBR* encodes the receptor of the APOB protein and is upregulated in lung tissues during infection with *Staphylococcus pneumoniae* (Salas et al. 2014).

These results indicate that populations from the Andean highlands have undergone selection in genes that offset pathogenic burden (*TRIM31*), that contribute to parasite dampening (*DVL2*), and that protect against bacterial infection (*APOBR*).

3.5 Discussion

The "Mars-relevant" [*sic*] environments of high altitude -- arid, with low oxygen, high UV, and extreme cold -- have led to adaptive evolution in a variety of species spanning from microbiota to amniotes (Dib et al. 2008, Zhang et al. 2016, Kereszturi et al. 2020). For humans inhabiting the Andean Altiplano, prior studies have focused on adaptations to hypoxic stress (Beall 2006, 2014; Bigham et al. 2009, 2010; Brutsaert et al. 2019); it is less clear how populations from the high Andes adapt to frigid montane environments.

This study sought evidence to support the hypothesis that populations from high altitude have genetic adaptations not only to hypoxia, but also to hypothermia. Cold stress, which is enhanced by hypoxia, can be a significant fitness-reducing stressor that leads to injury and even death (Kottke et al. 1948, Johnston et al. 1996, Granberg 1991, Hampton 1981). As such, it is critical to understand how populations inhabiting high altitude extremes simultaneously protect against low oxygen availability and low ambient temperature. To identify regions of the genome undergoing adaptive evolution, a selection scan was performed using one frequency-based test of population differentiation (LSBL), and one test that identifies long-ranging, segregating haplotypes (XP-nSL) (Shriver et al. 2004, Szpiech et al. 2021). These selection scans identified a number of SNPs that were highly-differentiated or that were embedded within selective sweep regions, offering strong evidence of recent population-specific evolution.

3.5.1 Genetic Evidence for Evolutionary Changes in Thermoregulatory Pathways

Several genes implicated in cold-induced thermogenesis (CIT) showed signatures of strong selection in the form of high-scoring haplotypes. CIT is a physiological response to the stimulus of low ambient temperatures, involving a variety of acclimatory behaviors such as shivering, increased rate of breathing, and vasoconstriction (Castellani and Young 2016). One gene implicated in CIT, Dynein Cytoplasmic 1 Heavy Chain 1, or *DYNC1H1*, was located in the middle of a one megabase sweep region on chromosome 14. *DYNC1H1* encodes a large subunit of the cytoplasmic dynein complex (Poirier et al. 2013). Dyneins are activated by binding with dynactin; fueled by ATP, the dynein-dynactin complexes move along microtubules to transport viruses, membrane-bound organelles, RNAs, and a variety of proteins (Reck-Peterson et al. 2018). Dynein is related to lipid metabolism, brown adipose tissue morphology, and cold tolerance, and thus is central to thermoregulatory responses to low ambient temperature (Eschbach et al. 2011). *NR1D1* and *ESRRG,* two other genes related to cold-induced thermogenesis (Liu et al. 2013, Müller et al. 2020), likewise contained high scoring haplotypes. Similar to cold-induced thermogenesis, the genes *CDH8* and *LPL* are known to respond to cold stimulus and both were centrally located in sweep regions (Suzuki and Takeichi 2008, Carmona et al. 2005). *LPL*, which encodes an enzyme found in cells lining muscular capillaries and adipose tissues (Nedergaard et al. 2011), contained four variants that presented an exceptionally tall, narrow peak falling within the 99.75%ile of XP-nSL scores; given the significant height but relatively short range of this haplotype, it is likely this gene is undergoing recent and strong selection.

Body temperature homeostasis through the recruitment of brown adipose tissue (BAT), a heat-generating form of fat, is under selection in various cold adapted groups (Daanen et al.

2015, Hancock et al. 2011, Racimo et al. 2015). BAT is a structure that is deeply conserved across mammals, and its ability to generate heat confers a thermoregulatory response to cold known as nonshivering thermogenesis (NST) (Lidell et al. 2013, Muzik et al. 2013, Oelkrug et al. 2015, Nedergaard and Cannon 2018). Activated BAT depots produce significantly more heat than resting muscle alone, thus providing an energetically-efficient means of mediating body temperature without the need to shiver (Steegmann 2007, van Marken Lichtenbelt 2009). In adults, inducible brown fat (aka "beige", or "iBAT") can be recruited from stem cells within white adipose tissue (WAT) either during cold exposure, after eating a high-fat food item, or by therapeutics targeting genes in the BAT thermogenesis pathway (Nicholls and Locke 1984, Schulz et al. 2011, Din et al. 2018, Levy et al. 2018, Hadi et al. 2019, Blondin et al. 2020, O'Mara et al. 2020, Sun et al. 2020). In neonates lacking sufficient muscle tone to shiver, cold-induced NST allows them to maintain safe body temperatures in a tenable, energy-optimizing manner, such that BAT thermogenesis has long been considered a potential target for adaptive evolution (Steegmann 2007, Sazzini et al. 2014, Levy et al. 2021).

Brown fat-mediated thermogenic pathways rely on a variety of genes that regulate the storage and breakdown of fatty acids, adipogenesis, the production and metabolism of glucose, and mitochondrial protein uncoupling (Devlin 2015). The primary regulators of BAT thermoregulation are genes in the mitochondrial protein uncoupling family (UCP) (Calderon-Dominguez et al. 2016). The UCP pathway is critical for NST given that these uncoupling proteins are cold inducible (Oulett et al. 2012, Hasan and Mahmood 2013, van der Lans et al. 2013). Variants within *UCP1* contribute to enhanced heat production during cold exposure, and there is evidence that this family underwent selection during migrations Out of Africa (Nishimura et al. 2017, Hancock 2011). Our study detected evolutionary changes in genes

involved in the *formation* -- but not UCP-mediated signaling -- of brown adipose tissue. This might suggest that UCP genes are fairly conserved across the three populations in this analysis, whereas genes influencing BAT production are not. Two such genes detected by selection scans are *ZNF516* and *METRNL*, both of which contribute to brown adipose cell differentiation (GO:0050873; Li et al. 2017, Jamal et al. 2020).

It is possible that selection on carnitine palmitoyltransferases (CPTs), which facilitate the entry of free fatty acids (FFAs) into mitochondria, could enhance mitochondrial protein uncoupling during cold exposure (Calderon-Dominguez et al. 2016). This study detected evidence of selection in the gene *CPT1A,* which triggers brown fat thermogenesis and has been shown to be under selection in populations from Siberia (Din et al. 2018, Cardona et al. 2014). The gene thyroid adenoma-associated protein (*THADA*), identified here through our LSBL analysis, is known to contribute to a muscle-based form of nonshivering thermogenesis that is not inducible by cold (Chatterjee and Perrimon 2018, Bal and Periasamy 2020). *THADA* is an uncoupler (and colocalizer) of SERCA, an ATP-dependent calcium pump that uses energy derived from ATP hydrolysis to transport calcium ions into the endoplasmic reticulum (ER) (Bal and Periasamy 2020). The amount of Ca^{2+} that penetrates the ER is reduced when *THADA* uncouples ATP hydrolysis from Ca^{2+} transport; this mechanism results in the release of energy in the form of heat (Moraru et al. 2017). The *THADA* gene is under selection in cold-adapted Siberians, and shows evidence of strong evolutionary divergence between living humans and Neandertals (Cardona et al. 2014, Green et al. 2010). Finally, thyroid hormones are known to contribute to body temperature regulation, and it is possible that selection on cold-inducible genes related to thyroid might contribute to enhanced body temperature homeostasis (Leonard et al. 2005, Snodgrass et al. 2005, Warner et al. 2013, Qi et al. 2014, Solmonson and Mills 2016).

Two genes influencing thyroid behavior, *DUOX2* and *DUOXA1* (Wang et al. 2020, Hulur et al. 2011), contained highly-differentiated SNPs between the three populations that were statistical outliers for LSBL. The influence of DUOX-family genes on body temperature regulation is uncertain but warrants further investigation. *PRKG1* was identified as a selection-nominated candidate gene for cold adaptation by both the LSBL and the XP-nSL analyses. This gene helps regulate platelet activation and smooth muscle contraction (Diamond et al. 2013, Hofmann et al. 2013, Zhang et al. 2018), which are believed to help offset the effects of high-altitude hypoxia. In fact, the *PRKG1* gene was previously identified as being under selection in other Andean populations (Eichstaedt et al. 2015). In cold climates, the association of *PRKG1* with vasodilation/vasoconstriction may help warm the extremities during prolonged exposure to low ambient temperatures. Of note, *PRKG1* was identified as under selection in Greenlandic Inuit in response to cold exposure (Fumagalli et al. 2015).

3.5.2 Genetic Evidence for Niche-Specific Adaptation

Given its position in the tropics and its thin atmosphere, the Andean Plateau is bombarded with extraordinarily high levels of UV radiation (Piazena 1996). In fact, the highest sustained UV radiation levels to reach Earth's surface were detected above 4300 mASL in Bolivia over the course of two months, with dosimeters registering a UV index (UVI) of over 43.3 (Cabrol et al. 2014). High levels of UV radiation can damage superficial skin cells, the eyes, and cause DNA damage that can lead to melanoma (Sample and He 2019). Conversely, exceptionally low levels of UV lead to diminished vitamin D production, causing immune deficiency as well as rickets, which can impact the process of childbirth and development (Innes et al. 2002). Over the course of some two million years outside of Africa (but in particular since

the late Pleistocene), human populations have offset the stress of latitudinal changes in UV levels with various dietary adaptations (i.e., to counteract low vitamin D), cultural buffers (e.g., skin coverings), and recent adaptive evolution that mediates melanin production in skin and hair (Jablonski and Chaplin 2017, Deng and Xu 2018, Lasisi and Shriver 2018).

Despite the fact that much of the body (except face and eyes) are typically protected by clothing and other skin coverings, it is possible that selection helps to offset the DNA-damaging effects of high UV radiation in altitude-adapted Peruvians. One gene that helps to offset low levels of vitamin D showed evidence of a recent selective sweep in Peruvian Quechua, and is known to be under selection in Tibetans (Hu et al. 2017). Seven genes detected in selection scans were associated with the body's response to UV stress, perhaps buffering against UV exposure unique to the high-altitude tropics. *MITF* mediates the development and behavior of pigment-producing melanocytes, and thus plays a central role in skin pigmentation (GO:0043473). Mutations within *DDB2* are associated with xeroderma pigmentosum (OMIM: 278730) and are implicated in high UV hypersensitivity, reduced skin pigmentation, and extremely elevated risk of sun-induced skin cancers such as melanoma (Abbotts et al 2019). *VDR* encodes the vitamin D3 receptor and was recently described as being under selection in Tibetans (Hu et al. 2017). It is possible that this *VDR* variant is protective against low vitamin D levels resulting either from diet or from covering much of one's skin at high altitude. *BBS5* (OMIM: 615983) is often associated with severe pigmentary retinopathy and photoreceptor damage (Bolch et al. 2016). Given that both *MMP9* and *BBS5* are related to pigmentation and are localized to the eye, it is possible that selection might protect against UV-related retinal damage given that this region of the body (the face and eyes) typically remains uncovered at altitude.

As expected, given the significant impact of hypoxia on human health, a number of genes undergoing selection in Peruvian Quechua were associated with responses to low oxygen availability. Seventeen genes detected through selection scans were putatively adaptive to high altitude and were present in the Gene Ontology dataset: thirteen were associated with responses to hypoxia (GO:0001666), three contributed to vasodilation (GO:0042311), and one regulated heart rate via cardiac conduction (GO:0086091). One gene related to vasodilation (*PRKG1*) and two genes related to hypoxia responses (*MIEF1, RYR2*) were detected by multiple tests. Several genes that were putatively adaptive to hypoxia contained highly-differentiated SNPs (rs6505483 in *NOS2*) or high-scoring haplotypes (rs149348765 in *HIF1A*). A number of candidate windows overlapping genes related to altitude adaptation were not included in the GO database. For example, the Peruvian dataset revealed selection on the gene *ATG5*, which is putatively adaptive to cold and high altitude, and ATG5 proteins interact with both *THADA* and *CTNNA3* via *USHBP1*, all of which are under selection.

3.5.3 Limitations and Alternate Approaches

Selection scans of genome data are effective methods of identifying pairwise differences in evolutionary trajectories between groups (Shriver et al. 2004), yet they are not without limitations. A shortcoming of our study is that it is constrained by the use of SNPs, which are essentially known genetic variants. Our scans were able to identify divergence between populations at loci included in the SNP array, yet variants that are not called (or known) were necessarily omitted. This alone does not invalidate our findings, yet opens up the potential to perform targeted sequencing of candidate-nominated genes (i.e., for sequence-based tests). Additionally, while selection scans have the power to identify evolutionary divergence or

coalescence, the absence of functional validation makes it impossible to know whether genes showing signals of selection actually contribute to reproductive fitness in human populations. One final drawback is that haplotype-based tests of selection were conducted using populations inhabiting the extremes of the environmental spectrum -- the hot, humid rainforest of Central America and the cold, arid Andes. Understandably, each population will show significant evolutionary divergence for genes that are putatively adaptive to their particular environments, but how these compare to selection scans against data derived from a control "temperate" climate sample is yet to be determined.

One issue potentially affecting our conclusions is that demographic factors often mimic the effects of natural selection: in situations where sample sizes are small, or gene flow is inhibited by geographic or geological barriers, populations will exhibit a reduction in genetic diversity not as a result of selection but rather as a result of drift. In particular, given the relative isolation of the high Andes compared to the lowland rainforests of Mesoamerica, it is possible that signals of genetic differentiation (e.g., LSBL) are somewhat skewed. Considering that Mexican Mayans and Peruvian Quechua descend from a more recent, geographically-isolated ancestor, branch lengths calculated for the Han Chinese sample are expectedly longer. Additionally it is worth mentioning that soft sweeps, which select on standing variation, might resemble drift in that whole distinct haplotypes containing neutral mutations can be swept up to high frequency. Considering that we applied haplotype-based tests of selection to our dataset, and conducted both LSBL and XP-nSL for both windows and SNPs, we are confident that our results are relatively robust to the effects of drift.

The genes identified in this selection scan should be investigated in future association studies examining functional variants contributing to body temperature homeostasis. Given that a

number of genes contribute to putatively-adaptive phenotypes in Peruvian Quechua, there will likely be detectable associations of genotypes under selection and physiological responses to cold stress. For example, nonshivering thermogenesis mediated by brown adipose tissue can be induced with only slight drops in ambient temperature (Devlin 2015). Cold challenges, where participants experience a slight drop in ambient or skin surface temperature, are known to trigger brown fat thermogenesis that can be detected through thermal imaging (Law et al. 2018). This would provide a noninvasive means of validating whether genes in these pathways contribute to an adaptive "heat production" phenotype for populations inhabiting cold montane environments.

3.5.4 Conclusions

Humans inhabiting high latitude zones have undergone strong selection in genes that facilitate body temperature regulation. Despite having tundra habitats similar to Siberia or Alaska, high altitude environments of the American tropics are often not considered to be cold climate zones. As such, evidence for cold climate adaptation in humans is limited to low-altitude populations from the global north. It is likely that in high-altitude, cold-climate environments such as the Peruvian Andes, the ability to buffer against hypothermia would confer a significant adaptive benefit, particularly for individuals experiencing hypoxia, for whom the ability to regulate body temperature is significantly impaired. We hypothesized that among the Peruvian Quechua, selection scans would detect evidence of hard sweeps surrounding genes that protect against cold stress. In this study, we identified a number of regions (e.g., *PRKG1*, *THADA*) previously described as undergoing selection in populations from Greenland and Siberia (Fumagalli et al. 2015, Cardona et al. 2014). Additionally, compared to Mexican Mayans (a related group that is putatively adapted to heat), the Peruvian Quechua sample shows evidence of

directional selection in genes related to: cold-induced thermogenesis (*ESRRG, IL18R1, ABHD6, AARDC3, RB1, DYNC1H1, NR1D1, PCTP*); differentiation of thermoregulatory brown fat cells (*EBF2, METRNL, ZNF516);* and thyroid function (DUOX family) which might contribute to body temperature regulation. Other genes undergoing selection in this Andean community protect against parasites and pathogens (*DVL2, LMLN*) help to offset the stress of high UV radiation (*DDB2*), and protect against low levels of vitamin D (*VDR*). Viewed in sum, these findings support the hypothesis that populations from the Andean highlands have undergone local evolutionary changes that offset not only the effects of low oxygen availability, but also year-round cold temperatures, niche-specific parasites, and high levels of UV. These results are intriguing given that they inform us not only about how populations adapt to novel environments over short evolutionary time scales, but also in that they provide some of the first evidence of local adaptation to thermal stress in a South American context. This sheds light onto broader evolutionary changes associated with dispersal into cold environments, such as those experienced by early hominins during the colonization of relatively high latitude and high-altitude zones (Yang et al. 2017, Nielsen et al. 2017, Ossendorf et al. 2019).

3.6 Tables and Figures

Table 3.1: Putatively Cold-Adaptive Genes detected in Selection Scans

Gene	Pathway	Top SNP	SNP Position	Test	Result
ESRRG	Cold-induced thermogenesis (GO:0106106)	rs1856521	Chr1:216832876	LSBL	0.2304
EIF2B3	Response to heat (GO:0009408)	rs538439403	Chr1:45347460	XP-nSL	0.3329
FAF1	Heat shock protein binding (GO:0031072)	rs12065210	Chr1:50942784	LSBL*	0.3910
IL18R1	Cold-induced thermogenesis (GO:0106106)	rs13015714	Chr2:102971865	LSBL*	0.4294
THADA	Adaptive thermogenesis (GO:1990845)	rs10179648	Chr2:43808065	LSBL*	0.3293
ABHD6	Cold-induced thermogenesis (GO:0106106)	AX-83055620	Chr3:58242335	XP-nSL	0.3329
DNAJC18	Heat shock protein binding (GO:0031072)	rs10900864	Chr5:138773090	Window LSBL	0.1634
ARRDC3	Cold-induced thermogenesis (GO:0106106)	rs566525954	Chr5:90674622	XP-nSL	0.3553
ATG5	Vasodilation (GO:0042311)	rs478310	Chr6:106665752	LSBL	0.6317
LPL	Response to cold (GO:0009409)	rs145657341	Chr8:19809322	XP-nSL	0.3873
EBF2	Brown fat cell differentiation (GO:0050873)	rs6557876	Chr8:25900675	Window XP-nSL	4.4770
PSIP1	Response to heat (GO:0009408)	rs142155589	Chr9:15466828	XP-nSL*	0.3624
PRKG1	Vasodilation (GO:0042311)	rs61849212	Chr10:54048119	XP-nSL	0.3664
CTNNA3	Cardiac conduction (GO:0086091)	rs10997077	Chr10:68118323	LSBL	0.4030
CPT1A	Fatty Acid Metabolism (Cardona et al. 2014)	rs41302429	Chr11:68529155	XP-nSL	0.3669
CLPB	Response to heat (GO:0009408)	rs144942416	Chr11:72019648	XP-nSL	0.4887
RB1	Cold-induced thermogenesis (GO:0106106)	rs406098	Chr13:48963784	LSBL	0.3456
DYNC1H1	Cold-induced thermogenesis (GO:0106106)	rs142883042	Chr14:102514949	XP-nSL	0.4108
HIF1A	Heat shock protein binding (GO:0031072)	rs149348765	Chr14:62204819	XP-nSL	0.3535
BDKRB2	Vasodilation (GO:0042311)	rs1046248	Chr14:96703484	XP-nSL	0.3344
DUOX2	Thyroid hormone generation (GO:0006590)	rs57659670	Chr15:45398438	LSBL	0.2809
DUOXA1	Thyroid hormone generation (GO:0006590)	rs61751061	Chr15:45409732	LSBL	0.2994
CDH8	Response to cold (GO:0009409)	rs17379848	Chr16:61947630	LSBL*	0.1189
NR1D1	Cold-induced thermogenesis (GO:0106106)	rs141144358	Chr17:38251385	LSBL	0.3932

PCTP	Cold-induced thermogenesis (GO:0106106)	rs79436929	Chr17:53849202	LSBL	0.3389
METRNL	Brown fat cell differentiation (GO:0050873)	AX-82988002	Chr17:81043039	LSBL	0.2136
ZNF516	Brown fat cell differentiation (GO:0050873)	rs77998951	Chr18:74198976	LSBL	0.4004

Asterisks indicate variants that were outliers for both SNP- and window-based versions of the corresponding tests.

Table 3.2: Genes offering putative adaptations to high-altitude stressors.

Gene	Stressor	Pathway
CHRNB2	Altitude Hypoxia	Response to hypoxia (GO:0001666)
HIPK2	Altitude Hypoxia	Response to hypoxia (GO:0001666)
LOXL2	Altitude Hypoxia	Response to hypoxia (GO:0001666)
MIEF1	Altitude Hypoxia	Response to hypoxia (GO:0001666)
NOS2	Altitude Hypoxia	Response to hypoxia (GO:0001666)
PAM	Altitude Hypoxia	Response to hypoxia (GO:0001666)
PRKG1	Altitude Hypoxia	Vasodilation (GO:0042311)
PSMA4	Altitude Hypoxia	Response to hypoxia (GO:0001666)
RBX1	Altitude Hypoxia	Response to hypoxia (GO:0001666)
ROCK2	Altitude Hypoxia	Response to hypoxia (GO:0001666)
RYR2	Altitude Hypoxia	Response to hypoxia (GO:0001666)
SH2B1	Altitude Hypoxia	Blood coagulation (GO:0007596)
SH2B3	Altitude Hypoxia	Blood coagulation (GO:0007596)
TRPC6	Altitude Hypoxia	Response to hypoxia (GO:0001666)
ATG5	Altitude/Temperature	Vasodilation (GO:0042311)
BDKRB2	Altitude/Temperature	Vasodilation (GO:0042311)
CTNNA3	Altitude/Temperature	Regulation of heart rate by cardiac conduction (GO:0086091)
HIF1A	Altitude/Temperature	Hypoxic response (GO:0001666), HSP binding (GO:0031072)
PRKG1	Altitude/Temperature	Vasodilation (GO:0042311)
AKR1B1	Aridity	Water homeostasis (GO:0030104)
CLDN4	Aridity	Water homeostasis (GO:0030104)
CLN3	Aridity	Water homeostasis (GO:0030104)
FLG	Aridity	Water homeostasis (GO:0030104)
LSR	Aridity	Water homeostasis (GO:0030104)
TP63	Aridity	Water homeostasis (GO:0030104)
ABHD6	Cold/Heat	Cold-induced thermogenesis (GO:0106106)
ARRDC3	Cold/Heat	Cold-induced thermogenesis (GO:0106106)
CDH8	Cold/Heat	Response to cold (GO:0009409)
CLPB	Cold/Heat	Response to heat (GO:0009408)

CPT1A	Cold/Heat	Fatty Acid Metabolism (Cardona et al. 2014)
DNAJC12	Cold/Heat	Heat shock protein binding (GO:0031072)
DNAJC18	Cold/Heat	Heat shock protein binding (GO:0031072)
DUOX2	Cold/Heat	Thyroid hormone generation (GO:0006590)
DUOXA1	Cold/Heat	Thyroid hormone generation (GO:0006590)
DYNC1H1	Cold/Heat	Cold-induced thermogenesis (GO:0106106)
EBF2	Cold/Heat	Brown fat cell differentiation (GO:0050873)
EIF2B1	Cold/Heat	Response to heat (GO:0009408)
EIF2B3	Cold/Heat	Response to heat (GO:0009408)
ESRRG	Cold/Heat	Cold-induced thermogenesis (GO:0106106)
FAF1	Cold/Heat	Heat shock protein binding (GO:0031072)
IL18R1	Cold/Heat	Cold-induced thermogenesis (GO:0106106)
LPL	Cold/Heat	Response to cold (GO:0009409)
METRNL	Cold/Heat	Brown fat cell differentiation (GO:0050873)
NR1D1	Cold/Heat	Cold-induced thermogenesis (GO:0106106)
PCTP	Cold/Heat	Cold-induced thermogenesis (GO:0106106)
PSIP1	Cold/Heat	Response to heat (GO:0009408)
RB1	Cold/Heat	Cold-induced thermogenesis (GO:0106106)
THADA	Cold/Heat	Adaptive thermogenesis (GO:1990845)
ZNF516	Cold/Heat	Brown fat cell differentiation (GO:0050873)
ADAMTS20	UV Radiation	Pigmentation (GO:0043473)
AP3B1	UV Radiation	Pigmentation (GO:0043473)
BBS5	UV Radiation	Pigmentation (GO:0043473)
DDB2	UV Radiation	Response to UV (GO:0009411)
MITF	UV Radiation	Pigmentation (GO:0043473)
MMP9	UV Radiation	Pigmentation (GO:0043473)

Table 3.3: Variants under selection in the region spanning HYPK.

Genomic Position	dbSNP	XP-nSL	LSBL	Alleles	Gene	Distance to *HYPK*
Chr15:44089414	rs143233262	0.4418	—	M [ATG] > T [ACTTG]	*SERINC4/SERF2*	3kb Upstream
Chr15:44090798	rs3759791	0.4477	0.2185	C/G	*SERINC4/SERF2*	2kb Upstream
Chr15:44091386	rs3784275	0.4489	0.2209	A/C	*SERINC4/SERF2*	2kb Upstream
Chr15:44093927	rs12702	0.4583	0.2098	S [TCT] > P [CCT]	*HYPK*	0

Figure 3.1: Inhabited High-Altitude Regions of the Planet

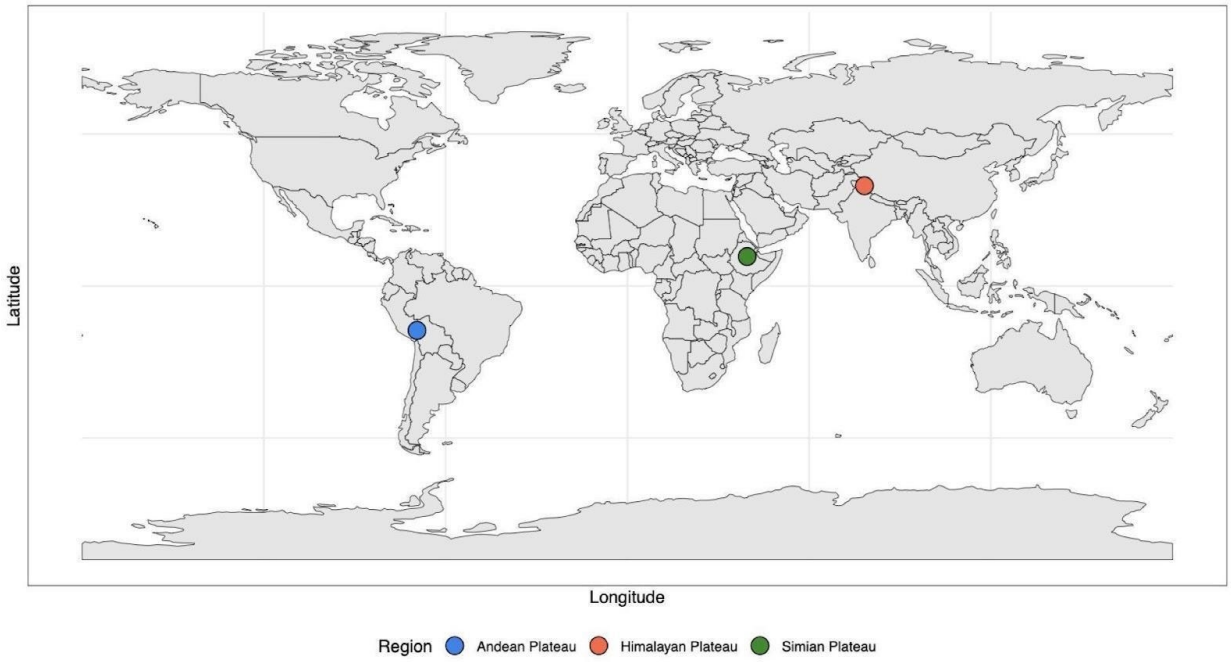

Map of high altitude adapted populations discussed in the text. There are three populations that inhabit regions in excess of 2,500 m above sea level. These are Ethiopian highlanders from the Simian Plateau (green), various populations from the Qinghai-Tibet Plateau (orange), and populations from the Andean Altiplano.

Figure 3.2: Diagram of LSBL Branching

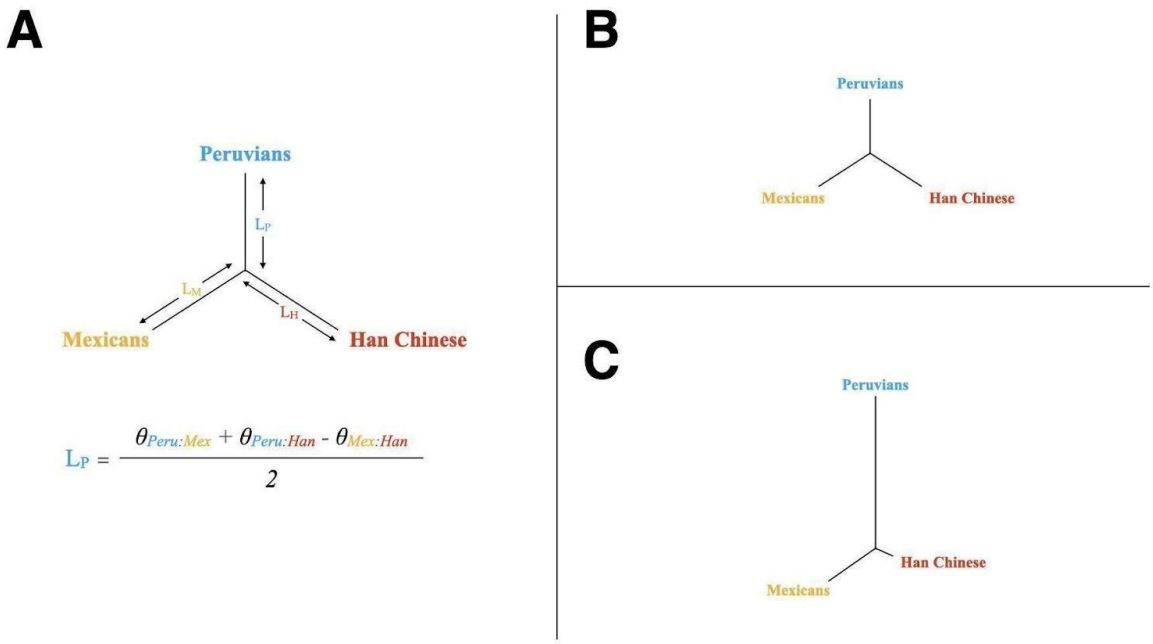

Diagram of Locus-specific branch length (LSBL) estimates. Panel A: formula for calculating branch lengths. Panel B: Equidistance of branch lengths, indicating no significant evolutionary change. Panel C: A long branch indicating population-specific evolutionary change.

Figure 3.3A: Results of Population Structure and Admixture Analysis

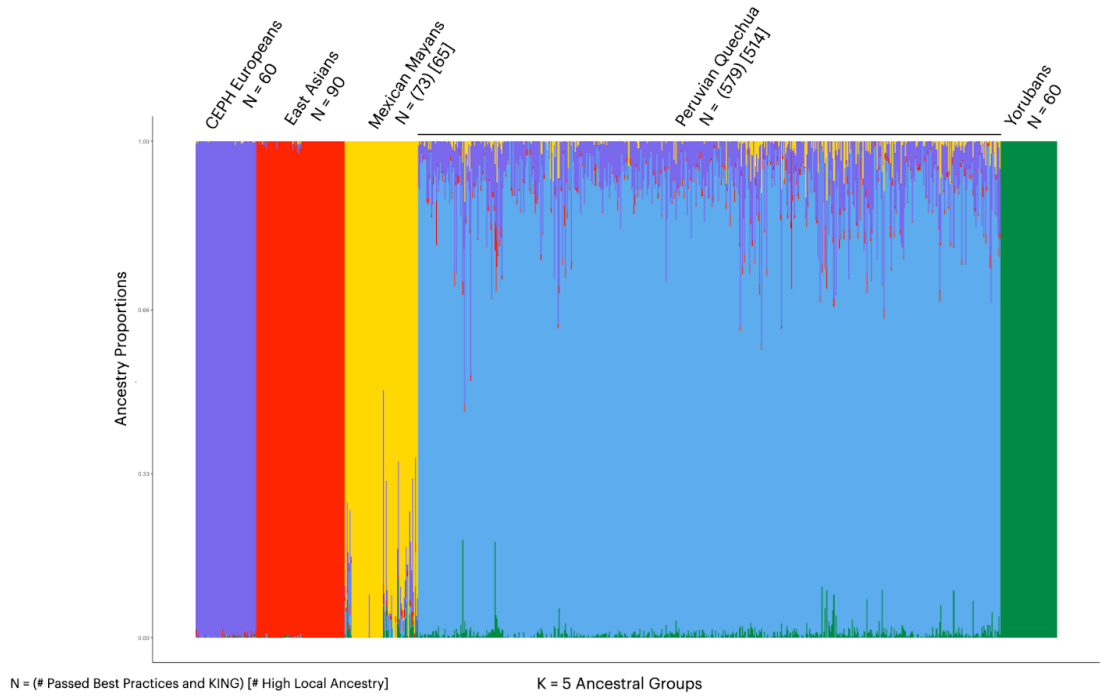

Results of ADMIXTURE analysis. Each vertical bar represents one individual, and the proportions of colors within bars correspond to the amount of ancestry (ancestry proportions) for K = 5 ancestral groups. Purple indicates ancestry similar to CEPH Europeans. Red corresponds with inferred East Asian ancestry. Gold indicates Mexican Mayan ancestry. Blue indicates Peruvian Quechua ancestry. Green indicates ancestry similar to Yoruban Africans.

Figure 3.3B: Results of Population Structure and Admixture Analysis

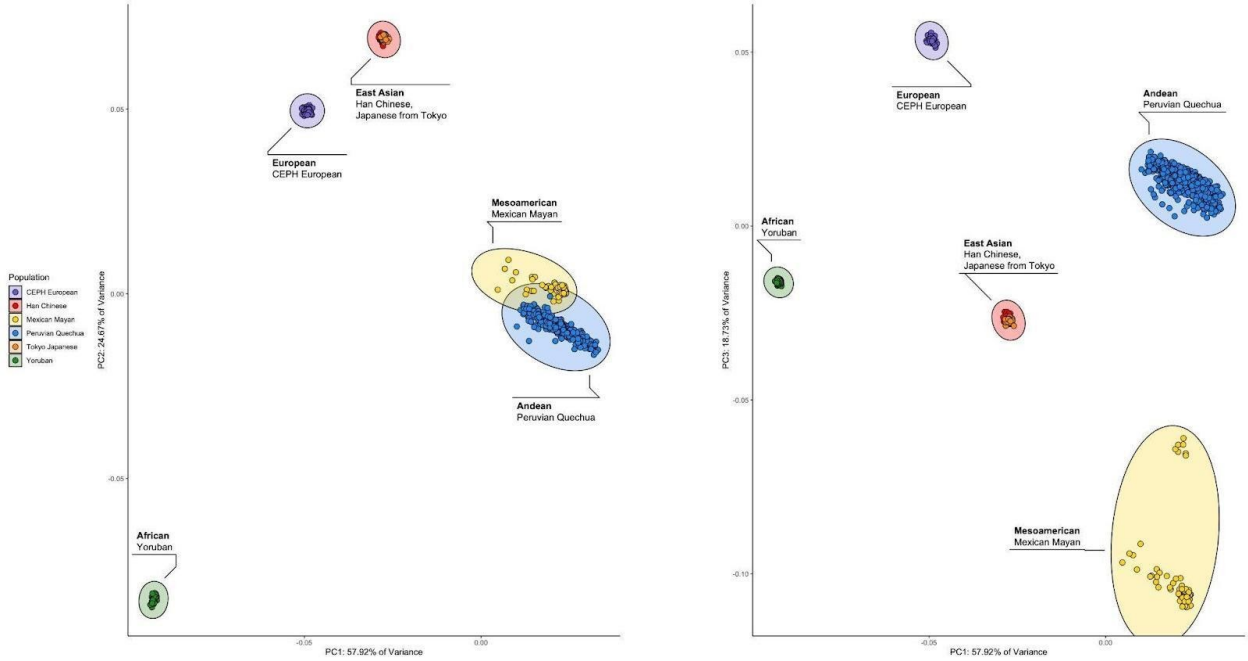

PCA was used to detect population structure and individuals with high levels of admixed ancestry. Each dot represents an individual. Ellipses indicate 95% CI for population clusters. Colors correspond to populations. The X axis of each graph represents the PC1 score, which accounted for 57.92% of variance. Left Panel: PC1 plotted against PC2, which accounted for 24.67% of variance. Right Panel: PC1 plotted against PC2, which account for 18.73% of variance.

Figure 3.4: Sweep Region Surrounding CLPB

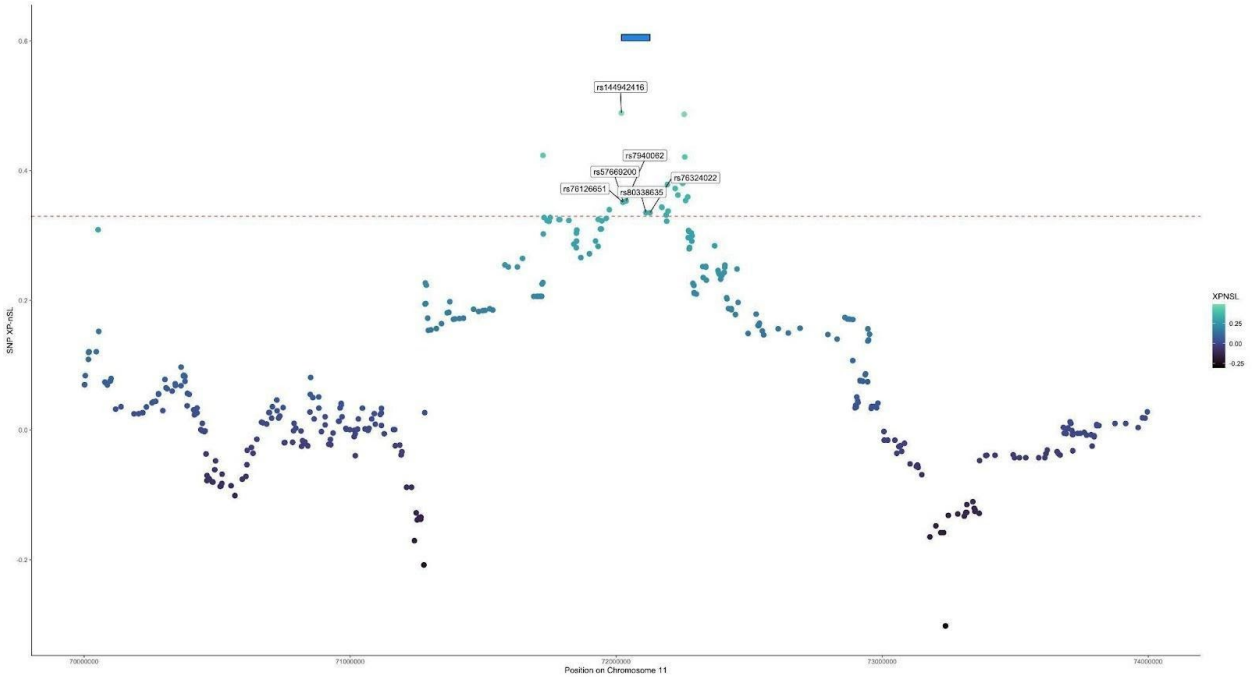

High scoring haplotype detected around *CLPB*. Each dot represents a SNP. Location on the X axis represents position on Chromosome 11. Both the color of the dot and location along the Y axis correspond with XP-nSL scores. The 99.5% genome-wide threshold for SNP XP-nSL scores (0.3296) is indicated by the red dotted line: labeled points (SNPs) indicate variants within the coding region of the gene that were considered to be statistically significant. Blue bar corresponds to the coding region of the gene.

Figure 3.5: Sweep Region Surrounding LPL

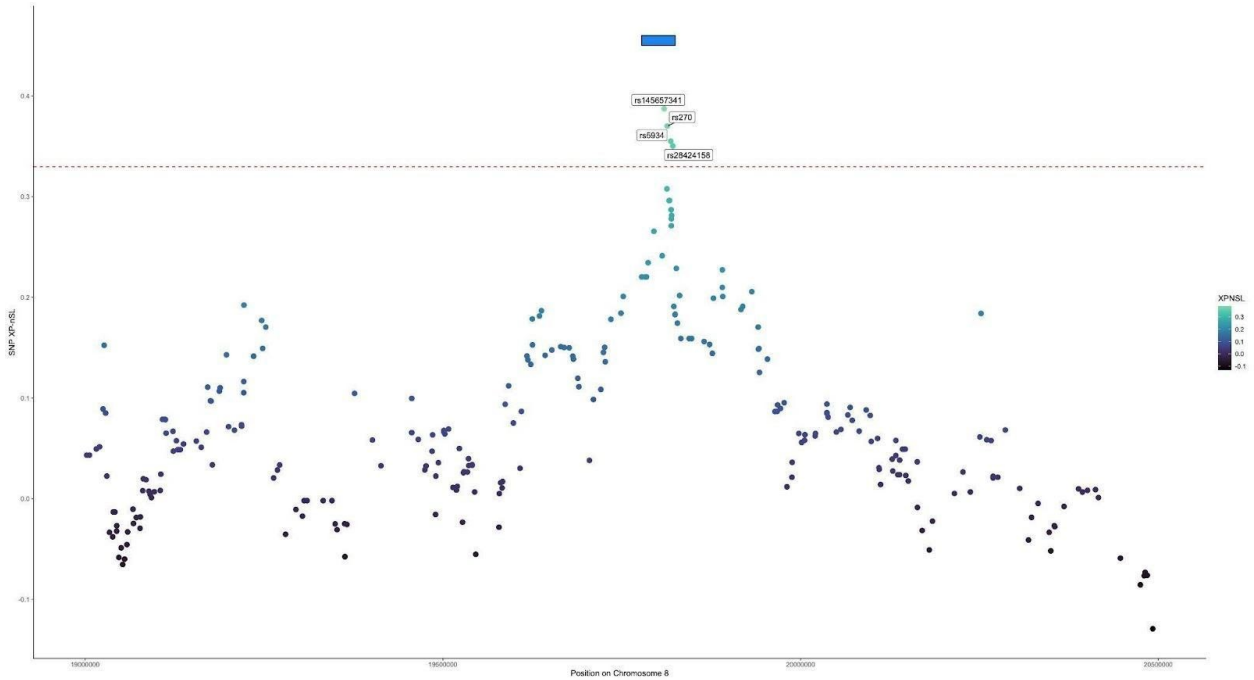

High scoring haplotype detected around *LPL*. Each dot represents a SNP. Location on the X axis represents position on Chromosome 8. Both the color of the dot and location along the Y axis correspond with XP-nSL scores. The 99.5% genome-wide threshold for SNP XP-nSL scores (0.329 is indicated by the red dotted line: labeled points (SNPs) indicate variants within the coding region of the gene that were considered to be statistically significant. Blue bar corresponds to the coding region of the gene.

Figure 3.6: High Scoring Haplotype Surrounding DYNC1H1

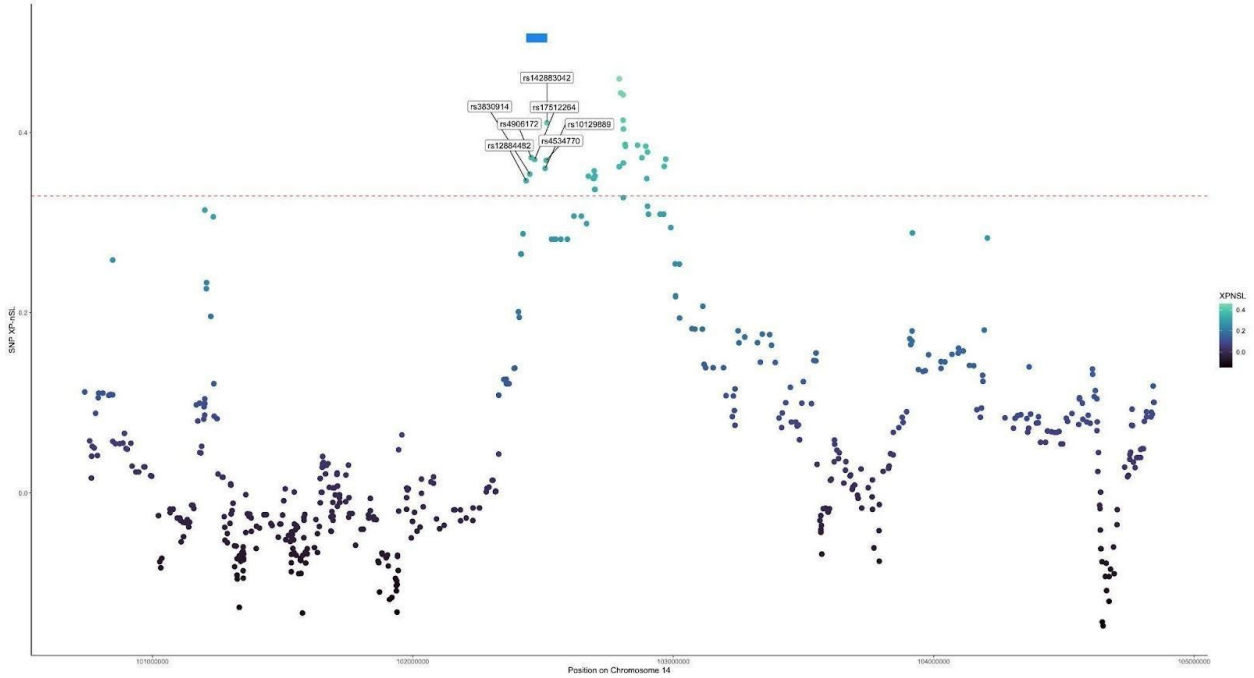

High scoring haplotype detected around *DYNC1H1*. Each dot represents a SNP. Location on the X axis represents position on Chromosome 14. Both the color of the dot and location along the Y axis correspond with XP-nSL scores. The 99.5% genome-wide threshold for SNP XP-nSL scores (0.3296) is indicated by the red dotted line: labeled points (SNPs) indicate variants within the coding region of the gene that were considered to be statistically significant. Blue bar corresponds to the coding region of the gene.

Figure 3.7: Outlier SNP in HIF1A

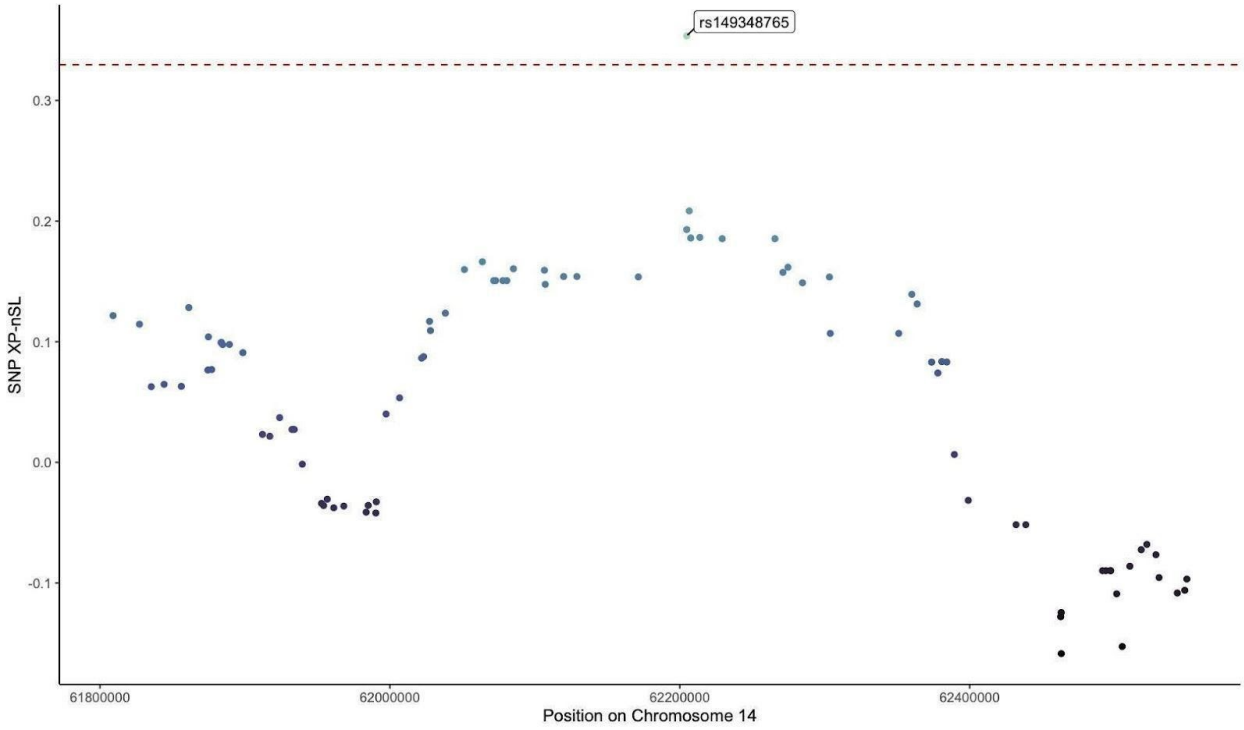

High scoring variant within around *HIF1A*. Each dot represents a SNP. Location on the X axis represents position on Chromosome 14. Both the color of the dot and location along the Y axis correspond with XP-nSL scores. The 99.5% genome-wide threshold for SNP XP-nSL scores (0.329 is indicated by the red dotted line: labeled points (SNPs) indicate variants within the coding region of the gene that were considered to be statistically significant.

Figure 3.8: Protein-protein interaction of Candidate Genes

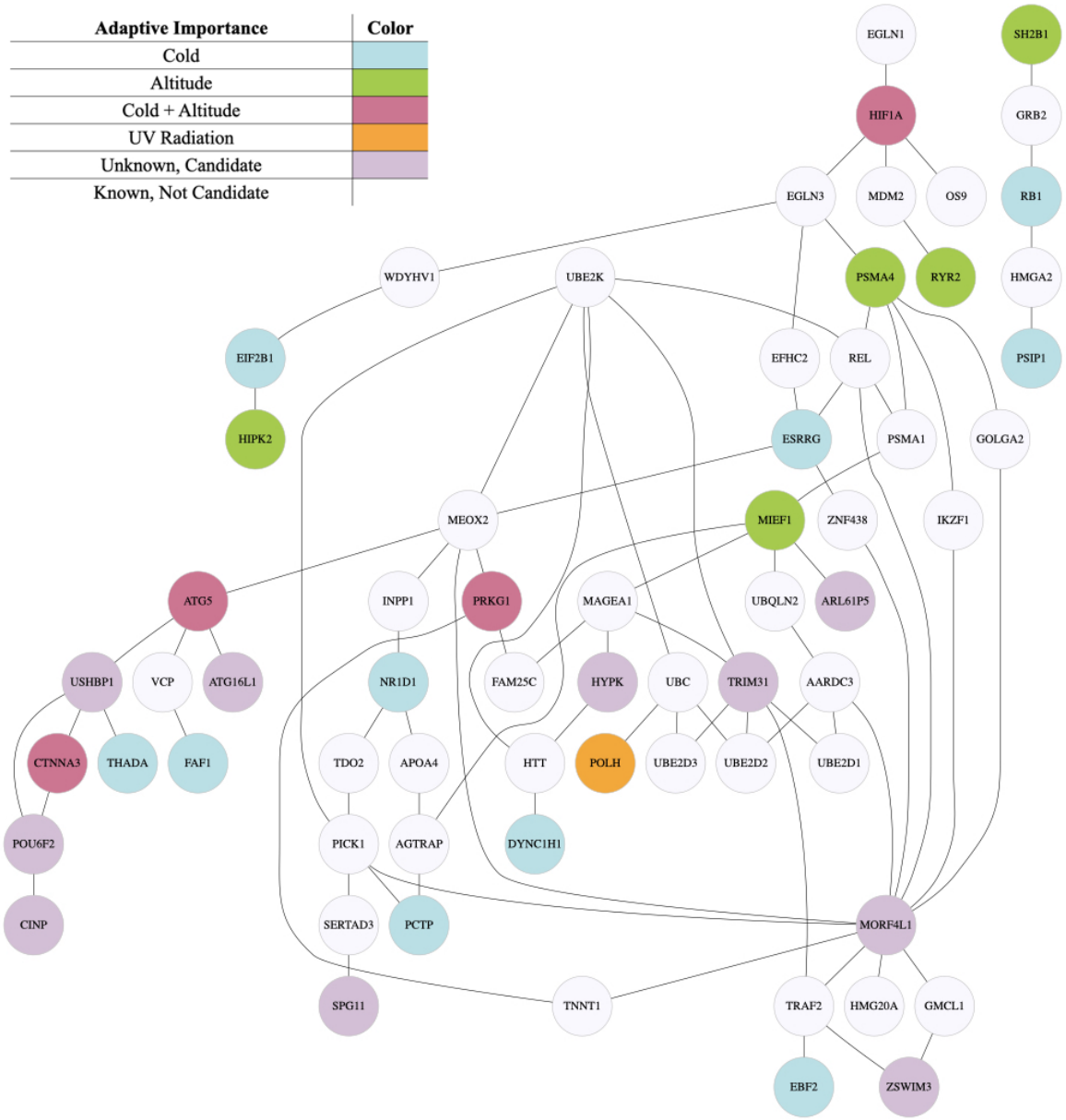

Protein interaction network for genes identified with adaptive significance at high altitude.

Figure 3.9: High-scoring Haplotype within VDR

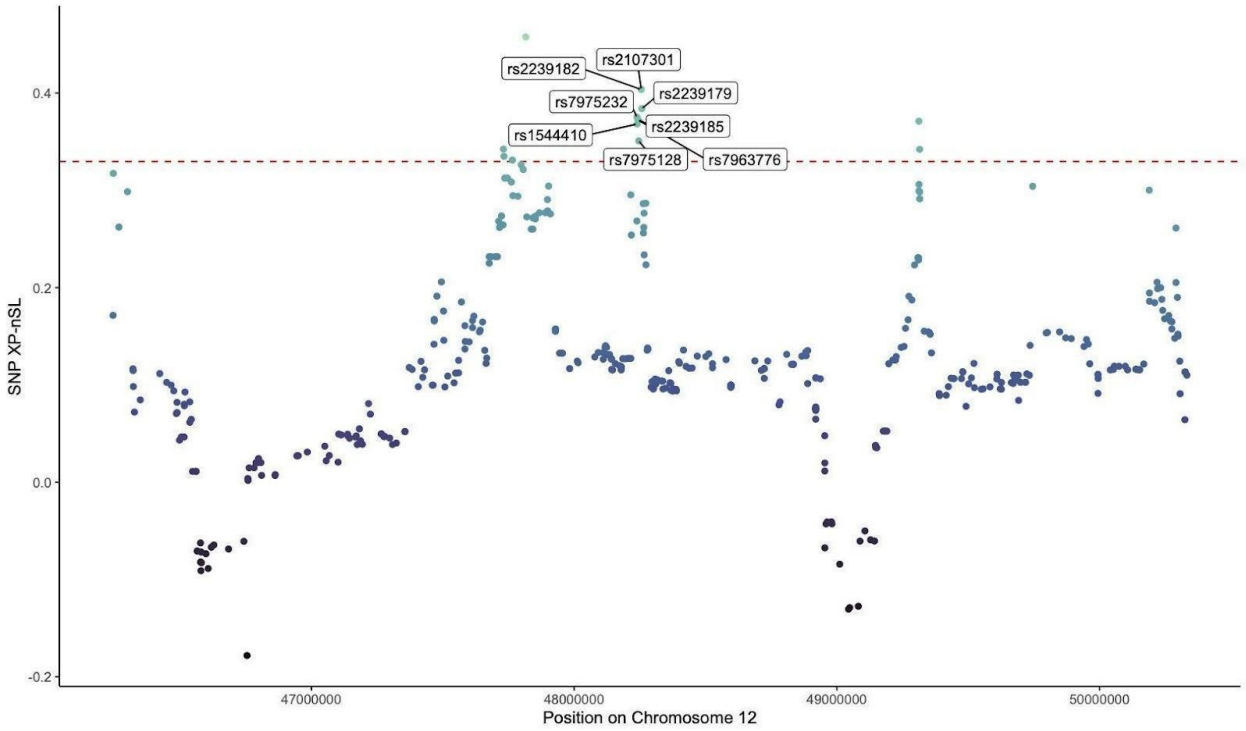

High scoring haplotype detected around *VDR*. Each dot represents a SNP. Location on the X axis represents position on Chromosome 12. Both the color of the dot and location along the Y axis correspond with XP-nSL scores. The 99.5% genome-wide threshold for SNP XP-nSL scores (0.329 is indicated by the red dotted line: labeled points (SNPs) indicate variants within the coding region of the gene that were considered to be statistically significant.

Figure 3.10 (Supplemental Figure 1): Koppen Climate Map of Peru

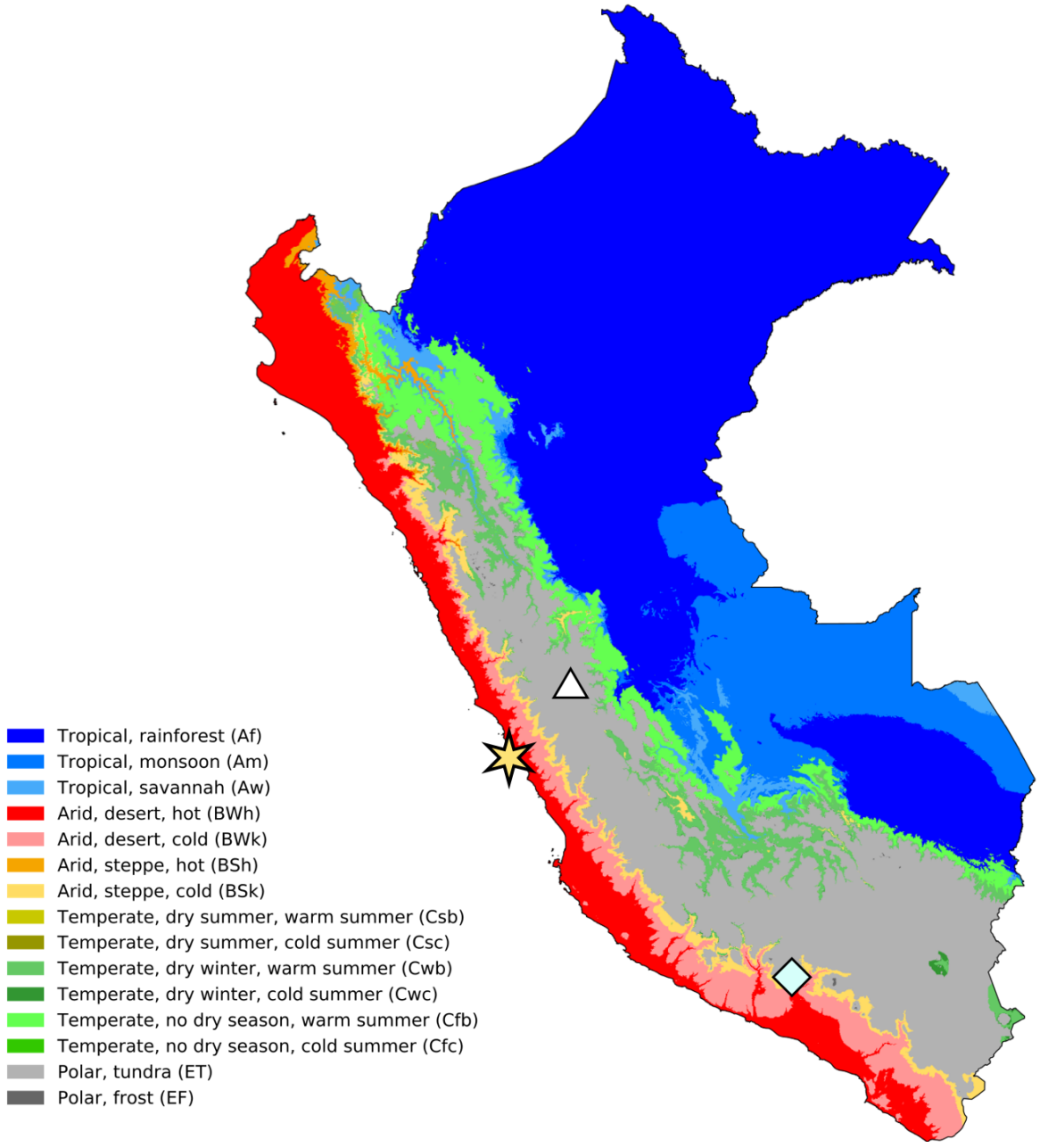

Koppen climate map of Peru modified from Beck et al. (2018). The triangle shows location of Cerro de Pasco, one of the recruitment sites; the star indicates the location of Lima, Peru, the second recruitment site. Diamond indicates the location of Cuncaicha, the ancient high-altitude archaeological site described by Rademaker et al. (2014) that dates back to 12,400 years before present. Color of the terrain corresponds with the climates listed in the legend.

Figure 3.11 (Supplemental Figure 2): SNPs within DUOX showing Divergence

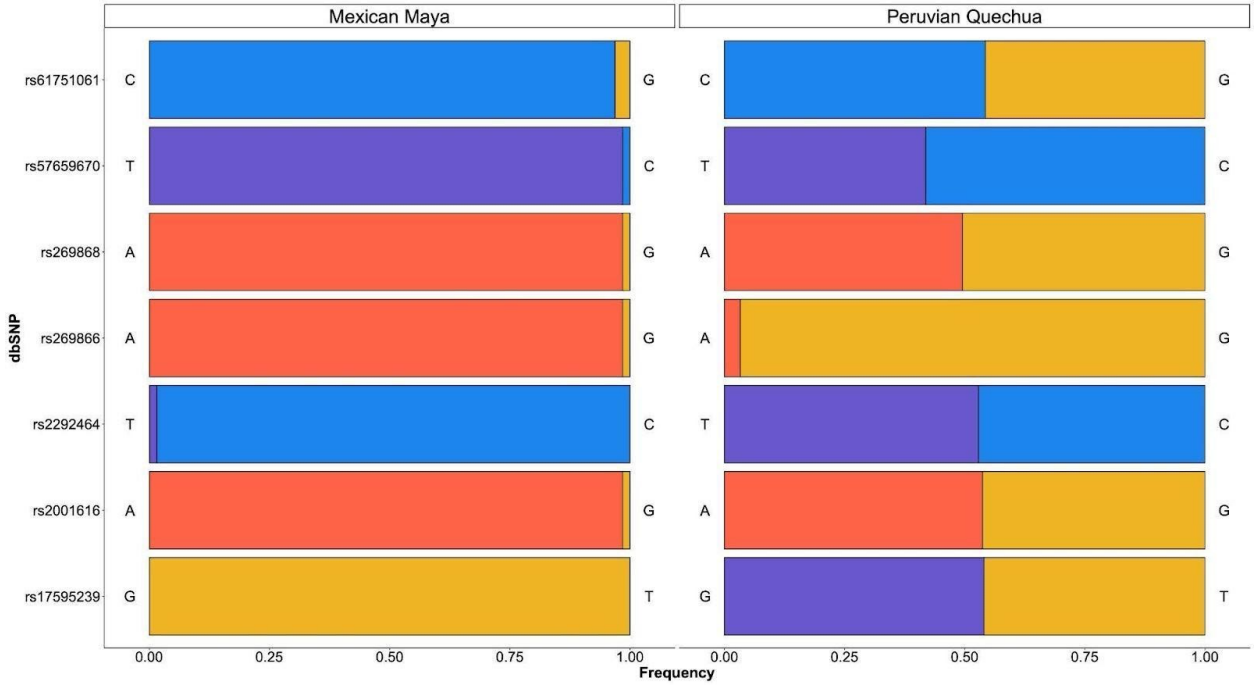

SNPS in the DUOX family that are highly differentiated between Mexican Mayans (left) and Peruvian Quechua (right). X axis represents frequency. Y axis represents SNPs, labeled with their dbSNP rsID. Colors correspond to bases.

Chapter 4 Facial Anatomy and Cold Climate Adaptation

4.1 Craniofacial Adaptations to Cold Climate Stress

Evidence for local adaptation can be seen in populations that inhabit various climatological extremes. These adaptations come in the form of physiological, anatomical, and genetic innovations to offset the stressors unique to particular ecological regimes (Scheinfeldt and Tishkoff 2013). One hazardous environment in which humans have thrived is that of high altitude. The high Andes, which have been occupied for over 10,000 years (Rademaker et al. 2014), have a climate marked by low oxygen availability, extreme cold, strong winds, and significant humidity gradients. For every 1000 meters gained in altitude, temperatures lapse at a rate of about 6 degrees Celsius, which in the Andean highlands creates tundra-like environments where there is often permanent snow and ice (Brush 1982, Minder et al. 2010). In the coldest months, the Andean Altiplano is very dry (near-zero percent humidity), and average night time temperatures are near or below freezing for much of the year (Baker 1963). However, extreme weather events (e.g., cold surges) and past climatic shifts would have made living in this region far more hostile than it is today.

During the Little Ice Age, the Peruvian Andes were blanketed by glaciers, and throughout the region ambient temperatures may have been colder by some 4.6 degrees Celsius (Polissar et al. 2006, Vuille et al. 2008). Andean populations have buffered against this persistent cold by using shelter, clothing, and fire (Baker 1963). However, even with cultural adaptations, and in tandem with other physiological stressors such as hypoxia, the ability to thermoregulate can be significantly compromised (Kottke et al. 1948, Johnston et al. 1996). During cold exposure,

humans experience a suite of physiological changes including peripheral vasoconstriction, increases in blood pressure, shivering, and increased total energy expenditure. Crucially, cold is a known contributor to impaired cardiovascular function and even death at high altitude (Ocobock 2016, Granberg 1991, Hampton 1981). Furthermore, individuals experiencing hypoxia exhibit reduced physiological responses to cold stimulus, which further drives down core body temperature (Kottke et al. 1948, Johnston et al. 1996). Given the multiplicative effects of cold and hypoxia, it is likely that altitude-adapted populations have undergone selection to low ambient temperatures. In particular, it is possible that the skull and face have undergone evolutionary changes considering that these anatomical components usually remain cold exposed and are critical for normal bodily function related to temperature homeostasis (e.g., gas exchange, respiration).

While there is little reported regarding human anatomy and cold climate adaptation [at high elevation, one might expect craniofacial changes in extreme high-altitude populations to mirror changes seen in humans that live in extremely high latitude regions of the planet]. Indeed, increased facial and nasal projection, morphology that has been proposed as an evolutionary adaptation that facilitates the warming of cold air (Fukase et al. 2016, Leong and Eccles 2009, de Azevedo et al. 2017, Churchill 2014) is seen in some living humans and also in classically cold-adapted populations such as Neanderthals. Additionally, evidence from traditional morphometrics studies in human populations suggests that sagittal measurements of both midfacial and nasal protrusion (both relative and absolute) tightly correspond to climate variables, whereas transverse measurements do not (Carey and Steegmann 1981). It is argued that adaptation of the skull and face is largely restricted to groups inhabiting “extremely” [*sic*] cold environments such as those of high latitude (Hubbe et al. 2009). Following the model of Thomson, who observed that variation

in nasal size corresponds with climate variables, humans from cold regions are expected to exhibit higher and larger noses compared to humans from warm regions (Thomson and Dudley Buxton 1923). In a similar vein, populations from cold, dry climates exhibit greater nasion-prosthion height, greater nasal height, and longer simotic subtense (i.e., projection of the nasal bridge from the simotic chord, the minimum horizontal breadth of the nasal) (Schwartz and Tattersall 1996).

Evidence from global human populations indicates that nasal projection is greater in populations inhabiting cold relative to hot regions, and is greater for populations inhabiting regions that are arid relative to humid (Carey and Steegman 1981). Related to this is the size of the internal nasal fossa, with longer and taller nasal fossa seen in colder, drier environments, whereas shorter, smaller nasal fossa are seen in tropical environments (Maddux et al. 2016). Similarly, the nasal turbinates of populations from the Arctic Circle are superoinferiorly and mediolaterally larger than those from populations inhabiting humid, warm regions of equatorial Africa (Marks et al. 2019). Additionally, cold-adapted populations from the circumpolar north have a significantly more narrow and elongated upper nasal passage (which redirects incoming air away from passage along the nasal floor) and an overall greater surface area-to-volume ratio of the nose (Noback et al. 2011): this increases the area over which cold, dry air comes into contact with the nasal mucosa (Yokley 2009). Finally, studies of airflow dynamics, heating, and moisture exchange in 3D reconstructions indicate that the majority of nasal conditioning occurs before air reaches the nasopharynx, and turbulence of inspired air begins at the back of the nasal vestibule (i.e., at the start of the bony nose) (Doorly et al. 2008a, Doorly et al. 2008b). In 3D nasal models developed by Naftali et al. (2005), it was shown that 92% of necessary warming and 96% of necessary humidifying was accomplished by the nose (Issakhov et al. 2021). Together these data suggest that the nasal passage

functions much like an airlock, in which both heat and moisture are exchanged to make inspired air less harsh for the lungs.

Clinical studies that have isolated the effect of cold air inhalation reveal that breathing in cold air triggers bronchoconstriction, increased heart rate, increased systolic and diastolic blood pressure, increased blood pH, and increased concentration of the partial pressure of oxygen (PO_2) and oxygen (O_2) in arterial blood (Hattenhauer and Neill 1975, Fontanari et al. 1996, Heindl et al. 2004). Considering the stress of low oxygen availability, physiological changes associated with breathing in cold, dry mountain air could be particularly harmful. Given that the high Andes are both exceptionally arid and have low temperatures for the majority of the year, it is possible that communities such as the Peruvian Quechua have evolved craniofacial adaptations to condition inspired cold air (Noback et al. 2011, Marks et al. 2019).

Understanding the correlates of diversity seen in facial phenotypes contributes to our knowledge not only of niche-specific adaptation, but also to our understanding of facial variation in deeper evolutionary timescales (Schwartz and Tattersall 1996, Antón and Kuzawa 2017). Given the lack of cartilaginous preservation on subfossil humans, it is crucial to determine how variation in soft tissue anatomy corresponds with general changes in the skeletal midface, as well as climatological factors, sexual dimorphism, and other components related to local adaptation (Franciscus and Trinkaus 1981, Yokley 1999, Noback et al. 2011). The goal of this project is to test the relationship between environmental factors such as aridity and cold and variation in craniofacial shape. Specifically, I predict that the highland Peruvian population will exhibit an enlarged nasal cavity and more projecting midface, two traits believed to contribute to thermal stasis (Noback et al. 2011). To test this hypothesis, a geometric morphometrics approach was used to identify craniofacial changes associated with climate variables between two populations: (1) the

putatively cold-adapted Peruvian Quechua from the high Andes, and (2) Mayans from Mexico, a population that inhabits a hot, humid climate in which there is no apparent need to moisten and warm inspired air.

4.2 Methods

4.2.1 Participant Recruitment

Study participants from two populations were included in this study: (A) individuals of Peruvian Quechua ancestry, from the cold, arid environment of the high Andes, and (B) Mexican Mayans from the humid, hot environments of Mexico's Yucatan peninsula. Participants were recruited as part of a larger effort to understand physiological and genomic adaptations to high-altitude environmental stressors including but not limited to hypoxia, cold, and ultraviolet radiation. Peruvian Quechua participants (N = 102; Female = 47; Males = 55) were recruited from Cerro de Pasco, Peru (4,300 m) in July of 2017 by a research team from the University of Michigan, Syracuse University, and Universidad Peruano Cayetano Heredia. Peruvian study participants were born, raised, and resided at high altitude, and their parents and both sets of grandparents were of high-altitude ancestry. Mexican Mayan participants consisted of Tzeltal, Tzotzil, or Ch'ol-speaking individuals who were recruited in Palenque, Chiapas, Mexico (N = 100; Female = 46; Males = 54) during the summer of 2015 by a research team from the University of Michigan and Centro de Investigaciones Docencia y Económica (CIDE). Peruvian and Mexico study participants were unrelated adults, between the ages of 18 and 35, in good health and with no apparent craniofacial trauma that would influence the results of this study. Forty of the Peruvian participants contributed whole blood samples for DNA extraction; for

these individuals, self-reported sexes were verified with SNP data, and were used to filter out any closely-related individuals.

At the time of study enrollment, all study participants provided written informed consent in Spanish. The Peruvian arm of the research was approved by the Institutional Review Boards of the University of Michigan, Syracuse University, and Universidad Peruana Cayetano Heredia, and the Mexican arm by the Institutional Review Boards of the University of Michigan and Centro de Investigaciones Docencia y Economica.

4.2.2 Data Collection

Digital facial stereophotogrammetry is a well-established method of creating a dense 3D point cloud by stitching together a series of overlapping 2D images (Claes et al. 2018, Zaidi et al. 2017. To reconstruct facial anatomy for each participant, three stereoscopic images (a.k.a., an image-set) were taken for each face by a trained technician using a Vectra H1 handheld 3D imaging system (Canfield Scientific, Parsippany, NJ). These three images (or observations) were collected simultaneously while the imaging system was tethered directly to a computer: this provided instant feedback to the technician so that they could be sure that the software did not flag any QC errors in the creation of a 3D image. From this 3D image, the Vectra software system (Canfield Scientific, Parsippany, NJ) automatically detected facial features and assigned five positional landmarks: two were placed on the inner corners of the eyes, two on the lateral-most corners of the mouth, and one at the foremost position of the nose (a.k.a. tip of the nose), which were verified by the technician at the time of data collection. If there were any detected errors in automated landmark placement (i.e., positional landmarks flagged by Vectra), the technician then re-photographed the participant. Only the 3D images for which the Vectra software was able to automatically digitize the five

positional landmarks were retained for this study (i.e., no images that required manual landmark digitization were used in analysis).

The resulting 3D images were processed by trained collaborators at Pennsylvania State University. Following the method described by Claes et al. (2018), collaborators cropped the 3D images close to the face and removed any hair, ears, or other obstructions that may have entered the margins of the 3D images. Using the five positional landmarks, the stereoscopic facial scans were aligned and oriented as digital reconstructions in 3D space. Next, an anthropometric mask (AM) was mapped to this standardized surface template, establishing a spatially-dense quasilandmark (QL) configuration (N_{QL} = 7,160) for each participant. This method of 3D phenotyping was performed using the MeshMonk toolkit in MatLab (Mathworks, Natick, MA). Facial size was calculated as the centroid size of all QL configurations, and was produced within a generalized Procrustes analysis (GPA) framework. Centroid size was calculated as the square root of the sum of squared distances from each landmark to the geometric center of the configuration (i.e., the midpoint of all points in the 3D anthropometric mask). The outputs of these standardized point clouds were compiled into a single CSV file of 3D coordinate data (i.e., X, Y, and Z coordinates), then were imported into R.

This automated method often is used in genome-wide association studies to quantify the genetic contribution to facial shape (Claes et al. 2018, Zaidi et al. 2017). The pointcloud generated by this phenotyping method is very precise: a study by our collaborators (White et al. 2019, who developed this method) indicates that there is ~32% less variance in automated landmark placement (0.27 mm) than what is observed in repeated manual landmark placement by trained technicians (0.3974 mm). Additionally, White et al. (2019) report that the delta (i.e., linear distance) between manually- and automatically-digitized landmarks is less than 0.7 mm,

suggesting that the automated method (three simultaneous facial observations) is comparable to repeated human-mediated landmark digitization.

4.2.3 Statistical Analysis

To identify population structure and to check for mis-mapped facial configurations, principal component analysis (PCA) and canonical variate analysis (CVA) were performed in R. PCA was performed to reduce dimensionality of the data, and the top two PCs were exported for CVA. CVA minimizes within-group variation while maximizing population differentiation, allowing an observer to identify population clusters within variate space. PCA and CVA were conducted in R using the GeoMorph package and were graphed using the ggplot2 and ggforce packages (Adams et al. 2020, Pederson and RStudio 2021).

To detect variation in midfacial projection associated with population affinity, landmarks along the sagittal plane were isolated for analysis (Figure 1). A total of 106 landmarks located along the sagittal plane were extracted and 'flattened', a process that removed slight horizontal (i.e., left or right) deviations from the midline when crania were oriented in standard anatomical positions. While midfacial variation is not restricted to soft tissue of the sagittal plane, these 106 landmarks are informative for several reasons: (1) the focus of this research is to investigate variation in maximal protrusion along the midline of the face; for a given cross-section of the human face, the anterior-most landmark on that plane tends to fall along the sagittal line; (2) the tip of the nose and the maxilla are the most protrusive components of facial anatomy, and (3) previous morphometrics studies such as that of Carey and Steegmann (1981) suggest that sagittal measurements of midfacial and nasal protrusion tightly correspond to climate variables, whereas transverse measurements are not as closely related to climate. These 106 landmarks were analyzed using the GeoMorph package in R (Adams et al. 2020). With the resulting datasets of

scaled linear distances, Procrustes ANOVA was used to test the null hypothesis of no difference in the projection along the facial midline when controlling for size and grouping variables of population affinity and sex. This was completed in R using the procD.lm() function, with which 1000 permutations of the model were performed. Results were considered significant at the 95% confidence level.

To visualize changes in midfacial projection between groups, consensus crania were generated for populations and sexes using the gpagen() function in R. Consensus crania are produced by calculating the mean X,Y coordinate per landmark across individuals within a sample. In other words, consensus crania represent the "average face" for each sex within a population. A consensus cranium was produced for each population by sex and again using all individuals to produce a global consensus. To model variation in nasal and midfacial projection, interlandmark distances were calculated for the following traits: 1. height of the bony nasal aperture, measured as the length of the segment between nasion and subnasale, 2. projection of nasal cartilage, measured from subnasale to tip of the nose, 3. chord length of the nasal ridge, measured from nasion to the tip of the nose, and 4. the external nasal profile (ENP). Distances were computed using the interlmkdist() function in GeoMorph (Adams et al. 2020). The length of ENP was calculated by adding consecutive interlandmark distances (again using interlmkdist()) between the 22 quasilandmarks that are distributed between the tip of the nose and nasion.

To test the null hypothesis of no differences in size or length in mean interlandmark distances, a global Procrustes ANOVA was performed using Geomorph in R. This method has been widely applied to human and non-human primate crania and various human postcranial elements (Profico et al. 2017, Fricano and DeLeon 2020, Ricklan et al. 2020, Uy et al. 2020). To

identify which specific changes in midfacial configuration vary between populations, pairwise t-tests were calculated using the stat_compare_means() function in R: these pairwise tests used the null hypothesis of no difference in interlandmark distances between samples and sexes as interactions. The resulting p-values were adjusted following Holm and Bonferroni, and were considered significant at the 95% confidence level. The distributions of interlandmark distances were represented in boxplots generated using the ggplot2 package, with Holm and Bonferroni-adjusted p-values calculated using compare_means() function in R (R Core Team 2021).

4.3 Results

4.3.1 Population Clustering

The first and second principal components (PCs) accounted for 27.89% and 17.91% of the variance respectively. The first PC separates each population, whereas the second PC separates populations by sex (Figure 2A, Figure 2B). Exporting these two PCs to produce canonical variate (CV) scores yielded similar results. The majority of variation in the CV space could be attributed to sex (CV1 = 63.55%), and population affinity (CV2 = 31.99%). To identify which components of population clustering were associated with putatively-adaptive changes in midfacial anatomy, a geometric morphometrics framework was applied to craniofacial landmarks distributed along the sagittal plane.

4.3.2 Population-Specific Variation in Midfacial Anatomy

To test the null hypothesis of no statistically-significant difference between populations in terms of midfacial projection (i.e., protrusion along the sagittal plane of the face), a Procrustes

ANOVA was performed using 106 landmarks distributed across the sagittal plane of the face (Supplementary Table 4.1). Results of the Procrustes ANOVA indicated that there were statistically-significant differences in midfacial projection associated with centroid size ($p < 0.001$, $F = 21.7411$, $Z = 4.8483$), population affinity ($p < 0.001$, $F = 4.7965$, $Z = 2.9101$), sex ($p < 0.001$, $F = 17.6097$, $Z = 5.1841$), and the interaction of centroid size and sex ($p < 0.001$, $F = 3.559$, $Z = 2.2606$).

For the 212 total landmark variables (i.e. 106 QLs with distinct X and Y coordinates), 95 had significant differences in their positioning in 3D space: from these, 23 landmarks showed differences resulting from population affinity (either alone or in combination with interacting variables). Population affinity without interactions with centroid size or sex predicted the 3D positioning of 17 different landmarks. Notably, these included three landmarks distributed across the subnasal clivus (QL50 through QL52), which mirrors the height of the nasal aperture. The remaining landmarks that reached significance for population affinity alone included seven landmarks distributed about the lower lip (horizontal orientation of QL32 and QL33, vertical orientation of QL35 through QL38) and the horizontal (anteroposterior) orientation of four landmarks on the chin (QL24 through QL27) and mentolabial sulcus (QL28 through QL31). For the remaining landmarks distributed across the face (i.e., excluding landmarks that are distributed across the mandibular tissues), there were statistical differences in the horizontal orientation of two landmarks located on the upper lip -- QL41 and QL42 -- corresponding to population and sex (Population: $p = 0.0481$, Sex: $p = 0.0432$) and for population as well as sex when controlling for centroid size (Population: $p = 0.0496$, Sex*Centroid: $p = 0.0454$). Centroid size was more significantly associated than other variables followed by population affinity (QL51: $p = 0.0395$).

Increased nasal projection, which is thought to be adaptive for the warming and conditioning of air, is a putative cold climate adaptation that one might expect to see in the Peruvian Quechua sample. Instead of modeling for population affinity alone, it is important to account for sex as a covariate in order to account for different developmental schedules and morphological variation seen between males and females (see Section 4.2). In this study, statistically-significant differences were observed between populations and sexes for components of nasal projection (Table 2). There were significant differences in the projection of nasal cartilage between Mayan females and Quechua females (p_{HB} = 0.013), Mayan females and Quechua males (p_{HB} = 0.0001), and Mayan males compared to Quechua males (p_{HB} = 0.035) (Figure 3).

For the length of the nasal ridge, measured as a chord spanning the nasion to the tip of the nose, statistically-significant differences were observed between Quechua and Mayan females (p_{HB} = 0.0034), Mayan females and Quechua males (p_{HB} = 1.4 x 10^{-6}), and between males from both groups (p_{HB} = 0.00034) (Figure 4). For height of the bony nasal aperture, modeled as the linear distance from nasion to subnasale, statistically-significant differences were detected between Mayan males and Quechua males (p_{HB} = 0.032) as well as Mayan females and Quechua males (p_{HB} = 0.0016) (Figure 5).

To identify differences in nasal size that might result from changes in the external shape of the nose, interlandmark distances were calculated for consecutive QLs ranging from nasion to the tip of the nose (Figure 6). This model of the length of the ENP was statistically significant between all groups except for within Mayans. The most significant difference was shown between Quechua males and Mayan females (p_{HB} = 8.3 x 10^{-9}), followed by the comparison of

both sets of males (p_{HB} = 9.9 x 10^{-8}). Additional differences in ENP length were significant among females (p_{HB} = 0.0012) and Mayan Males compared to Quechua females (p_{HB} = 0.014).

One method of identifying how variables such as centroid size or facial size contribute to variation in shape is through Procrustes ANOVA. Here, a Procrustes ANOVA was performed to identify whether this apparent difference in ENP length was the result of variation in facial size (i.e., centroid size) or other factors (i.e., sex, population affinity). Results revealed no association with centroid size, but significant relationships with population ($p < 0.001$), sex ($p < 0.008$), and the interaction between centroid size and population ($p < 0.034$). While the lengthened ENP observed in both Peruvian samples was associated with sex, this described only a small proportion of the observed variance ($R^2 = 0.0330$); conversely, population affinity predicts roughly 20% of the variance in the model ($R^2 = 0.1924$).

In order to visualize these differences in midfacial projection between populations as well as for each population compared to the global consensus cranium, crania were aligned along their positional landmarks, after which deformation grids of the sagittal plane were produced (Figure 7). In both populations, males had a more protrusive midface than females as was indicated by the more anterior position of landmarks within the sagittal plane. For each sex, the Quechua sample had a more protrusive midface than the Mayan sample. Overall, projection of the midface was most pronounced in Quechua males. Viewed in the context of the deformation grids, the greater linear distance in nasal protrusion in Mayan males relative to their male Quechuan counterparts (i.e., for the cartilaginous portion of the nose) appears to result from both a superior positioning of the tip of the nose in the Mexican sample and an anterior placement of subnasale in the Peruvian sample (Figure 8). Additionally, the bridge of the nose is far higher in the Andean sample relative the Mesoamerican sample when accounting for sex. The position of

the tip of the nose in Quechua females approximates that of Mayan males, while the nasal bridge in Mayan males remains slightly more protrusive than Quechua females. Mayan females have the least elongated (i.e., most posteriorly placed) nasal complex out of the four subsamples. Finally, both male and female Mayans have an apparently shorter face compared to Peruvian participants, evident by the inferior position of the uppermost QLs and the superior position of the lower QLs relative to the Peruvian sample.

4.4 Discussion

The morphometrics analysis of this study tested the null hypothesis of no difference in midfacial projection between Peruvian Quechua and Mexican Mayan samples. This is a proximate model for how groups living in distinct environments may develop unique morphological responses to combat climatological stressors (e.g., low temperatures and high aridity). Our results showed significant associations of population affinity with differences not only in midfacial projection but also in nasal form, rejecting the null hypothesis of no difference. Specifically, our results indicate that for each sex, the mean of the Quechua sample has greater average height of the bony nasal aperture and nasal ridge length than their counterparts from the Yucatan. This appears to be driven primarily as a result of an anterior positioning of the maxilla in the Quechua sample, which leads to an extension in the overall length of the ENP. This also explains the statistically-significant differences in the orientation of the subnasal clivus and the horizontal positioning of soft tissues in the upper lip.

The ability to offset environmental stress is crucial for human populations who settle novel ecological niches. While evolutionary adaptations to altitude-induced hypoxia have been observed in populations from the Andes, little attention has been paid to how these communities adapt to cold climate stress (Bigham et al. 2009, 2010; Brutsaert et al. 2019). Temperatures lapse

by about six degrees Celsius for every 1000 meters gained above sea level, and coupled with variable humidity and high winds, these high-altitude zones promote environments that are relatively hostile for human occupation (Minder et al. 2010). Furthermore, individuals experiencing hypoxia have decreased thermoregulatory output, which increases the severity of cold exposure. Despite these factors, between one-quarter and one-half of the populations of Peru, Ecuador, and Bolivia live above the 2,500 meter threshold that defines high altitude (Tremblay and Ainslie 2021). It is unclear whether such populations from the high Andes have evolved to offset the stress of low ambient temperatures, especially as it pertains to anatomical changes in the face and skull. Analysis of craniofacial variation in putatively cold-adapted populations can reveal the components of facial anatomy that are perhaps adaptive to the stressors of cold, thin atmosphere.

4.4.1 Phenotypic Plasticity and Anatomical Variation in Human Crania

In addition to putative evolutionary adaptations that influence skeletal morphology, the human skull exhibits an incredible amount of phenotypic plasticity. Phenotypic plasticity can be recognized as changes in attributes (here, in the skull) not resulting from underlying genetic change but rather as a response to environmental stimuli (Antón and Kuzawa 2017) or from neutral evolutionary change (Howells 1973, von Cramon-Taubadel and 2008). A significant proportion of changes in craniofacial shape derive not necessarily from genetics but from masticatory behavior, with unrelated human populations converging on similar craniofacial morphologies resulting from diet (Katz et al. 2017). Notably, populations that derive significant caloric input from soft or liquid food sources have less robust masticatory apparatus given that biomechanical loading of the skull is relaxed (Strait et al. 2007).

Morphological analyses between dairying and cereal-cultivating subsistence communities show differences in the size of the anterior temporalis, masseter, and medial pterygoid muscles, the height of the palatal vault and "peaked"-ness [*sic*] of the cranial vault, as well as maxillary/palatal length (Katz et al. 2017). At the extremes of the global human habitation range, where climate is either too hot or too cold for subsistence agriculture to take place, reduced reliance on agricultural food-stuffs might mask or amplify putative evolutionary adaptations to the skull and face.

Further evidence of the plasticity of cranial form was reported in the classic publication by Franz Boas (1912). This study investigated the role of environment in influencing skull morphology in European migrants from Southern and Central Europe, and American-born children from these same immigrant communities. The results showed that while there is variation in ancestral cranial form, and while population-level differences may not be completely eliminated, cranial phenotypes among European-migrant children (e.g., cephalic index) converged on similar forms regardless of their ancestry. This indicated that high degrees of heritability in cranial form were minimized when environmental stimuli were changed or removed. In other words, while genetic factors undoubtedly play some role determining in skull shape (e.g., at the genus level), changes in craniofacial form are not independent of any shared combination of climatological, dietary, or experiential factors faced by a given population at a given moment in time (Antón and Kuzawa 2017).

Unlike the rest of the human cranium, which can apparently be modified by environmental factors, it appears that normal *nasal* morphology is highly canalized, and that adult nasal shape is solidified very early in life (Shaffer et al. 2016, Zaidi et al. 2017, Claes et al. 2018, Butaric et al. 2021). The implication of this is that components of nasal morphology *not* attributable to

environmental stimuli may be driven either by neutral evolutionary change or environmentally-mediated selection (Zaidi et al. 2017). It is possible that some combination of genotype and environment contribute to adaptive differences in craniofacial form that help to offset the burden of high altitude, cold climate, and super-arid conditions.

4.4.2 Sexual Dimorphism and Human Cranial Variation

In humans, an individual's sex is determined by a suite of genetic and developmental variables variables that creates a continuum of highly polymorphic sex characteristics (Astorino 2019). At the extremes of this distribution, individuals have classicially been assigned as female or male given the appearance of "typical" [sic; Astorino 2019] traits: these differences are often summarized as sexual dimorphism, a concept that is of particular importance to skeletal biology, evolutionary science, and anthropological archaeology (Frayer and Wolpoff 1985, Larsen 2003, Garvin et al. 2017, Best et al. 2018, Dunsworth 2020). While the term dimorphism incorrectly implies the existence of a sex binary, it is a useful descriptor to examine how sex corresponds to components of anatomy and physiology.

While not a primary focus of our research, this study identified differences in components of facial anatomy that spanned both the variables of population affinity and sex (e.g., ENP between Mayan Female and Quechua Male). Sex was a significant predictor for 73 possible orientations (vertical or horizontal placement of midsagittal QLs), and the interaction of sex with either population affinity and/or centroid size account for an additional 83 significant differences in QL placement. Across the landmark dataset, this influence of sex on facial anatomy was widespread enough that sex was a significant contributor to population clustering (CV1 = 63.55% of variance).

Previous studies of local adaptation in craniofacial anatomy have showed similar results of sex-based differences in facial form within and between populations, and it appears that some components of sexual dimorphism in the face might appear as early as one year of age (e.g., forehead recession in males relative to females; Matthews et al. 2016; Bastir et al. 2011, Bejdová et al. 2013). This process of differentiation derives from a set of developmental changes in utero, which following different developmental and experiential trajectories in early life, manifest as a spectrum of skeletal, muscular, and hormonal differences between individuals (Dunsworth 2020). During puberty and ultimately adulthood, distinct reproductive endpoints, investment strategies, and survival goals all act to shape components of average female and male body morphology that can be gleaned from the skeleton (Fuentes 2021).

One component of dimorphism that is likely a significant contributor to variation seen in morphometrics studies is that males, on average, tend to be larger than their female counterparts (for landmarks distributed across a 3D face, this is seen as differences in centroid size). This disparity in size is likely not the result of selection for larger males, but rather might be a byproduct of sex-specific differences in the duration of growth periods and other constraints on females (e.g., increased estrogen leading to earlier growth arrest; Dunsworth 2020). Similar to what is seen in the postcranial skeleton, hormonal differences are known to broadly influence aspects of facial morphology. For example, a twenty-year follow-up study by Whitehouse et al. (2015) showed that variables such as prenatal testosterone exposure were significantly associated with how feminized or masculinized an individual's face appears in adulthood. Altered hormonal production leads to changes in craniofacial morphology as has been demonstrated in both animal models and clinical settings (Haralabakis and Dagalakis 1980, Pirinen 1994). As such, developmental differences

related to hormone production and growth likely contribute to sex-based differences in cranial morphology.

4.4.3 Geometric Morphometric Analysis of Variation in Midfacial Projection

The Mexican Mayan and Peruvian Quechua communities are fairly closely related at the genomic level, yet they inhabit distinct environments: Mexican Mayans in a hot, humid region; Peruvian Quechua in a cold, arid region. In the interest of identifying how adaptation to local climate stress may influence craniofacial morphology, this study applied a geometric morphometric framework to identify population-specific changes in midfacial projection. To this end, data from spatially-dense 3D point clouds were generated for Peruvian Quechua, a putatively cold-adapted group from the high Andes, and Mexican Mayans, a population inhabiting a humid subtropical region of the Yucatan Peninsula. One hundred and six landmarks distributed along the sagittal plane were isolated from 3D facial reconstructions and were analyzed to identify variation in midfacial projection. Procrustes ANOVA revealed statistically-significant differences in midsagittal facial configuration related to centroid size, population affinity, sex, and the interaction between centroid size and sex; this rejects the null hypothesis of no differences in facial shape, indicating that each population has distinct components of midfacial morphology. This alone neither answers whether these differences in facial anatomy result from changes encoded in DNA, nor does this answer whether craniofacial differences arose from drift or selection: however, it indicates that there are statistically-significant differences in the “average” face between populations.

To identify which components of midfacial anatomy varied between groups, interlandmark distances were calculated between QLs distributed along the midfacial sagittal plane. These results revealed that the Peruvian Quechua possess a longer nasal ridge, a taller nasal cavity seen only between males from each group, and an overall lengthened size of the ENP. These significant differences in the length of the ENP were not the result of an overall larger face (modeled by centroid size) and were weakly predicted by sex, but more strongly by population affinity. Additionally, the Peruvian sample has a more anterior position of the alveolar process of the maxilla, which resulted in a forward shift in the entirety of the external nose and upper lip: three landmarks located on the subnasal clivus -- QL50 through QL52 -- were statistically significant between populations even without the effect of sex, indicating divergence in the orientation/position of this component of the midface (Table 1). Unexpectedly, the Mexican Mayan sample had greater projection of the cartilaginous portion of the nose, but it is likely a result of a posterior position of the subnasal clivus coincident with a superior shift in the orientation of the tip of the nose. This is likely related to a relatively down-turned nose in the Peruvian sample, which minimizes the linear distance between the subnasale and tip of the nose. Together these results align with the expectation that cold-climate, high altitude-adapted populations would have a larger, more protrusive nasal chamber as has been described for Fuegians, Aleutian Islanders, and Siberians (Noback et al. 2011).

In these populations, lengthening of the ENP is suggested to increase the volume and turbulence of air that can be retained within this nasal-midfacial complex. This larger chamber would enhance the moistening and warming capabilities of the internal face as it exposes a greater amount of air to nasal mucosa, a trait that would be beneficial in environments where the air is dry and cold (Yokley 2009). In particular, this higher SA:V ratio allows a greater amount

of inspired air to flow across the nasal mucosa, a process which facilitates the exchange of heat and moisture of air before it enters the lungs (Marks et al. 2019). As such, putatively cold-adapted populations are predicted to have a relatively large nasal complex compared to related populations inhabiting warmer environments.. This study showed a statistically-significant difference in the projection and height of the nasal profile in Peruvian Quechua relative to Mexican Maya. Additionally, the anterior positioning of midfacial landmarks within Peruvian Quechua, along with the shortened projection of the nasal cartilage, may be a factor that drives enhanced turbulence of inspired air, a critical function for body temperature regulation that leads to the mixture of inspired air within the boundary layer of the nasal mucosa (Noback et al. 2011).

4.4.4 Error and Uncertainty

Potential sources of uncertainty in geometric morphometrics include: measurement error, specifically from the incorrect placement of landmarks; error due to improper specimen/sample preparation (e.g., if a fossil is reconstructed in an inaccurate manner); and errors due to inconsistencies in the positioning of photogrammetric equipment, resulting in the skewing of images (i.e., parallax) (Fruciano 2016). Repeated measures are a method of assessing uncertainty (Arnqvist and Mårtensson 1998). To do this, either an observer can generate data multiple times on the same participant, or multiple observers can generate data in tandem (Fruciano 2016). In either case, error is understood to be low if there is a high degree of concordance between measurements. Several studies have shown that measurement error from digitization is relatively low compared to variation among individuals (Debat et al. 2003, Breuker et al. 2006).

To minimize error from poor landmark registration, this study used an accurate, automated method that collected three synchronous stereoscopic images of the face. Any image-

set that passed QC was stitched together and used to create a point cloud from which 3D coordinates per landmark per individual were used. Analysis by our collaborators revealed that this method of positional phenotyping with MeshMonk is accurate within 1.26 mm of average error (White et al. 2019). Given that landmark digitization was automated, and given the stringent filtering criteria omitted any stereoscopic image-set that failed QC (i.e., that required manual landmark placement), there is little potential for observer error related to the placement of landmarks.

4.4.5 Results in the Context of Previous Work and Limitations

The results of this study in some ways run contrary to previous work investigating the effects of climate on midfacial anatomy. While several authors have investigated how factors such as temperature and humidity influence nasal form, these studies have primarily worked with populations that inhabit sea level, albeit at high *latitude* (Wolpoff 1968, Carey and Steegmann 1981). Our results show that a low-latitude, high-altitude population shows components of midfacial anatomy that mirror what is seen in populations from the Arctic, despite residing in the tropics. For example, Peruvian Quechua participants have a larger and more protrusive midface, similar to what is seen in populations from much higher latitudes such as Tierra del Fuego, Alaska, and northernmost Eurasia (Noback et al. 2011).

Studies like that of Carey and Steegmann (1981) showed that protrusion of the nasal complex was strongly associated with a decrease in absolute humidity and latitude, with absolute rather than relative humidity being the best predictor of nasal protrusion. Our results indicate that altitudinal differences perhaps play just as important a role in shaping human variation. Much like traveling northward, ascent to high altitude subjects humans to cold stress (and low oxygen)

and thus might trigger adaptive responses (Brush 1982, Minder et al. 2010). While other regions of the American tropics are generally warm and humid, the Andes are dominated by low ambient temperature and high wind speed, with variable atmospheric moisture content depending on altitude (Maddux et al. 2016). This means models of anatomical variation might not show particularly strong associations with latitude unless they control for altitude.

One limitation of this study is that the geometric morphometrics framework derived from 3D stereophotogrammetry relies on superficial landmark placement. The superficial components of craniofacial variation are important for understanding how the external anatomy of the face corresponds with population affinity, but the positioning of these features at best only approximates underlying (fine-scale) morphological changes in the skull. As such, this project would be greatly enhanced with more information about population-specific changes in thickness of cartilage and nasal bone as well as the positioning of nasal bones relative to the skin and cartilage. If this methodological approach were applied to minimally-invasive forms of imaging such as craniofacial CT scans, we could have an even greater understanding of how soft tissues such as the cartilage at the tip of the nose change in response to environmental factors. Additionally, gathering data regarding the relationship of external nasal topography to the volume of the nasal cavity would provide insight as to the adherence of these midfacial phenotypes to ecogeographic rules like those of Bergmann, Allen, and Thompson (Bergmann 1847, Allen 1877, Thompson and Buxton 1923). The functional significance of these changes can be identified during a cold challenge, in which thermal imaging can be used to identify changes in skin surface temperature resulting from the inspiration of cold, dry air. This could be tested against a variety of nasal or midfacial phenotypes, changing variables such as ambient temperature, humidity, and duration of cold exposure.

A related issue is derived from the statistical analysis of quasilandmarks regardless of species: for QLs that are distributed along a given surface on the basis of linear distance (e.g., distribute 10 equally-spaced landmarks along a chord *AB*), there might not be any specific relationship between spatial variables and the actual function for the corresponding anatomical unit. For example, an observer might detect statistical differences in length between two random QLs distributed along the dorsal fin of a fish, yet this variation in shape or distance might be meaningless if it does not capture biologically-meaningful variation. For this dataset, the quasilandmarks distributed along the sagittal plane contained a number of canonical landmarks that are associated with both Mendelian traits and putatively-adaptive functions (e.g., tip of nose, subnasal clivus, tip of lip, glabella); however, it also included landmarks for which the evolutionary or morphological significance is somewhat unclear (e.g., the ninth quasilandmark between a given chord *BC*). To not lose the forest for the trees, this study paid particular attention to variation in shape as it pertains to the superficial equivalents (i.e., soft-tissue landmarks) of skeletal landmarks that are widely represented in morphological analyses of hominid remains (Franciscus 1999) and living human groups (Zaidi et al. 2017, Fukase et al. 2016, Claes et al. 2018).

A second limitation of this project is that it used only two populations inhabiting opposite extremes of an environmental spectrum: cold, arid environments of high altitude and hot, humid environments of the tropics. By including Indigenous communities from warm, arid environments (e.g., the American Southwest) and cold, boreal environments (e.g., maritime provinces of Canada), we could better understand how midfacial variation correlates with changes along the spectrum of variable temperature and humidity. This is of particular interest considering that at the global scale, some of the largest or most projecting midfaces are in

populations descended from warm, semi-arid environments such as southern Europe (de Azevedo et al. 2017).

Perhaps the largest drawback to this study was that it examines statistical differences in phenotype without investigating underlying genetic or epigenetic changes that might contribute to midfacial form. Many changes in midfacial anatomy are the result of mutations in genes that are active during early development (Gokhman et al. 2020). Maternal stress is known to contribute to phenotypic changes in newborns and this process is critical for neonate survival especially in environmental extremes; it is possible that this happens for aspects of facial anatomy. The adaptive nature of these changes, such as changes in the microvascular vessel density of babies born at altitude, undoubtedly play significant roles in the story of human dispersal into novel ecological niches (Gassman et al. 2016).

While there is a large heritable component underlying midfacial anatomy, there are three arguments that could not be addressed by this project in the absence of genetic data (Richmond et al. 2018). These are that: (1) changes in craniofacial anatomy are the result of environment alone (i.e., same genotype, different phenotype); (2) putative evolutionary changes in midfacial anatomy are the result of drift, not selection (i.e., different genotype by neutral evolution); and (3) differences in midfacial anatomy are the result of recent adaptive evolution private to the high Andes. Each of these could be addressed by conducting sequence-based tests of selection in regions of the genome associated with craniofacial anatomy. One component that might be addressed is examining the effect of diet and other environmental stimuli on craniofacial form; while the shape of the entire skull is widely-reported to be plastic in nature, the attribution of variables such as food toughness on midfacial/nasal anatomy is not particularly clear in these two populations (Gravlee et al. 2003, Antón and Kuzawa 2017, Katz et al. 2017). Both Peruvian

Quechua and Mexican Mayan communities rely on a variety of domesticated plants, but the attribution of potato-based (Peruvian) versus maize-based (Mexican) diets to the phenotypes discussed here could easily be explored. Similar to the work of Boas (1912), our study could be expanded to investigate components of craniofacial anatomy in Mexican Mayan and Peruvian Quechua expatriate or migrant communities (e.g., in the United States), who have converged on similar diets or inhabit similar environments (e.g., a humid subtropical zone). Additionally, how indicators of health and wellbeing (e.g., body mass index, stature, and seated height) covary with components of craniofacial anatomy warrants investigation.

A final drawback to this study is that while it supports the hypothesis that populational affinity is associated with variation in protrusion along the sagittal plane, this study did not examine whether or not transverse landmarks (i.e., going horizontally across the face) do the same. Part of this was by design, given that previous studies such as that of Carey and Steegmann (1981) report an association of environmental factors with variation along the facial midline. Yet without an ability to calculate internal nasal volume from stereophotogrammetry alone, understanding the contribution of midfacial variation in transverse landmarks would have been informative.

4.4.6 Conclusion

This study showed that changes in craniofacial anatomy correspond with the suite of climatological variables unique to high altitude: low ambient temperatures, a humidity/aridity axis, high winds, and low oxygen availability. In this study, we demonstrate that components of craniofacial anatomy such as the lengthened external nasal passage with shortening of nasal cartilage are significantly differentiated between populations inhabiting cold/arid and hot/humid

environments. In putatively cold-adapted groups from high latitude, these changes of midfacial anatomy are hypothesized to facilitate the warming and moistening of harsh mountain air, and thus contribute to body temperature homeostasis (Yokley 2009, Maddux et al. 2016). This evidence of changes in facial shape warrants further investigations as to the ways in which the entire midfacial complex -- from sagittal, transverse, volumetric, and 3D points of view -- contributes to body temperature homeostasis. If validated in this manner, these results align with preliminary data from population genetics which point to a scenario in which Peruvian Quechua have adapted not only to the stress of high altitude but also of low ambient temperatures (Chapter 2).

4.5 Tables and Figures

Table 4.1: Significant results of ANOVA on midsagittal landmarks

Region of the Face: Landmark	Coefficient	Estimate	Std Error	T Value	Pr(>|t|)
Subnasal Clivus: Vertical orientation of QL 50 [50X]	Centroid Size : Population	1.48E-05	7.46E-06	1.98	0.04915
Subnasal Clivus: Vertical orientation of QL 51 [51X]	Centroid Size : Population	1.56E-05	7.54E-06	2.068	0.03999
Subnasal Clivus: Vertical orientation of QL 52 [52X]	Centroid Size : Population	1.60E-05	7.70E-06	2.073	0.0395
Subnasal Clivus: Vertical orientation of QL 50 [50X]	Population	-8.09E-02	4.07E-02	-1.99	0.04801
Subnasal Clivus: Vertical orientation of QL 51 [51X]	Population	-8.53E-02	4.11E-02	-2.073	0.03945
Subnasal Clivus: Vertical orientation of QL 52 [52X]	Population	-8.70E-02	4.20E-02	-2.073	0.0395
Upper Lip: Horizontal orientation of QL 41 [41Y]	Centroid Size : Population : Sex	3.04E-06	1.54E-06	1.976	0.0496
Upper Lip: Horizontal orientation of QL 42 [42Y]	Centroid Size : Population : Sex	3.18E-06	1.58E-06	2.014	0.0454
Upper Lip: Horizontal orientation of QL 41 [41Y]	Population : Sex	-1.65E-02	8.29E-03	-1.989	0.0481
Upper Lip: Horizontal orientation of QL 42 [42Y]	Population : Sex	-1.73E-02	8.50E-03	-2.035	0.0432

Table 4.2: Results of pairwise T-Tests. Groups are color-coordinated to align with boxplots.

Trait	Group 1	Group 2	Holm-Bonferroni Adjusted *p*	Significance Level
External Nasal Profile	Maya Female	Maya Male	0.2400	
	Maya Female	Quechua Female	0.0012	**
	Maya Female	Quechua Male	8.30E-09	****
	Maya Male	Quechua Female	0.0110	**
	Maya Male	Quechua Male	9.90E-08	****
	Quechua Male	Quechua Female	0.0060	**
Projection of Nasal Cartilage	Maya Female	Maya Male	0.3000	
	Maya Female	Quechua Female	0.0130	**
	Maya Female	Quechua Male	0.0001	****
	Maya Male	Quechua Female	0.3000	
	Maya Male	Quechua Male	0.0350	*
	Quechua Male	Quechua Female	0.3000	
Height of Bony Nasal Aperature	Maya Female	Maya Male	0.4000	
	Maya Female	Quechua Female	0.1000	
	Maya Female	Quechua Male	0.0016	***
	Maya Male	Quechua Female	0.4000	
	Maya Male	Quechua Male	0.0320	*
	Quechua Male	Quechua Female	0.4000	
Chord of Nasal Ridge	Maya Female	Maya Male	0.1200	
	Maya Female	Quechua Female	0.0034	***
	Maya Female	Quechua Male	1.40E-06	****

	Maya Male		Quechua Female	0.1200	
	Maya Male		Quechua Male	0.0003	****
	Quechua Male		Quechua Female	0.0880	

Figure 4.1: Anthropomorphic Mask of spatially-dense quasilandmarks

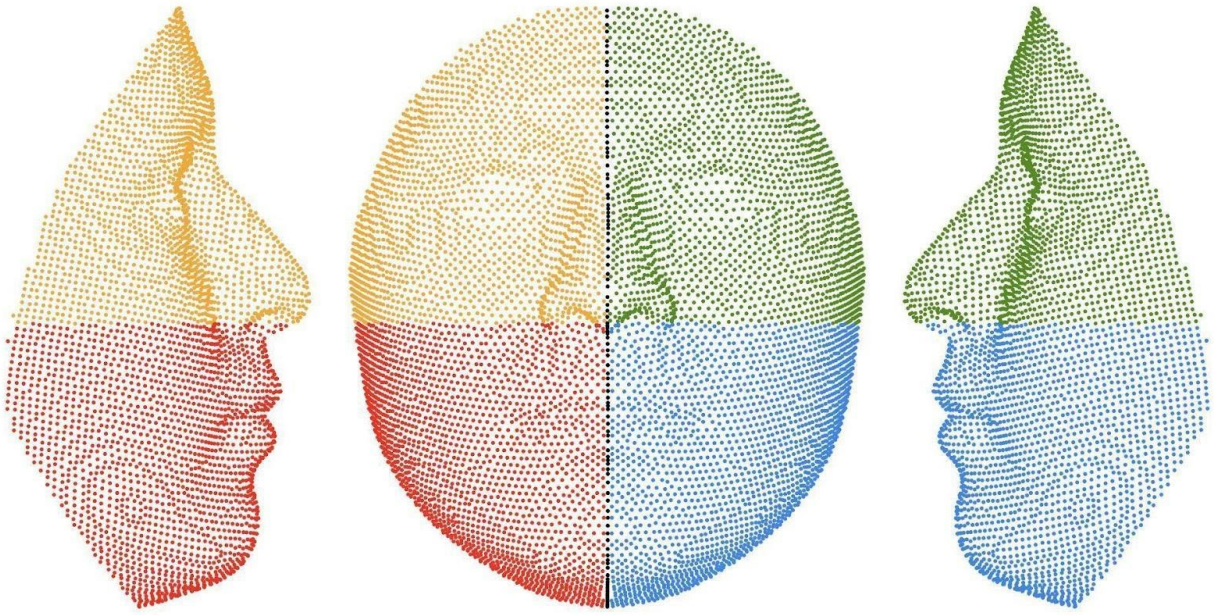

The black dots indicate landmarks on the midsagittal plane that were extracted for analysis. Given that these landmarks are occupying the same plane, coordinate data describing the lateral orientation of landmarks were removed, creating a “flattened” image. The resulting data, which was relevant to vertical and horizontal orientation of landmarks, were then used to detect changes in midfacial projection.

Figure 4.2: PCA Results

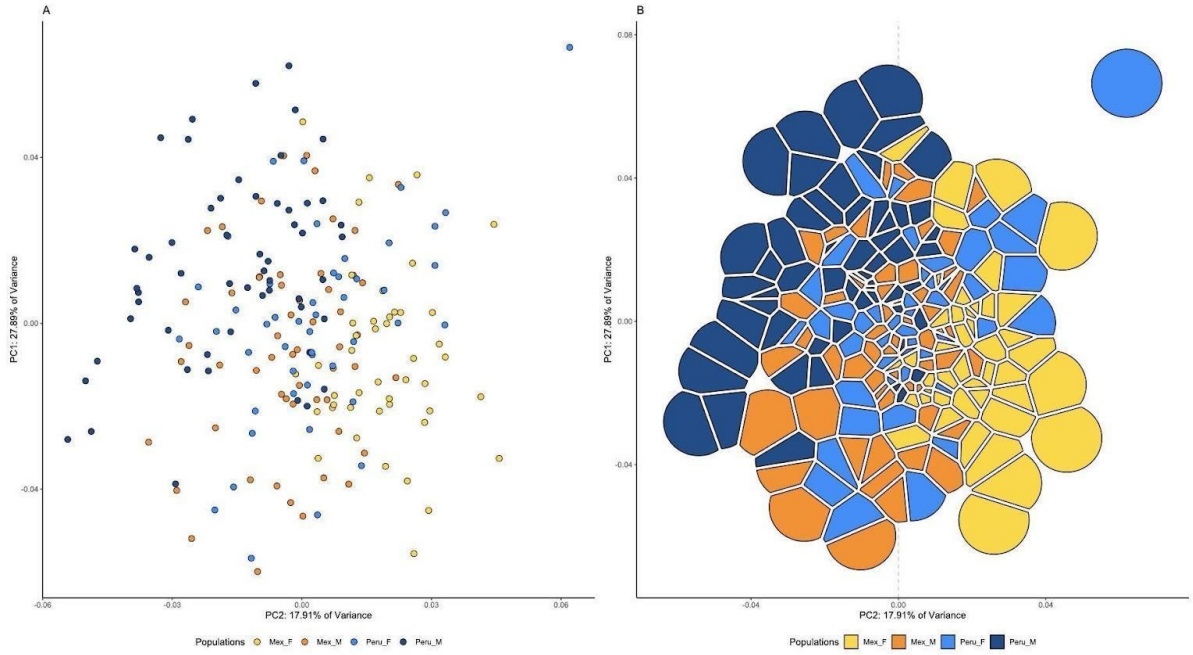

Panel A: PCA results calculated with the full dataset of craniofacial landmarks. Each point represents an individual. Paanel B: PCA results presented as a dense point cloud removing space between individuals. PC1 explains 27.89% of the variation, whereas PC2 accounts for 17.91% of the variation.

Figure 4.3: CVA Results

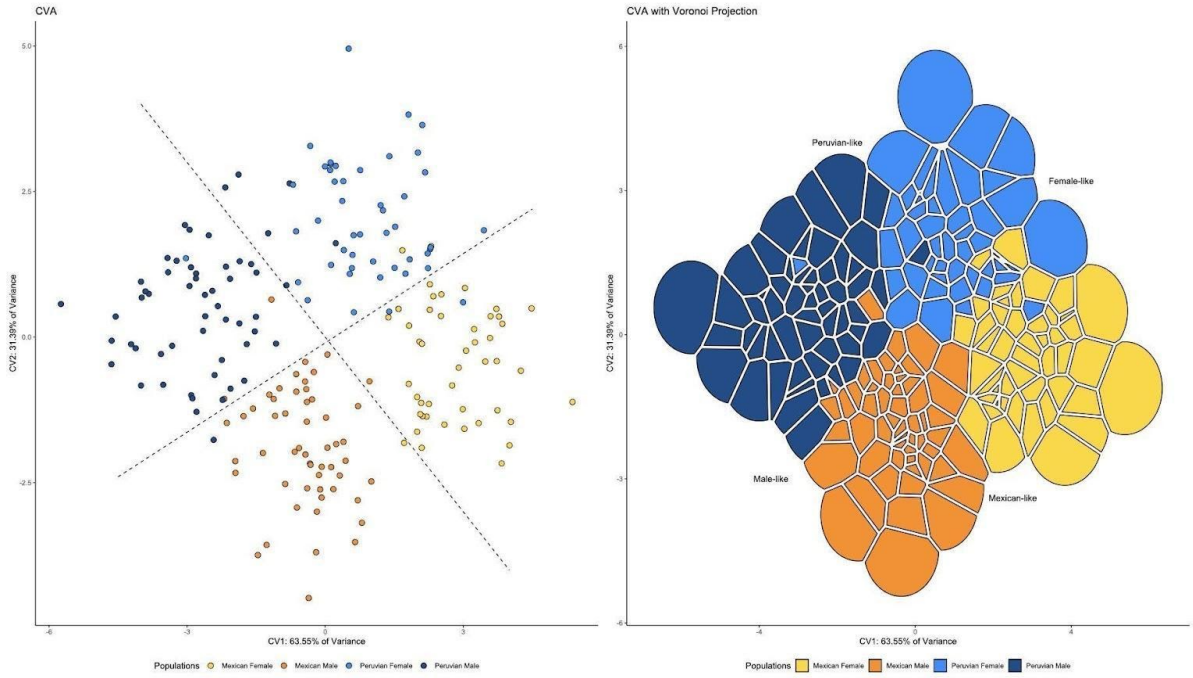

Panel A: CVA results calculated with the first two PCs. Each point represents an individual. Panel B: CVA results presented as a dense point cloud removing space between individuals. Relative to PC, the CVA minimizes variation within and maximizes variation between population clusters. Here, CV1 accounts for nearly two thirds of the variation and corresponds to sex. CV2 accounts for roughly the final third of variation and corresponds to population affinity.

Figure 4.4: Boxplot of ILD from subnasale to tip of the nose.

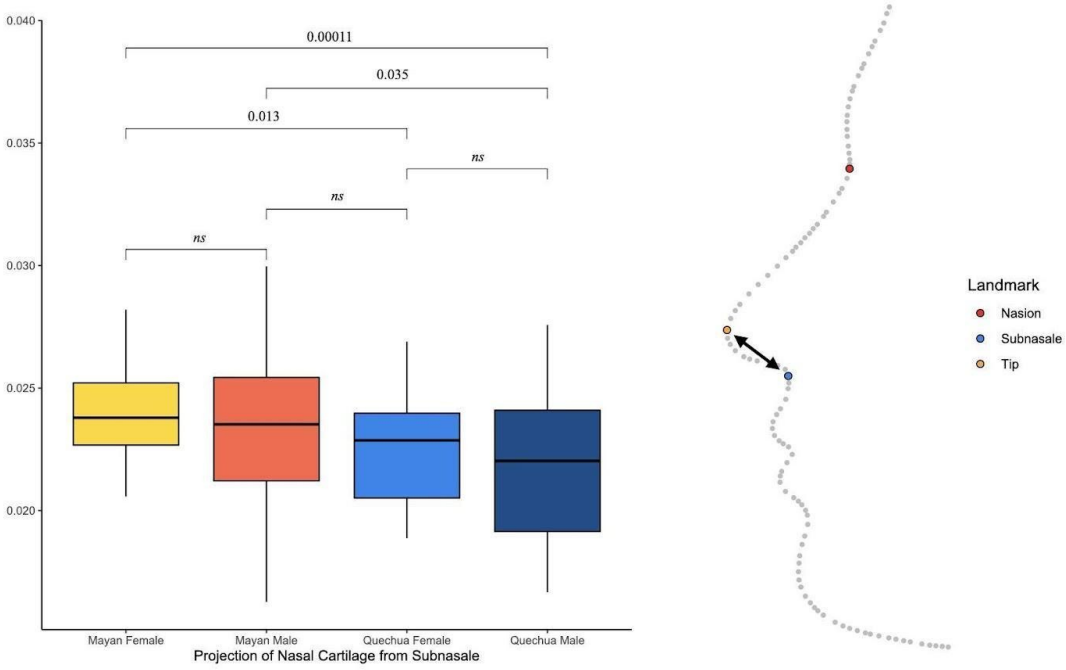

Figure 4.5: Boxplot ILD from nasion to tip of the nose.

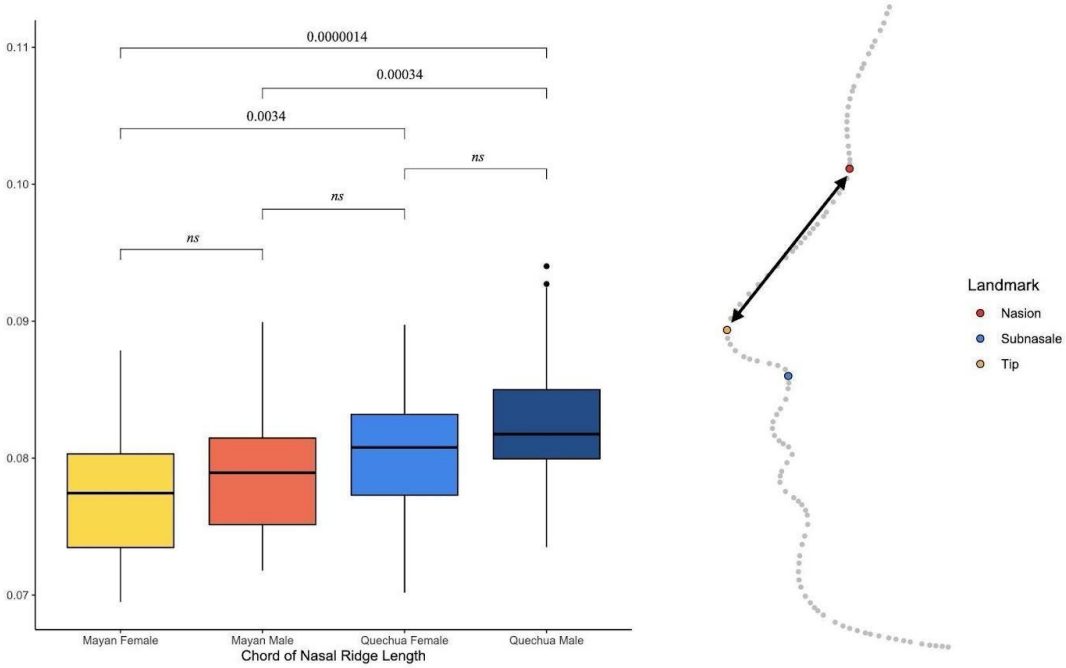

Figure 4.6: Boxplot of ILDs approximating the height of nasal cavity

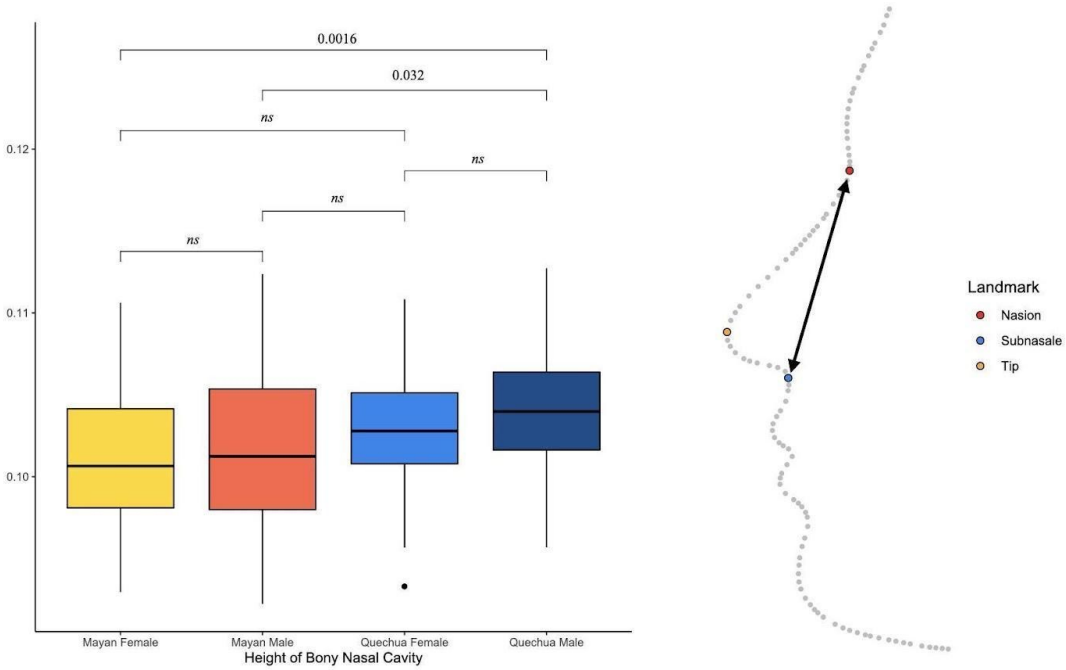

Figure 4.7: Boxplot of concatenated ILDs showing length of nasal profile

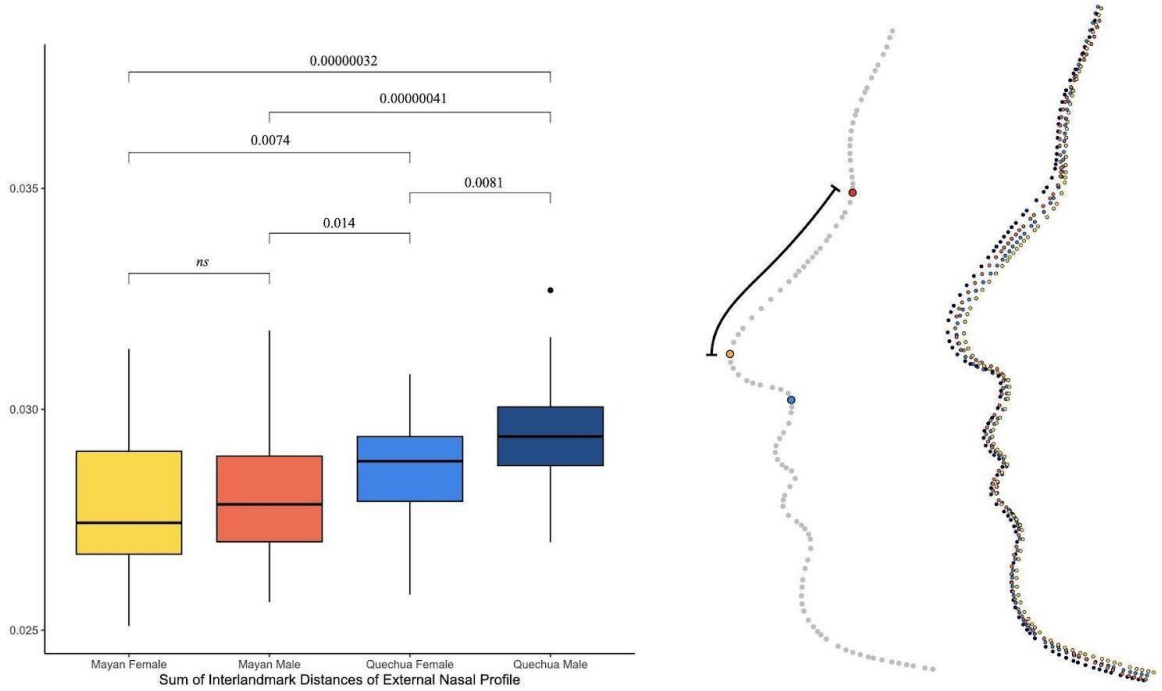

External nasal profile (ENP) was measured from the nasion to the tip of the nose. The image on the far right represents the compared mean midfacial profile for each population. Colors are consistent throughout: yellow dots = Mayan females; orange dots = Mayan males; light blue dots = Quechua females; dark blue dots = Quechua males.

Figure 4.8: Sex-specific deformation grids of midfacial profile

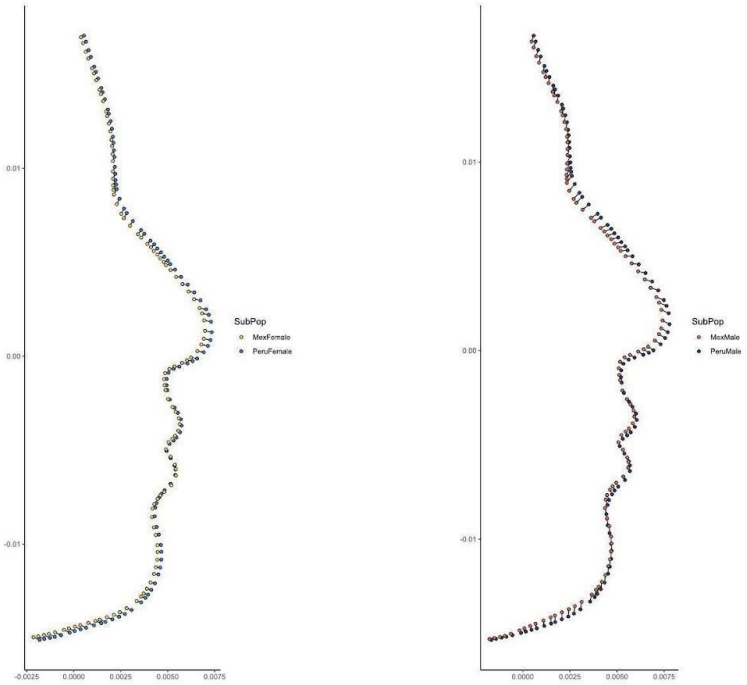

Left panel: females. Right panel: males.

Table 4.3: (Supplemental Table 1): Extended Results from ANOVA (significant hits only)

Label	Facial Component	Coefficient	Estimate	SE	Pr(>|t|)	Sig Level
Chin Projection: Horizontal orientation of QL 24 [24Y]	Chin Projection	[cs:PopAffin]	-4.56E-06	1.96E-06	0.0213	*
Chin Projection: Horizontal orientation of QL 24 [24Y]	Chin Projection	[PopAffin]	2.47E-02	1.07E-02	0.022	*
Chin Projection: Horizontal orientation of QL 25 [25Y]	Chin Projection	[cs:PopAffin]	-5.33E-06	2.05E-06	0.00996	**
Chin Projection: Horizontal orientation of QL 25 [25Y]	Chin Projection	[PopAffin]	2.87E-02	1.12E-02	0.01087	*
Chin Projection: Horizontal orientation of QL 26 [26Y]	Chin Projection	[cs:PopAffin]	-5.71E-06	2.11E-06	0.00756	**
Chin Projection: Horizontal orientation of QL 26 [26Y]	Chin Projection	[PopAffin]	3.06E-02	1.15E-02	0.00851	**
Chin Projection: Horizontal orientation of QL 27 [27Y]	Chin Projection	[cs:PopAffin]	-5.62E-06	2.14E-06	0.00918	**
Chin Projection: Horizontal orientation of QL 27 [27Y]	Chin Projection	[PopAffin]	3.01E-02	1.16E-02	0.01045	*
Lower Lip: Horizontal orientation of QL 32 [32Y]	Lower Lip	[cs:PopAffin]	-4.98E-06	2.32E-06	0.0327	*
Lower Lip: Horizontal orientation of QL 32 [32Y]	Lower Lip	[PopAffin]	2.68E-02	1.26E-02	0.0349	*
Lower Lip: Horizontal orientation of QL 33 [33Y]	Lower Lip	[cs:PopAffin]	-4.89E-06	2.36E-06	0.0398	*
Lower Lip: Horizontal orientation of QL 33 [33Y]	Lower Lip	[PopAffin]	2.63E-02	1.29E-02	0.0426	*
Lower Lip: Horizontal orientation of QL 34 [34Y]	Lower Lip	[cs:PopAffin]	-4.74E-06	2.39E-06	0.0483	*
Lower Lip: Vertical orientation of QL 35 [35X]	Lower Lip	[cs:sex: PopAffin]	-1.06E-05	4.64E-06	0.0242	*
Lower Lip: Vertical orientation of QL 35 [35X]	Lower Lip	[cs:PopAffin]	1.77E-05	7.44E-06	0.0184	*
Lower Lip: Vertical orientation of QL 35 [35X]	Lower Lip	[cs:sex]	1.40E-05	3.39E-06	5.63E-05	***
Lower Lip: Vertical orientation of QL 35 [35X]	Lower Lip	[cs]	-2.73E-05	5.40E-06	9.87E-07	***
Lower Lip: Vertical orientation of QL 35 [35X]	Lower Lip	[PopAffin:sex]	5.71E-02	2.50E-02	0.0235	*
Lower Lip: Vertical orientation of QL 35 [35X]	Lower Lip	[PopAffin]	-9.78E-02	4.06E-02	0.0169	*
Lower Lip: Vertical orientation of QL 35 [35X]	Lower Lip	[sex]	-7.64E-02	1.84E-02	5.02E-05	***
Lower Lip: Vertical orientation of QL 35 [35X]	Lower Lip	Intercept	2.12E-01	2.98E-02	1.92E-11	***

Lower Lip: Vertical orientation of QL 36 [36X]	Lower Lip	[cs:sex: PopAffin]	-1.05E-05	4.44E-06	0.0191	*
Lower Lip: Vertical orientation of QL 36 [36X]	Lower Lip	[cs:PopAffin]	1.72E-05	7.11E-06	0.0164	*
Lower Lip: Vertical orientation of QL 36 [36X]	Lower Lip	[cs:sex]	1.34E-05	3.23E-06	4.88E-05	***
Lower Lip: Vertical orientation of QL 36 [36X]	Lower Lip	[cs]	-2.64E-05	5.16E-06	7.27E-07	***
Lower Lip: Vertical orientation of QL 36 [36X]	Lower Lip	[PopAffin:sex]	5.71E-02	2.39E-02	0.0177	*
Lower Lip: Vertical orientation of QL 36 [36X]	Lower Lip	[PopAffin]	-9.54E-02	3.88E-02	0.0147	*
Lower Lip: Vertical orientation of QL 36 [36X]	Lower Lip	[sex]	-7.41E-02	1.76E-02	3.87E-05	***
Lower Lip: Vertical orientation of QL 36 [36X]	Lower Lip	Intercept	2.03E-01	2.84E-02	1.67E-11	***
Lower Lip: Vertical orientation of QL 37 [37X]	Lower Lip	[cs:sex: PopAffin]	-9.51E-06	4.27E-06	0.027209	*
Lower Lip: Vertical orientation of QL 37 [37X]	Lower Lip	[cs:PopAffin]	1.56E-05	6.85E-06	0.023889	*
Lower Lip: Vertical orientation of QL 37 [37X]	Lower Lip	[cs:sex]	1.23E-05	3.12E-06	0.000108	***
Lower Lip: Vertical orientation of QL 37 [37X]	Lower Lip	[cs]	-2.46E-05	4.97E-06	1.54E-06	***
Lower Lip: Vertical orientation of QL 37 [37X]	Lower Lip	[PopAffin:sex]	5.21E-02	2.30E-02	0.02484	*
Lower Lip: Vertical orientation of QL 37 [37X]	Lower Lip	[PopAffin]	-8.66E-02	3.73E-02	0.021472	*
Lower Lip: Vertical orientation of QL 37 [37X]	Lower Lip	[sex]	-6.83E-02	1.70E-02	8.16E-05	***
Lower Lip: Vertical orientation of QL 37 [37X]	Lower Lip	Intercept	1.91E-01	2.74E-02	5.00E-11	***
Lower Lip: Vertical orientation of QL 38 [38X]	Lower Lip	[cs:sex: PopAffin]	-8.61E-06	4.15E-06	0.039296	*
Lower Lip: Vertical orientation of QL 38 [38X]	Lower Lip	[cs:PopAffin]	1.42E-05	6.65E-06	0.034443	*
Lower Lip: Vertical orientation of QL 38 [38X]	Lower Lip	[cs:sex]	1.14E-05	3.03E-06	0.000225	***
Lower Lip: Vertical orientation of QL 38 [38X]	Lower Lip	[cs]	-2.32E-05	4.83E-06	3.16E-06	***
Lower Lip: Vertical orientation of QL 38 [38X]	Lower Lip	[PopAffin:sex]	4.73E-02	2.24E-02	0.035557	*
Lower Lip: Vertical orientation of QL 38 [38X]	Lower Lip	[PopAffin]	-7.88E-02	3.63E-02	0.03106	*
Lower Lip: Vertical orientation of QL 38 [38X]	Lower Lip	[sex]	-6.32E-02	1.65E-02	0.000167	***

Lower Lip: Vertical orientation of QL 38 [38X]	Lower Lip	Intercept	1.80E-01	2.66E-02	1.38E-10	***
Mentolabial Sulcus: Horizontal orientation of QL 28 [28Y]	Mentolabial Sulcus	[cs:PopAffin]	-5.40E-06	2.12E-06	0.0115	*
Mentolabial Sulcus: Horizontal orientation of QL 28 [28Y]	Mentolabial Sulcus	[PopAffin]	2.90E-02	1.15E-02	0.0129	*
Mentolabial Sulcus: Horizontal orientation of QL 29 [29Y]	Mentolabial Sulcus	[cs:PopAffin]	-5.24E-06	2.14E-06	0.015	*
Mentolabial Sulcus: Horizontal orientation of QL 29 [29Y]	Mentolabial Sulcus	[PopAffin]	2.82E-02	1.16E-02	0.0164	*
Mentolabial Sulcus: Horizontal orientation of QL 30 [30Y]	Mentolabial Sulcus	[cs:PopAffin]	-5.16E-06	2.20E-06	0.0199	*
Mentolabial Sulcus: Horizontal orientation of QL 30 [30Y]	Mentolabial Sulcus	[PopAffin]	2.78E-02	1.20E-02	0.0213	*
Mentolabial Sulcus: Horizontal orientation of QL 31 [31Y]	Mentolabial Sulcus	[cs:PopAffin]	-5.09E-06	2.24E-06	0.0243	*
Mentolabial Sulcus: Horizontal orientation of QL 31 [31Y]	Mentolabial Sulcus	[PopAffin]	2.75E-02	1.22E-02	0.0259	*
Submandibular: Horizontal orientation of QL 1 [1Y]	Submandibular	[cs:sex: PopAffin]	-3.53E-06	1.68E-06	0.0372	*
Submandibular: Horizontal orientation of QL 1 [1Y]	Submandibular	[cs:sex]	3.01E-06	1.23E-06	0.0151	*
Submandibular: Horizontal orientation of QL 1 [1Y]	Submandibular	[PopAffin:sex]	1.92E-02	9.06E-03	0.0356	*
Submandibular: Horizontal orientation of QL 1 [1Y]	Submandibular	[sex]	-1.63E-02	6.67E-03	0.0153	*
Submandibular: Horizontal orientation of QL 1 [1Y]	Submandibular	Intercept	2.54E-02	1.08E-02	0.0192	*
Submandibular: Horizontal orientation of QL 2 [2Y]	Submandibular	[cs:sex:PopAffin]	-3.50E-06	1.67E-06	0.0378	*
Submandibular: Horizontal orientation of QL 2 [2Y]	Submandibular	[cs:sex]	2.99E-06	1.22E-06	0.0153	*
Submandibular: Horizontal orientation of QL 2 [2Y]	Submandibular	[cs]	-3.84E-06	1.95E-06	0.05	*
Submandibular: Horizontal orientation of QL 2 [2Y]	Submandibular	[PopAffin:sex]	1.90E-02	9.02E-03	0.0362	*
Submandibular: Horizontal orientation of QL 2 [2Y]	Submandibular	[sex]	-1.62E-02	6.65E-03	0.0155	*
Submandibular: Horizontal orientation of QL 2 [2Y]	Submandibular	Intercept	2.52E-02	1.07E-02	0.0201	*
Submandibular: Horizontal orientation of QL 3 [3Y]	Submandibular	[cs:sex]	2.85E-06	1.26E-06	0.0245	*
Submandibular: Horizontal orientation of QL 3 [3Y]	Submandibular	[PopAffin:sex]	1.83E-02	9.29E-03	0.0498	*
Submandibular: Horizontal orientation of QL 3 [3Y]	Submandibular	[sex]	-1.55E-02	6.84E-03	0.0247	*

Submandibular: Horizontal orientation of QL 3 [3Y]	Submandibular	Intercept	2.41E-02	1.11E-02	0.0306	*
Subnasal Clivus: Vertical orientation of QL 50 [50X]	Subnasal Clivus	[cs:PopAffin]	1.48E-05	7.46E-06	0.04915	*
Subnasal Clivus: Vertical orientation of QL 50 [50X]	Subnasal Clivus	[cs]	-1.32E-05	5.41E-06	0.0153	*
Subnasal Clivus: Vertical orientation of QL 50 [50X]	Subnasal Clivus	[PopAffin]	-8.09E-02	4.07E-02	0.04801	*
Subnasal Clivus: Vertical orientation of QL 50 [50X]	Subnasal Clivus	Intercept	8.30E-02	2.98E-02	0.00587	**
Subnasal Clivus: Vertical orientation of QL 51 [51X]	Subnasal Clivus	[cs:PopAffin]	1.56E-05	7.54E-06	0.03999	*
Subnasal Clivus: Vertical orientation of QL 51 [51X]	Subnasal Clivus	[cs]	-1.33E-05	5.47E-06	0.01598	*
Subnasal Clivus: Vertical orientation of QL 51 [51X]	Subnasal Clivus	[PopAffin]	-8.53E-02	4.11E-02	0.03945	*
Subnasal Clivus: Vertical orientation of QL 51 [51X]	Subnasal Clivus	Intercept	8.02E-02	3.02E-02	0.00848	**
Subnasal Clivus: Vertical orientation of QL 52 [52X]	Subnasal Clivus	[cs:PopAffin]	1.60E-05	7.70E-06	0.0395	*
Subnasal Clivus: Vertical orientation of QL 52 [52X]	Subnasal Clivus	[cs]	-1.28E-05	5.58E-06	0.0232	*
Subnasal Clivus: Vertical orientation of QL 52 [52X]	Subnasal Clivus	[PopAffin]	-8.70E-02	4.20E-02	0.0395	*
Subnasal Clivus: Vertical orientation of QL 52 [52X]	Subnasal Clivus	Intercept	7.33E-02	3.08E-02	0.0181	*
Upper Lip: Horizontal orientation of QL 41 [41Y]	Upper Lip	[cs:sex: PopAffin]	3.04E-06	1.54E-06	0.0496	*
Upper Lip: Horizontal orientation of QL 41 [41Y]	Upper Lip	[PopAffin:sex]	-1.65E-02	8.29E-03	0.0481	*
Upper Lip: Horizontal orientation of QL 42 [42Y]	Upper Lip	[cs:sex: PopAffin]	3.18E-06	1.58E-06	0.0454	*
Upper Lip: Horizontal orientation of QL 42 [42Y]	Upper Lip	[PopAffin:sex]	-1.73E-02	8.50E-03	0.0432	*

Figure 4.9: (Supplemental Figure 1): Deformation grid for Mexican Mayans relative to Global Consensus.

Dots indicate the position of landmarks for the population in question. Arrows point towards the location of the global mean, and lengths are relative to the linear distance towards the global consensus.

Figure 4.10 (Supplemental Figure 2): Deformation grid for Peruvian Quechua relative to Global Consensus.

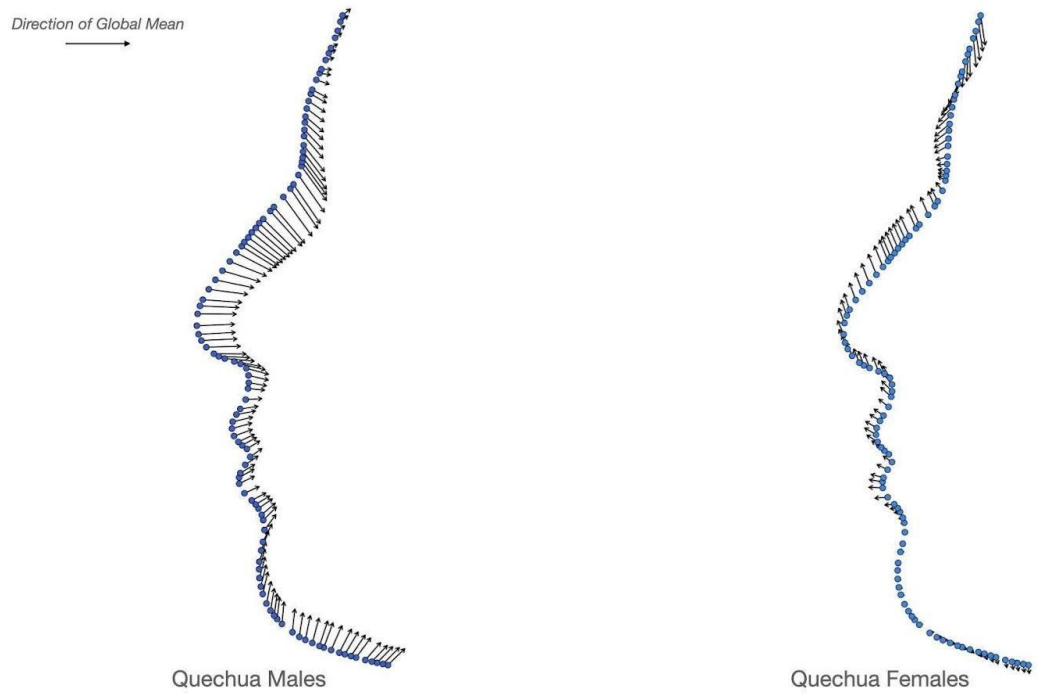

Dots indicate the position of landmarks for the population in question. Arrows point towards the location of the global mean, and lengths are relative to the linear distance towards the global consensus.

Chapter 5 Conclusion

This dissertation examined the effects of thermal stress on adaptive changes among Peruvian Quechua and Mexican Mayans. To do this, a combination of population genetic selection scans and morphometric analyses were conducted to test the following hypotheses: (1) are populations from Mesoamerica adapted to high heat index?, (2) are populations from the high Andes adapted to low ambient temperatures?, and (3) do components of facial anatomy in Peruvian Quechua mirror what is seen in high latitude, cold-adapted populations?

We were interested in these questions primarily given the dearth of knowledge about thermal stress in contexts outside of the cold and in the global north. More generally, we were interested in how these components of local adaptation were manifested in populations who have occupied their homelands for relatively short periods of time (<14,000 years) (González et al. 2014, Rademaker et al. 2014). Despite the fact that the earliest humans were a tropical species, there is little genetic evidence for recent evolutionary adaptation to high ambient temperatures. While there is ample evidence suggesting that populations from the Andes are adapted to hypoxic conditions of high altitude, there is no genetic evidence for cold climate adaptation for any of the communities that inhabit the tundra-like environments found at high elevation. To this end, we conducted selection scans using genome-wide microarray data from Indigenous American populations hailing from the tropical rainforests of southern Mexico and from high altitude regions of Peru. For each group, we interrogated SNP data for evidence of recent selective sweeps in genes that protect against different forms of thermal stress. Finally, we

conducted geometric morphometrics analysis on 3D facial reconstructions to identify which components of midfacial anatomy correspond with local climate variables.

5.1 Primary Research Objectives

5.1.1 Heat Adaptation in Mexican Mayans

The objective of this chapter was to address the question: *Do Mexican Mayans show genetic adaptations to heat stress?*

To test the hypothesis that Indigenous Mesoamerican populations are adapted to hot, humid environments, we applied selection scans to SNP data from Tzeltal, Tzotil, and Ch'ol-speaking Mayans recruited from the Yucatan Peninsula in Mexico. Using two different tests, we were able to identify regions of the genome that showed evidence of local evolutionary change unique to Mexican Mayans: the first test, locus-specific branch length (LSBL), is designed to identify regions of high genetic differentiation between three related populations (Mexican Mayans, Han Chinese, and Peruvian Quechua); the second test, XP-nSL, calculates the number of segregating sites along a given genomic tract between two populations (Mexican Mayans and Peruvian Quechua), identifying regions of low genetic variation defined by high-frequency haplotypes (Shriver et al. 2004, Ferrer-Admettla et al. 2014)

While this study did not conduct functional validation to quantify the phenotype contribution of genetic variation in candidate-nominated genes (e.g., protein expression assays during a thermal challenge), it identified classic signals of evolutionary divergence between the study populations. Among Mexican Mayans, regions of high differentiation and low genetic diversity spanned numerous genes that previously have been shown to influence thermoregulation and bodily water/salt maintenance. This pattern was seen in the heat shock

protein-encoding gene *HSPA12A*, the exceptionally high haplotype scores in *BAG6*, and the steep peak of XP-nSL values surrounding the DUOX family of genes. The gene *BDKRB2*, which is related to "vasodilation" (GO: 0042311), exhibits very low genetic variation in Mexican Mayans, which is a hallmark of recent selection. Additionally, was evidence of strong selection on seven genes implicated in bodily responses to high temperatures, three were involved in "response to heat" (GO:0034605): *YWHAE, NUP88*, and *RPTOR*; three were related to "heat shock protein binding" (GO: 0030544, GO: 0031072) or were genes encoding heat shock proteins: *BAG6, FAF1, HSPA12A*; and one was related to "cellular response to heat stress" (R-HSA-3371556). Three genes related to lipid metabolism (R-HSA-400206), a process implicated in body temperature regulation in classically cold adapted groups, were also identified as having undergone recent evolutionary change: *ABCA1, ABCA4*, and *PPARG*. Finally – and in addition to evidence of selection on the DUOX family of genes – there was a visible fingerprint of selection on *TPO*, which is also implicated in thyroid hormone generation (GO:0006590).

This result aligns with the findings of perhaps the only other population genetics study related to heat adaptation, in which Malaspinas et al. (2016) detected selection on thyroid-related genes in Aboriginal Australian communities. Several genes related to salt/water homeostasis also revealed evidence of selection. The gene *TPK1,* implicated in both aquaporin-mediated transport (R-HSA-445717) and renal water homeostasis mediated by vasopressin (R-HSA-432040), contained an exceptionally divergent branch (rs28692603: LSBL = 0.513). Four genes, *AKAP11, FLG, HYAL2,* and *NEDD4L*, were related to water homeostasis pathways (GO:0003091, GO:0070295, GO:0030104). The gene *HSD17B4,* implicated in acid and bile salt metabolism (R-HSA-194068), contained eight SNPs that surpassed the significance threshold for XP-nSL, the highest of which was rs162196 (XP-nSL = 0.2299). This was interesting considering that

there was a relatively high number of SNPs that just barely surpassed the significance threshold, possibly implying that the region is located at the "shoulder" of a sweep region, or these variants are part of a haplotype that is currently undergoing a sweep.

Additional results detected selection on: genes implicated in psoriasis susceptibility, but that might confer accelerated wound healing (*PSORS1C1, PSORS1C2*); genes associated with parasite dampening, in particular related to Leishmaniasis (*TPK1, C3*); and various genes within the HLA family, which encode MHC class II antigen presentation. Together, these suggest that a significant environmental stressor is parasites and pathogens, which are known to increase in frequency and abundance within tropical regions (Guernier et al. 2004, Cashdan 2014).

An unexpected result was that selection scans detected recent selective sweeps shaping variation in genes that are classically associated with adaptive responses to cold stress through mitochondrial uncoupling (*NUBPL*, *ETFB*, and *NDUFAF6*) and lipid metabolism (*PPARG*). *NUBPL* was detected through a lone high scoring LSBL variant, which only indicates differentiation at this locus between Mexican Mayans, Peruvian Quechua, and Han Chinese. As such, it is possible that genes contributing to whole-body metabolism, perhaps related to the ability to release energy in the form of heat, contribute to body temperature regulation during heat stress.

The results of this chapter suggest that genes undergoing selection in Mexican Mayans contribute to offsetting local environmental stress, specifically in regards to heat exposure (*HSPA12A*), water loss (*NEDD4L*), pathogen abundance (*C3*), and whole body metabolism (*PPARG*). This increases our knowledge regarding putative evolutionary adaptations to heat stress (of which there are few), while also enriching our understanding of how populations that

descend from recently cold-adapted ancestors adapt to novel ecological extremes.

5.1.2 Cold Climate Adaptation in Peruvian Quechua

The aim of this chapter was to address the question: *do Peruvian Quechua show genetic adaptations to cold climate?* To test the hypothesis that Indigenous Andeans are adapted to cold, arid environments, we applied selection scans to SNP data from Peruvian Quechua recruited from Peru (N = 514). Again, we applied two tests of selection, LSBL and XP-nSL.

The Peruvian Quechua sample showed clear evidence of selection on genes related to cold-induced thermogenesis (GO:0106106) and brown fat cell differentiation (GO:0050873). Among these, eight genes were identified through highly-differentiated LSBL branches: *ESRRG, IL18R1, THADA, RB1, NR1D1, PCTP, METRNL,* and *ZNF516;* five genes were identified on the basis of belonging to high scoring haplotypes: *ABHD6, ARRDC3, LPL, EBF2,* and *DYNC1H1*. Haplotype scores for the gene *LPL,* related to response to cold (GO:0009409), were represented as a very tall, narrow peak, possibly indicating a past selective sweep that has been eroded by recombination. The gene *DYNC1H1*, which is implicated in cold-induced thermogenesis (GO:0106106), contained a cluster of very high scoring SNPs which suggests that this gene window is under directional selection. Perhaps the strongest evidence of selection related to cold stress was on the gene *CLPB,* which was encompassed by one of the highest ranked haplotypes in this study. Counterintuitively, *CLPB* is implicated in response to heat (GO:0009408), but at the cellular level this likely corresponds to general thermal stress related to swings in temperature. This partially explains why so many genes related to heat shock protein binding show signatures of selection in Peruvian Quechua (e.g., *DNAJC12, DNAJC18, EIF2B3, FAF1*).

Additional results showed selection on genes related to both cold and hypoxia, such as: *PRKG1, BDKRB2,* and *ATG5*, which are related to vasodilation (GO:0042311); *HIF1A*, which is related to both hypoxic response and heat shock protein binding (GO:0001666, GO:0031072); and *CTNNA3*, which is implicated in regulation of heart rate by cardiac conduction (GO:0086091). Finally, selection scans detected a number of genes within sweep regions that confer protective effects against high levels of UV radiation: *ADAMTS20*, *AP3B1*, *BBS5, DDB2, MITF*, and *MMP9;* as well as protect against low levels of vitamin D: *VDR*.

These results expand our understanding of human adaptation to cold climate by providing possibly the first evidence of genetic adaptations to cold stress in a South American context. Further, they reveal evidence of cold adaptation happening within the tropics, which is intriguing considering that altitude (and not latitude) is the variable that drives cold year-round temperatures in the high Andes. These results are critical to understanding not only how populations adapt to cold stress, but how populations living in high-altitude hypoxia can offset the effects of hypothermia. There is an apparent multiplicative effect of low oxygen availability and low ambient temperature in regards to bodily stress. It is possible that evolutionary adaptations in one pathway would dovetail with adaptations within the next (e.g., vasodilation offsetting hypoxia while facilitating thermoregulation). These findings help to address how populations can offset cold stress through various physiological pathways (e.g., brown fat thermogenesis, fatty acid metabolism), but also protect against the effects of cold at the cellular level. Viewed in sum, these results indicate that adaptation to high-altitude environments requires humans not only to be adapted to hypoxic conditions, but also to the stressors of low ambient temperature and high levels of UV, both of which are direct results of the thin

atmosphere of high elevation zones.

5.1.3 Midfacial Anatomy and Cold Climate Adaptation

The primary questions addressed by this chapter were: *Do changes in midfacial anatomy correspond to cold, arid environments? Specifically, do components of facial anatomy exhibited in Peruvian Quechua mirror morphological patterns observed in other putatively cold-adapted populations?* The focus of the final chapter was to investigate whether components of midfacial anatomy correspond to different environmental factors among two samples of Indigenous Americans -- Peruvian Quechua and Mexican Mayans. Data from spatially-dense 3D point clouds were analyzed within a geometric morphometrics framework, and were used to test the hypothesis that changes in midfacial projection were associated with cold, arid climate. Specifically, this chapter investigated whether or not a sample of digitally-reconstructed crania from Peruvian Quechua showed evidence of changes in the midface that are hypothesized to facilitate the warming and moistening of cold air (Schwartz and Tattersall 1996). Given the harsh breathing conditions of high-altitude environments, it was predicted that the Peruvian Quechua sample would reveal a lengthened external nasal passage (ENP). A longer, tubular ENP increases the area over which inspired air can come into contact with the nasal mucosa, increasing moisture and heat exchange within otherwise cold, dry air (Yokley 2009).

Analysis revealed statistically-significant differences in the external nasal profile, length of the nasal ridge, and height of the bony nasal aperture between Peruvians and Mexican Mayans. For every trait listed above, the Peruvian Quechua sample had greater interlandmark distances when matched for sex, indicating significant population-level divergence in each of these traits corresponding to lengthened ENP. Population affinity was a strong predictor of

maxillary and labial protrusion as well as overall size of the external nasal profile. Furthermore, the tip of the nose for the Peruvian Quechua sample was relatively downturned, and while more anteriorly placed overall, the Peruvian sample exhibited less projection of the nasal cartilage. Both of these factors are hypothesized to reduce heat loss during breathing, and to be beneficial for the mixture of cold, ambient air with warm, moistened air within the nasal cavity itself.

These changes in midfacial anatomy align with previous studies conducted with populations such as Fuegians, Aleutian Islanders, and Siberians -- all of which are putatively cold-adapted populations and who live at or near sea level (Wolpoff 1968, Noback et al. 2011). This provides indirect support for the hypothesis that this suite of changes in midfacial anatomy is adaptive to cold, arid environments such as those at high altitudes.

This study provided a unique opportunity to investigate not only the genetic contributions to thermal adaptation, but also how components of craniofacial anatomy vary between related populations that inhabit the cold/arid and hot/humid extremes of the American tropics. Prior to this study, it was unknown whether these populations exhibit evidence of genetic adaptation to local climate variables implicated in thermal stress. Furthermore, this project provides some of the first explicit evidence for genetic adaptations to heat stress in *any* human population, and is likely the first genetic evidence for cold climate adaptation in populations from the high Andes. Such results fill a significant gap in the understanding of how humans adapt to local environmental stressors, which in turn is critical for understanding broader questions about human evolutionary change, such as how humans survive in environmental extremes and undergo significant phenotypic change in relatively short evolutionary timespans.

5.2 Future Directions

Genotype-phenotype association studies are often performed in order to identify genetic variation contributing to phenotypes of interest (Alkorta-Aranburu et al. 2012; Jonnalagadda et al. 2019; Rawofi et al. 2017). Using available data presented in this dissertation including the Affymetrix Biobank Array data and the 3D facial data, a genome wide association study (GWAS) could be performed to understand how variation in selection-nominated genes associates with facial form. Future studies could expand GWAS to additional adaptive thermogenic phenotypes including skin surface temperatures, metabolic behaviors, and various physiological responses (e.g., shivering) that manifest during a cold challenge. Similarly, the strong evidence of selection on genes related to psoriasis susceptibility could be a second association study among Mexican Mayans. The fact that genes related to psoriasis simultaneously contribute to wound healing provides an interesting case study within Darwinian medicine; understanding how variants implicated in dermatological disorders undergo selection given putative protective effects from parasites (or other environmental factors) could be of clinical importance.

Together, the results presented in this dissertation identified population-specific patterns of genetic change and divergence in craniofacial morphology, which contribute to our knowledge of how climate might shape biological variation in cold/arid and hot/humid extremes. Nonetheless, there is more work to be done in order to fully appreciate the cost of cold stress in high-altitude environments. Given that bodily responses to cold stimulus are impaired during hypoxia, and considering that hypothermia and hypoxia often trigger similar physiological responses (e.g., hyperventilation), more work is needed in order to parse out the specific causative mechanisms underlying cold climate adaptation in the Andes. One method to address

this would be to identify patterns of evolutionary change along the entirety of the Andean Cordillera. Like the inhabitants of the Peruvian Andes, the peoples of Tierra del Fuego and southern Patagonia have lived in their respective homelands for thousands of years (de Saint Pierre et al. 2012, Dillehay et al. 2015). Like their neighbors to the north, these southernmost Andean communities likewise inhabit extreme cold, yet they live approximately at sea level. If these populations prove to be cold-adapted, it is possible that high-scoring, cold-adaptive haplotypes that are also protective against hypoxia (e.g., *PRKG1*) are under selection in cold-adapted lowland populations, which might indicate a deeply ancestral selective sweep has occurred. Conversely, there could be evidence of selection against certain high-frequency haplotypes in one population relative to the others, which could point towards genes or pathways that are beneficial to high altitude versus high latitude.

5.3 Concluding Remarks

In this dissertation, genetic and anatomical adaptations to local climate stress were identified using a combination of selection scans and geometric morphometrics. The results of this research reveal that populations from the hot, humid Yucatan Peninsula have markers of selection in genes related to cellular responses to heat stress (*BAG6*), water/salt balance (*NEDD4L*), and body temperature regulation (*DUOX2*). Conversely, populations inhabiting the Andean highlands exhibit changes in genes that counteract low ambient temperature through nonshivering thermogenesis (*THADA*), that buffer against UV radiation (*DDB2*), and that protect against hypoxic conditions of high elevation (*HIF1A*). These same Andean individuals reveal evidence of population-specific changes in midfacial anatomy that are associated with enhanced warming and conditioning of harsh montane air.

There are several limitations to this dissertation research, the first being that SNP data is essentially a measure of absence/presence at known polymorphic sites in the genome. While informative, SNP arrays are not designed to detect de novo mutations or variants that are unique to groups that are underrepresented in population genetics studies. Additionally, it is possible that variants under selection in Peruvian Quechua or Mexican Mayans were omitted or were filtered out during QC. A second limitation of this project is that while it had the power to detect selective sweeps in the form of allele frequency difference and highly-differentiated haplotypes, it did not include any sequence-based tests of selection or association testing. Finally, this project compared evolutionary changes in one population that inhabits extreme heat and humidity to another that lives in an environment that is extremely cold and arid: while this pairwise comparison might enhance signals of selection related to climate stress, it might simultaneously mask some evidence of local environmental adaptation. For example, both Peruvian Quechua and Mexican Mayan populations showed strong evidence of selection in heat shock proteins and genes related to thyroid function, but these populations live in essentially orthogonal environments. Replicating this study with a population from warm, arid environments (e.g, the Sechura Desert in Peru) and cold, humid environments (e.g., the Magellanic moors of Chile) can inform us of how evolutionary change happens along a temperature gradient as well as a humidity/aridity continuum.

Overall, this study found support for the hypotheses that Peruvians from high altitude constitute a genetically cold-adapted group, and that Mexican Mayans have genetic markers of adaptation to high heat index. These provide some of the first evidence for local climate adaptation in the Americas, and are informative about recent, rapid, and niche-specific evolutionary change.

Bibliography

1. Adams, D., Collyer, M., Kaliontzopoulou, A., Baken, E., 2021. geomorph: Geometric Morphometric Analyses of 2D/3D Landmark Data. R package version 4.0. https://cran.r-project.org/package=geomorph.

2. Afrane, Y.A., Githeko, A.K., Yan, G., 2012. The Ecology of Anopheles Mosquitoes under Climate Change: Case Studies from the Effects of Environmental Changes in East Africa Highlands. Annals of the New York Academy of Sciences 1249, 204–210. https://doi.org/10.1111/j.1749-6632.2011.06432.x

3. Aggarwal, A., Upadhyay, R., 2013. Heat Stress and Immune Function, in: Aggarwal, A., Upadhyay, R. (Eds.), Heat Stress and Animal Productivity. Springer, India, pp. 113–136. https://doi.org/10.1007/978-81-322-0879-2_5

4. Ahir, A., Guo, L., Hussain, A.A., Marshall, J., 2002. Expression of Metalloproteinases from Human Retinal Pigment Epithelial Cells and Their Effects on the Hydraulic Conductivity of Bruch's Membrane. Investigative Ophthalmology and Visual Science. 43, 458–465.

5. Åkesson, C.M., Matthews-Bird, F., Bitting, M., Fennell, C.-J., Church, W.B., Peterson, L.C., Valencia, B.G., Bush, M.B., 2020. 2,100 years of human adaptation to climate change in the High Andes. Nature Ecology and Evolution 4, 66–74. https://doi.org/10.1038/s41559-019-1056-2

6. Alkorta-Aranburu, G., Beall, C.M., Witonsky, D.B., Gebremedhin, A., Pritchard, J.K., Rienzo, A.D., 2012. The Genetic Architecture of Adaptations to High Altitude in Ethiopia. PLOS Genetics 8, e1003110. https://doi.org/10.1371/journal.pgen.1003110

7. Amorim, C.E.G., Nunes, K., Meyer, D., Comas, D., Bortolini, M.C., Salzano, F.M., Hünemeier, T., 2017. Genetic signature of natural selection in first Americans. PNAS 114, 2195–2199. https://doi.org/10.1073/pnas.1620541114

8. Arellano-Mendoza, M.-I., Saúl-Cano, A., 2016. Common Skin Diseases and Treatments in North America: Mexico, in: Kelly, A.P., Taylor, S.C., Lim, H.W., Serrano, A.M.A. (Eds.), Taylor and Kelly's Dermatology for Skin of Color. McGraw-Hill Education, New York, NY.

9. Arnqvist, G., Martensson, T., 1998. Measurement error in geometric morphometrics: Empirical strategies to assess and reduce its impact on measures of shape. Acta Zoologica Academiae Scientiarum Hungaricae. 44, 73 - 96

10. Astorino, C.M., 2019. Beyond Dimorphism: Sexual Polymorphism and Research Bias in Biological Anthropology. American Anthropologist 121, 489–490. https://doi.org/10.1111/aman.13224

11. Auger, N., Fraser, W.D., Smargiassi, A., Bilodeau-Bertrand, M., Kosatsky, T., 2017. Elevated outdoor temperatures and risk of stillbirth. International Journal of Epidemiology 46, 200–208. https://doi.org/10.1093/ije/dyw077

12. Ávila-Arcos, M.C., McManus, K.F., Sandoval, K., Rodríguez-Rodríguez, J.E., Villa-Islas, V., Martin, A.R., Luisi, P., Peñaloza-Espinosa, R.I., Eng, C., Huntsman, S., Burchard, E.G., Gignoux, C.R., Bustamante, C.D., Moreno-Estrada, A., 2020. Population History and Gene Divergence in Native Mexicans Inferred from 76 Human Exomes. Molecular Biology and Evolution 37, 994–1006. https://doi.org/10.1093/molbev/msz282

13. Baker, P.T., 1963. Adaptation to High Altitude Cold in the Andes. Pennsylvania State University, University Park.

14. Bal, N.C., Periasamy, M., 2020. Uncoupling of sarcoendoplasmic reticulum calcium ATPase pump activity by sarcolipin as the basis for muscle non-shivering thermogenesis. Philosophical Transactions of the Royal Society B: Biological Sciences 375, 20190135. https://doi.org/10.1098/rstb.2019.0135

15. Bar-Yosef, O., 1994. The lower paleolithic of the Near East. Journal of World Prehistory 8, 211–265. https://doi.org/10.1007/BF02221050

16. Bar-Yosef, O., Belfer-Cohen, A., 2001. From Africa to Eurasia — early dispersals. Quaternary International 75, 19–28. https://doi.org/10.1016/S1040-6182(00)00074-4

17. Bärtsch, P., Gibbs, J.S.R., 2007. Effect of Altitude on the Heart and the Lungs. Circulation 116, 2191–2202. https://doi.org/10.1161/CIRCULATIONAHA.106.650796

18. Basnyat Buddha, Starling Jennifer M., Schlossberg David, 2015. Infectious Diseases at High Altitude. Microbiology Spectrum 3, 3.4.26. https://doi.org/10.1128/microbiolspec.IOL5-0006-2015

19. Bastir, M., Godoy, P., Rosas, A., 2011. Common features of sexual dimorphism in the cranial airways of different human populations. American Journal of Physical Anthropology 146, 414–422. https://doi.org/10.1002/ajpa.21596

20. Basu, M., Pal, K., Prasad, R., Malhotra, A.S., Rao, K.S., Sawhney, R.C., 1997. Pituitary, gonadal and adrenal hormones after prolonged residence at extreme altitude in man. International Journal of Andrology 20, 153–158. https://doi.org/10.1046/j.1365-2605.1997.00046.x

21. Bates, G.P., Miller, V.S., 2008. Sweat rate and sodium loss during work in the heat. Journal of Occupational Medicine and Toxicology 3, 4. https://doi.org/10.1186/1745-6673-3-4

22. Bauer-Gottwein, P., Gondwe, B.R.N., Charvet, G., Marín, L.E., Rebolledo-Vieyra, M., Merediz-Alonso, G., 2011. Review: The Yucatán Peninsula karst aquifer, Mexico. Hydrogeology 19, 507–524. https://doi.org/10.1007/s10040-010-0699-5

23. Beall, C.M., 2006. Andean, Tibetan, and Ethiopian patterns of adaptation to high-altitude hypoxia. Integrative and Comparative Biology 46, 18–24. https://doi.org/10.1093/icb/icj004

24. Beall, C.M., 2014. Adaptation to High Altitude: Phenotypes and Genotypes. Annual Review of Anthropology 43, 251–272. https://doi.org/10.1146/annurev-anthro-102313-030000

25. Beall, C.M., Brittenham, G.M., Strohl, K.P., Blangero, J., Williams-Blangero, S., Goldstein, M.C., Decker, M.J., Vargas, E., Villena, M., Soria, R., Alarcon, A.M., Gonzales, C., 1998. Hemoglobin concentration of high-altitude Tibetans and Bolivian Aymara. American Journal of Physical Anthropology 106, 385–400. https://doi.org/10.1002/(SICI)1096-8644(199807)

26. Beall, C.M., Decker, M.J., Brittenham, G.M., Kushner, I., Gebremedhin, A., Strohl, K.P., 2002. An Ethiopian pattern of human adaptation to high-altitude hypoxia. Proceedings of the National Academy of Science 99, 17215–17218. https://doi.org/10.1073/pnas.252649199

27. Beck, H.E., Zimmermann, N.E., McVicar, T.R., Vergopolan, N., Berg, A., Wood, E.F., 2018. Present and future Köppen-Geiger climate classification maps at 1-km resolution. Scientific Data 5, 180214. https://doi.org/10.1038/sdata.2018.214

28. Bejdová, Š., Krajíček, V., Velemínská, J., Horák, M., Velemínský, P., 2013. Changes in the sexual dimorphism of the human mandible during the last 1200 years in Central Europe. HOMO 64, 437–453. https://doi.org/10.1016/j.jchb.2013.05.003

29. Beker, B.M., Beker, B.M., n.d. Human Physiology in Extreme Heat and Cold. https://doi.org/10.23937/iacph-2017/1710001

30. Belval, L.N., Morrissey, M.C., 2020. Physiological Response to Heat Stress, in: Adams, W.M., Jardine, J.F. (Eds.), Exertional Heat Illness: A Clinical and Evidence-Based Guide. Springer International Publishing, Cham, pp. 17–27. https://doi.org/10.1007/978-3-030-27805-2_2

31. Best, A., Lieberman, D.E., Kamilar, J.M., 2019. Diversity and evolution of human eccrine sweat gland density. Journal of Thermal Biology 84, 331–338. https://doi.org/10.1016/j.jtherbio.2019.07.024

32. Best, K.C., Garvin, H.M., Cabo, L.L., 2018. An Investigation into the Relationship between Human Cranial and Pelvic Sexual Dimorphism. Journal of Forensic Sciences 63, 990–1000. https://doi.org/10.1111/1556-4029.13669

33. Bigham, A., Bauchet, M., Pinto, D., Mao, X., Akey, J.M., Mei, R., Scherer, S.W., Julian, C.G., Wilson, M.J., Herráez, D.L., Brutsaert, T., Parra, E.J., Moore, L.G., Shriver, M.D., 2010. Identifying Signatures of Natural Selection in Tibetan and Andean Populations Using Dense Genome Scan Data. PLOS Genetics 6, e1001116. https://doi.org/10.1371/journal.pgen.1001116

34. Bigham, A.W., Lee, F.S., 2014. Human high-altitude adaptation: forward genetics meets the HIF pathway. Genes and Development 28, 2189–2204. https://doi.org/10.1101/gad.250167.114

35. Bigham, A.W., Mao, X., Mei, R., Brutsaert, T., Wilson, M.J., Julian, C.G., Parra, E.J., Akey, J.M., Moore, L.G., Shriver, M.D., 2009. Identifying positive selection candidate loci for high-altitude adaptation in Andean populations. Human Genomics 4, 79–90. https://doi.org/10.1186/1479-7364-4-2-79

36. Blackwell, J.M., Jamieson, S.E., Burgner, D., 2009. HLA and Infectious Diseases. Clinical Microbiology Reviews 22, 370–385. https://doi.org/10.1128/CMR.00048-08

37. Bojko, E.R., 1997. Metabolical changes induced by adaptation to circumpolar conditions in Spitsbergen. International Journal of Circumpolar Health 56, 134–141.

38. Bolch, S.N., Dugger, D.R., Chong, T., McDowell, J.H., Smith, W.C., 2016. A Splice Variant of Bardet-Biedl Syndrome 5 (BBS5) Protein that Is Selectively Expressed in Retina. PLoS One 11. https://doi.org/10.1371/journal.pone.0148773

39. Borda, V., Alvim, I., Mendes, M., Silva-Carvalho, C., Soares-Souza, G.B., Leal, T.P., Furlan, V., Scliar, M.O., Zamudio, R., Zolini, C., Araújo, G.S., Luizon, M.R., Padilla, C., Cáceres, O., Levano, K., Sánchez, C., Trujillo, O., Flores-Villanueva, P.O., Dean, M., Fuselli, S., Machado, M., Romero, P.E., Tassi, F., Yeager, M., O'Connor, T.D., Gilman, R.H., Tarazona-Santos, E., Guio, H., 2020. The genetic structure and adaptation of Andean highlanders and Amazonians are influenced by the interplay between geography and culture. Proceedings of the National Academy of Sciences USA 117, 32557–32565. https://doi.org/10.1073/pnas.2013773117

40. Bourgeon, L., Burke, A., Higham, T., 2017. Earliest Human Presence in North America Dated to the Last Glacial Maximum: New Radiocarbon Dates from Bluefish Caves, Canada. PLOS ONE 12, e0169486. https://doi.org/10.1371/journal.pone.0169486

41. Brake, D.J., Bates, G.P., 2003. Fluid losses and hydration status of industrial workers under thermal stress working extended shifts. Occupational Environmental Medicine 60, 90–96. https://doi.org/10.1136/oem.60.2.90

42. Bramble, D.M., Lieberman, D.E., 2004. Endurance running and the evolution of Homo. Nature 432, 345–352. https://doi.org/10.1038/nature03052

43. Breuker, C.J., Patterson, J.S., Klingenberg, C.P., 2006. A Single Basis for Developmental Buffering of Drosophila Wing Shape. PLOS ONE 1, e7. https://doi.org/10.1371/journal.pone.0000007

44. Bridges, L.E., 1949. Uttermost Part of the Earth. Dutton and Co., New York, NY.

45. Brooks, D.R., Ramirez-Rubio, O., Amador, J.J., 2012. CKD in Central America: A Hot Issue. American Journal of Kidney Diseases 59, 481–484. https://doi.org/10.1053/j.ajkd.2012.01.005

46. Bruckner, T.A., Modin, B., Vågerö, D., 2014. Cold ambient temperature in utero and birth outcomes in Uppsala, Sweden, 1915–1929. Annals of Epidemiology 24, 116–121. https://doi.org/10.1016/j.annepidem.2013.11.005

47. Brutsaert, T.D., Kiyamu, M., Elias Revollendo, G., Isherwood, J.L., Lee, F.S., Rivera-Ch, M., Leon-Velarde, F., Ghosh, S., Bigham, A.W., 2019. Association of EGLN1 gene with high aerobic capacity of Peruvian Quechua at high altitude. PNAS 116, 24006–24011.

48. Bubb, K.L., Bovee, D., Buckley, D., Haugen, E., Kibukawa, M., Paddock, M., Palmieri, A., Subramanian, S., Zhou, Y., Kaul, R., Green, P., Olson, M.V., 2006. Scan of Human Genome Reveals No New Loci Under Ancient Balancing Selection. Genetics 173, 2165–2177. https://doi.org/10.1534/genetics.106.055715

49. Cabrol, N.A., Feister, U., Häder, D.-P., Piazena, H., Grin, E.A., Klein, A., 2014. Record solar UV irradiance in the tropical Andes. Front. Environ. Sci. 2. https://doi.org/10.3389/fenvs.2014.00019

50. Calderon-Dominguez, M., Sebastián, D., Fucho, R., Weber, M., Mir, J.F., García-Casarrubios, E., Obregón, M.J., Zorzano, A., Valverde, Á.M., Serra, D., Herrero, L., 2016. Carnitine Palmitoyltransferase 1 Increases Lipolysis, UCP1 Protein Expression and Mitochondrial Activity in Brown Adipocytes. PLoS One 11. https://doi.org/10.1371/journal.pone.0159399

51. Cardona, A., Pagani, L., Antao, T., Lawson, D.J., Eichstaedt, C.A., Yngvadottir, B., Shwe, M.T.T., Wee, J., Romero, I.G., Raj, S., Metspalu, M., Villems, R., Willerslev, E., Tyler-Smith, C., Malyarchuk, B.A., Derenko, M.V., Kivisild, T., 2014. Genome-Wide Analysis of Cold Adaptation in Indigenous Siberian Populations. PLOS ONE 9, e98076. https://doi.org/10.1371/journal.pone.0098076

52. Carey, J.W., Steegmann, A.T., 1981. Human nasal protrusion, latitude, and climate. American Journal of Physical Anthropology 56, 313–319. https://doi.org/10.1002/ajpa.1330560312

53. Carmona, M.C., Hondares, E., Rodriguez de la Concepcion, M.L., Rodriguez-Sureda, V., Peinado-Onsurbe, J., Poli, V., Iglecias, R., Villaroya, F., Giralt, M., 2005. Defective thermoregulation, impaired lipid metabolism, but preserved adrenergic induction of gene expression in brown fat of mice lacking C/EBPβ. Biochemical Journal 389, 47–56. https://doi.org/10.1042/BJ20050009

54. Cashdan, E., 2014. Biogeography of Human Infectious Diseases: A Global Historical Analysis. PLoS One 9. https://doi.org/10.1371/journal.pone.0106752

55. Chakraborty, A., Maity, S., Sen, M., 2019. Wnt5A Signaling Antagonizes Leishmania donovani Infection, Vector-Borne Diseases - Recent Developments in Epidemiology and Control. IntechOpen. https://doi.org/10.5772/intechopen.87928

56. Chang, C.C., Chow, C.C., Tellier, L.C., Vattikuti, S., Purcell, S.M., Lee, J.J., 2015. Second-generation PLINK: rising to the challenge of larger and richer datasets. Gigascience 4, 7. https://doi.org/10.1186/s13742-015-0047-8

57. Charkoudian, N., 2016. Human thermoregulation from the autonomic perspective. Autonomic Neuroscience: Basic and Clinical 196, 1–2. https://doi.org/10.1016/j.autneu.2016.02.007

58. Churchill, S.E., 2014. Thin on the Ground: Neandertal Biology, Archeology, and Ecology. John Wiley & Sons.

59. Claes, P., Roosenboom, J., White, J.D., Swigut, T., Sero, D., Li, J., Lee, M.K., Zaidi, A., Mattern, B.C., Liebowitz, C., Pearson, L., González, T., Leslie, E.J., Carlson, J.C., Orlova, E., Suetens, P., Vandermeulen, D., Feingold, E., Marazita, M.L., Shaffer, J.R., Wysocka, J., Shriver, M.D., Weinberg, S.M., 2018. Genome-wide mapping of global-to-local genetic effects on human facial shape. Nature Genetics 50, 414–423. https://doi.org/10.1038/s41588-018-0057-4

60. Crawford, J.E., Amaru, R., Song, J., Julian, C.G., Racimo, F., Cheng, J.Y., Guo, X., Yao, J., Ambale-Venkatesh, B., Lima, J.A., Rotter, J.I., Stehlik, J., Moore, L.G., Prchal, J.T., Nielsen, R., 2017. Natural Selection on Genes Related to Cardiovascular Health in High-Altitude Adapted Andeans. The American Journal of Human Genetics 101, 752–767. https://doi.org/10.1016/j.ajhg.2017.09.023

61. Daanen, H.A.M., 2003. Finger cold-induced vasodilation: a review. European Journal of Applied Physiology 89, 411–426. https://doi.org/10.1007/s00421-003-0818-2

62. Dadvand Payam, Basagaña Xavier, Sartini Claudio, Figueras Francesc, Vrijheid Martine, de Nazelle Audrey, Sunyer Jordi, Nieuwenhuijsen Mark J., 2011. Climate Extremes and the Length of Gestation. Environmental Health Perspectives 119, 1449–1453. https://doi.org/10.1289/ehp.1003241

63. Danecek, P., Auton, A., Abecasis, G., Albers, C.A., Banks, E., DePristo, M.A., Handsaker, R.E., Lunter, G., Marth, G.T., Sherry, S.T., McVean, G., Durbin, R., 2011. The variant call format and VCFtools. Bioinformatics 27, 2156–2158. https://doi.org/10.1093/bioinformatics/btr330

64. Dávid-Barrett, T., Dunbar, R.I.M., 2016. Bipedality and hair loss in human evolution revisited: The impact of altitude and activity scheduling. Journal of Human Evolution 94, 72–82. https://doi.org/10.1016/j.jhevol.2016.02.006

65. de Azevedo, S., González, M.F., Cintas, C., Ramallo, V., Quinto-Sánchez, M., Márquez, F., Hünemeier, T., Paschetta, C., Ruderman, A., Navarro, P., Pazos, B.A., Silva de Cerqueira, C.C., Velan, O., Ramírez-Rozzi, F., Calvo, N., Castro, H.G., Paz, R.R., González-José, R., 2017. Nasal airflow simulations suggest convergent adaptation in Neanderthals and modern humans. PNAS 114, 12442–12447. https://doi.org/10.1073/pnas.1703790114

66. de Gabriel, J.R., 2015. Darwinian medicine and psoriasis. Actas Dermo-Sifiliográficas 106, 189–194. https://doi.org/10.1016/j.ad.2014.06.009

67. Debat, V., Béagin, M., Legout, H., David, J.R., 2003. Allometric and Nonallometric Components of Drosophila Wing Shape Respond Differently to Developmental

Temperature. Evolution 57, 2773–2784. https://doi.org/10.1111/j.0014-3820.2003.tb01519.x

68. Delaneau, O., Zagury, J.-F., Robinson, M.R., Marchini, J.L., Dermitzakis, E.T., 2019. Accurate, scalable and integrative haplotype estimation. Nature Communications 10, 5436. https://doi.org/10.1038/s41467-019-13225-y

69. Deng, L., Ruiz-Linares, A., Xu, S., Wang, S., 2016. Ancestry variation and footprints of natural selection along the genome in Latin American populations. Scientific Reports 6, 21766. https://doi.org/10.1038/srep21766

70. Devlin, M.J., 2015. The "Skinny" on brown fat, obesity, and bone. American Journal of Physical Anthropology 156, 98–115. https://doi.org/10.1002/ajpa.22661

71. Diamond, J.M., Akimova, T., Kazi, A., Shah, R.J., Cantu, E., Feng, R., Levine, M.H., Kawut, S.M., Meyer, N.J., Lee, J.C., Hancock, W.W., Aplenc, R., Ware, L.B., Palmer, S.M., Bhorade, S., Lama, V.N., Weinacker, A., Orens, J., Wille, K., Crespo, M., Lederer, D.J., Arcasoy, S., Demissie, E., Christie, J.D., 2014. Genetic Variation in the Prostaglandin E2 Pathway Is Associated with Primary Graft Dysfunction. American Journal of Respiratory and Critical Care Medicine 189, 567–575. https://doi.org/10.1164/rccm.201307-1283OC

72. Dib, J., Motok, J., Zenoff, V.F., Ordoñez, O., Farías, M.E., 2008. Occurrence of Resistance to Antibiotics, UV-B, and Arsenic in Bacteria Isolated from Extreme Environments in High-Altitude (Above 4400 m) Andean Wetlands. Current Microbiology 56, 510–517. https://doi.org/10.1007/s00284-008-9103-2

73. Donaldson, G.C., Keatinge, W.R., Saunders, R.D., 2003. Cardiovascular responses to heat stress and their adverse consequences in healthy and vulnerable human populations. International Journal of Hyperthermia 19, 225–235. https://doi.org/10.1080/0265673021000058357

74. Dunayevich, P., Baltanás, R., Clemente, J.A., Couto, A., Sapochnik, D., Vasen, G., Colman-Lerner, A., 2018. Heat-stress triggers MAPK crosstalk to turn on the hyperosmotic response pathway. Science Reports 8, 15168. https://doi.org/10.1038/s41598-018-33203-6

75. Dunsworth, H.M., 2020. Expanding the evolutionary explanations for sex differences in the human skeleton. Evolutionary Anthropology: Issues, News, and Reviews 29, 108–116. https://doi.org/10.1002/evan.21834

76. Eichstaedt, C.A., Antao, T., Cardona, A., Pagani, L., Kivisild, T., Mormina, M., 2015. Positive selection of AS3MT to arsenic water in Andean populations. Mutation Research/Fundamental and Molecular Mechanisms of Mutagenesis 780, 97–102. https://doi.org/10.1016/j.mrfmmm.2015.07.007

77. Epstein, Y., Yanovich, R., 2019. Heatstroke. New England Journal of Medicine. https://doi.org/10.1056/NEJMra1810762

78. Equihua, M., Ibáñez-Bernal, S., Benítez, G., Estrada-Contreras, I., Sandoval-Ruiz, C.A., Mendoza-Palmero, F.S., 2017. Establishment of Aedes aegypti (L.) in mountainous regions

in Mexico: Increasing number of population at risk of mosquito-borne disease and future climate conditions. Acta Tropica 166, 316–327. https://doi.org/10.1016/j.actatropica.2016.11.014

79. Ericsson, C.D., Steffen, R., Basnyat, B., Cumbo, T.A., Edelman, R., 2001. Infections at High Altitude. Clinical Infectious Diseases 33, 1887–1891. https://doi.org/10.1086/324163

80. Eriksson, A., Betti, L., Friend, A.D., Lycett, S.J., Singarayer, J.S., Cramon-Taubadel, N. von, Valdes, P.J., Balloux, F., Manica, A., 2012. Late Pleistocene climate change and the global expansion of anatomically modern humans. PNAS 109, 16089–16094. https://doi.org/10.1073/pnas.1209494109

81. Evans, D.G., Olarte, J., DuPont, H.L., Evans, D.J., Galindo, E., Portnoy, B.L., Conklin, R.H., 1977. Enteropathogens associated with pediatric diarrhea in Mexico City. The Journal of Pediatrics 91, 65–68. https://doi.org/10.1016/S0022-3476(77)80446-0

82. Fagundes, N.J.R., Tagliani-Ribeiro, A., Rubicz, R., Tarskaia, L., Crawford, M.H., Salzano, F.M., Bonatto, S.L., 2018. How strong was the bottleneck associated to the peopling of the Americas? New insights from multilocus sequence data. Genetics and Molecular Biology 41, 206–214. https://doi.org/10.1590/1678-4685-GMB-2017-0087

83. Favila, M.A., Geraci, N.S., Zeng, E., Harker, B., Condon, D., Cotton, R.N., Jayakumar, A., Tripathi, V., McDowell, M.A., 2014. Human Dendritic Cells Exhibit a Pronounced Type I IFN Signature following Leishmania major Infection That Is Required for IL-12 Induction. The Journal of Immunology 192, 5863–5872. https://doi.org/10.4049/jimmunol.1203230

84. Fehren-Schmitz, L., Harkins, K.M., Llamas, B., 2017. A paleogenetic perspective on the early population history of the high altitude Andes. Quaternary International, The Peopling of High-Altitude Landscapes of the Americas 461, 25–33. https://doi.org/10.1016/j.quaint.2017.01.003

85. Ferrer-Admetlla, A., Liang, M., Korneliussen, T., Nielsen, R., 2014. On detecting incomplete soft or hard selective sweeps using haplotype structure. Molecular Biology and Evolution 31, 1275–1291. https://doi.org/10.1093/molbev/msu077

86. Fischer, E.M., Sippel, S., Knutti, R., 2021. Increasing probability of record-shattering climate extremes. Nature Climate Change 1–7. https://doi.org/10.1038/s41558-021-01092-9

87. Fisher, G.J., Choi, H.-C., Bata-Csorgo, Z., Shao, Y., Datta, S., Wang, Z.-Q., Kang, S., Voorhees, J.J., 2001. Ultraviolet Irradiation Increases Matrix Metalloproteinase-8 Protein in Human Skin In Vivo. Journal of Investigative Dermatology 117, 219–226. https://doi.org/10.1046/j.0022-202x.2001.01432.x

88. Foundation for Statistical Computing, Vienna, Austria. https://www.R-project.org/.

89. Franciscus, R.G., 1999. Neandertal nasal structures and upper respiratory tract "specialization." PNAS 96, 1805–1809. https://doi.org/10.1073/pnas.96.4.1805

90. Franklinos, L.H.V., Jones, K.E., Redding, D.W., Abubakar, I., 2019. The effect of global change on mosquito-borne disease. The Lancet Infectious Diseases 19, e302–e312. https://doi.org/10.1016/S1473-3099(19)30161-6

91. Frayer, D.W., Wolpoff, M.H., 1985. Sexual Dimorphism. Annual Review of Anthropology 14, 429–473. https://doi.org/10.1146/annurev.an.14.100185.002241

92. Fruciano, C., 2016. Measurement error in geometric morphometrics. Development Genes and Evolution 226, 139–158. https://doi.org/10.1007/s00427-016-0537-4

93. Fuentes, A., 2021. Searching for the "Roots" of Masculinity in Primates and the Human Evolutionary Past. Current Anthropology 62, S13–S25. https://doi.org/10.1086/711582

94. Fukase, H., Ito, T., Ishida, H., 2016. Geographic variation in nasal cavity form among three human groups from the Japanese Archipelago: Ecogeographic and functional implications. American Journal of Human Biology 28, 343–351. https://doi.org/10.1002/ajhb.22786

95. Fumagalli, M., Moltke, I., Grarup, N., Racimo, F., Bjerregaard, P., Jørgensen, M.E., Korneliussen, T.S., Gerbault, P., Skotte, L., Linneberg, A., Christensen, C., Brandslund, I., Jørgensen, T., Huerta-Sánchez, E., Schmidt, E.B., Pedersen, O., Hansen, T., Albrechtsen, A., Nielsen, R., 2015. Greenlandic Inuit show genetic signatures of diet and climate adaptation. Science 349, 1343–1347. https://doi.org/10.1126/science.aab2319

96. G. Amorim, C.E., Nunes, K., Meyer, D., Comas, D., Bortolini, M.C., Salzano, F.M., Hünemeier, T., 2017. Genetic signature of natural selection in first Americans. PNAS 114, 2195–2199. https://doi.org/10.1073/pnas.1620541114

97. Gagge, A.P., Gonzalez, R.R., 2011. Mechanisms of Heat Exchange: Biophysics and Physiology, in: Comprehensive Physiology. John Wiley & Sons, Ltd, pp. 45–84. https://doi.org/10.1002/cphy.cp040104

98. Gagnon, D., Crandall, C.G., 2018. Sweating as a heat loss thermoeffector. Handbook of Clinical Neurology 156, 211–232. https://doi.org/10.1016/B978-0-444-63912-7.00013-8

99. Gallagher, S.A., Hackett, P.H., 2004. High-altitude illness. Emergency Medicine Clinics 22, 329–355. https://doi.org/10.1016/j.emc.2004.02.001

100. García-Trabanino, R., Jarquín, E., Wesseling, C., Johnson, R.J., González-Quiroz, M., Weiss, I., Glaser, J., José Vindell, J., Stockfelt, L., Roncal, C., Harra, T., Barregard, L., 2015. Heat stress, dehydration, and kidney function in sugarcane cutters in El Salvador – A cross-shift study of workers at risk of Mesoamerican nephropathy. Environmental Research 142, 746–755. https://doi.org/10.1016/j.envres.2015.07.007

101. Garvin, H.M., Elliott, M.C., Delezene, L.K., Hawks, J., Churchill, S.E., Berger, L.R., Holliday, T.W., 2017. Body size, brain size, and sexual dimorphism in Homo naledi from the Dinaledi Chamber. Journal of Human Evolution 111, 119–138. https://doi.org/10.1016/j.jhevol.2017.06.010

102. Gasparrini, A., Guo, Y., Hashizume, M., Lavigne, E., Zanobetti, A., Schwartz, J., Tobias, A., Tong, S., Rocklöv, J., Forsberg, B., Leone, M., Sario, M.D., Bell, M.L., Guo, Y.-L.L.,

Wu, C., Kan, H., Yi, S.-M., Coelho, M. de S.Z.S., Saldiva, P.H.N., Honda, Y., Kim, H., Armstrong, B., 2015. Mortality risk attributable to high and low ambient temperature: a multicountry observational study. The Lancet 386, 369–375. https://doi.org/10.1016/S0140-6736(14)62114-0

103. Gassmann, N.N., van Elteren, H.A., Goos, T.G., Morales, C.R., Rivera-Ch, M., Martin, D.S., Cabala Peralta, P., Passano del Carpio, A., Aranibar Machaca, S., Huicho, L., Reiss, I.K.M., Gassmann, M., de Jonge, R.C.J., 2016. Pregnancy at high altitude in the Andes leads to increased total vessel density in healthy newborns." Journal of Applied Physiology (Bethesda, Md. : 1985) vol. 121,3 (2016): 709-15. doi:10.1152/japplphysiol.00561.2016

104. Gastañaduy, P.A., Sánchez-Uribe, E., Esparza-Aguilar, M., Desai, R., Parashar, U.D., Patel, M., Richardson, V., 2013. Effect of Rotavirus Vaccine on Diarrhea Mortality in Different Socioeconomic Regions of Mexico. Pediatrics 131, e1115–e1120. https://doi.org/10.1542/peds.2012-2797

105. Gazal, S., Espinoza, J.R., Austerlitz, F., Marchant, D., Macarlupu, J.L., Rodriguez, J., Ju-Preciado, H., Rivera-Chira, M., Hermine, O., Leon-Velarde, F., Villafuerte, F.C., Richalet, J.-P., Gouya, L., 2019. The Genetic Architecture of Chronic Mountain Sickness in Peru. Frontiers in Genetics 10, 690. https://doi.org/10.3389/fgene.2019.00690

106. Gokhman, D., Nissim-Rafinia, M., Agranat-Tamir, L., Housman, G., García-Pérez, R., Lizano, E., Cheronet, O., Mallick, S., Nieves-Colón, M.A., Li, H., Alpaslan-Roodenberg, S., Novak, M., Gu, H., Osinski, J.M., Ferrando-Bernal, M., Gelabert, P., Lipende, I., Mjungu, D., Kondova, I., Bontrop, R., Kullmer, O., Weber, G., Shahar, T., Dvir-Ginzberg, M., Faerman, M., Quillen, E.E., Meissner, A., Lahav, Y., Kandel, L., Liebergall, M., Prada, M.E., Vidal, J.M., Gronostajski, R.M., Stone, A.C., Yakir, B., Lalueza-Fox, C., Pinhasi, R., Reich, D., Marques-Bonet, T., Meshorer, E., Carmel, L., 2020. Differential DNA methylation of vocal and facial anatomy genes in modern humans. Nature Communications 11, 1189. https://doi.org/10.1038/s41467-020-15020-6

107. Golant, A., Nord, R.M., Paksima, N., Posner, M.A., 2008. Cold Exposure Injuries to the Extremities: Journal of the American Academy of Orthopaedic Surgeons 16, 704–715. https://doi.org/10.5435/00124635-200812000-00003

108. González, A.H.G., Sandoval, C.R., Mata, A.T., Sanvicente, M.B., Stinnesbeck, W., 2008. The Arrival of Humans on the Yucatan Peninsula: Evidence from Submerged Caves in the State of Quintana Roo, Mexico 24.

109. Gordon, K., Blondin, D.P., Friesen, B.J., Tingelstad, H.C., Kenny, G.P., Haman, F., 2019. Seven days of cold acclimation substantially reduces shivering intensity and increases nonshivering thermogenesis in adult humans. Journal of Applied Physiology 126, 1598–1606. https://doi.org/10.1152/japplphysiol.01133.2018

110. Granberg, P.O., 1991. Human physiology under cold exposure. Arctic Medical Research 50 Suppl 6, 23–27.

111. Guernier, V., Hochberg, M.E., Guégan, J.-F., 2004. Ecology Drives the Worldwide Distribution of Human Diseases. PLoS Biology 2, e141. https://doi.org/10.1371/journal.pbio.0020141

112. Hampton, W.R., 1981. Hypothermia in winter and high altitude sports. Connecticut Medicine 45, 633–636.

113. Hancock, A.M., Clark, V.J., Qian, Y., Di Rienzo, A., 2011. Population Genetic Analysis of the Uncoupling Proteins Supports a Role for UCP3 in Human Cold Resistance. Molecular Biology and Evolution 28, 601–614. https://doi.org/10.1093/molbev/msq228

114. Hancock, A.M., Witonsky, D.B., Gordon, A.S., Eshel, G., Pritchard, J.K., Coop, G., Rienzo, A.D., 2008. Adaptations to Climate in Candidate Genes for Common Metabolic Disorders. PLoS Genetics 4, e32. https://doi.org/10.1371/journal.pgen.0040032

115. Haralabakis, H.N., Dagalakis, E.G., 1980. Effect of prednisolone and human growth hormone on growth of cranial bones and cranial base synchondroses in rats. European Journal of Orthodontics 2, 239–248. https://doi.org/10.1093/ejo/2.4.239

116. Harris, I., Osborn, T.J., Jones, P., Lister, D., 2020. Version 4 of the CRU TS monthly high-resolution gridded multivariate climate dataset. Scientific Data 7, 109. https://doi.org/10.1038/s41597-020-0453-3

117. Hassi, J., Sikkilä, K., Ruokonen, A., Leppäluoto, J., 2001. The pituitary-thyroid axis in healthy men living under subarctic climatological conditions. Journal of Endocrinology 169, 195–203. https://doi.org/10.1677/joe.0.1690195

118. Heeren, J., Scheja, L., 2018. Brown adipose tissue and lipid metabolism. Current Opinion in Lipidology 29, 180–185. https://doi.org/10.1097/MOL.0000000000000504

119. Hoffmann, S., He, S., Ehren, M., Ryan, S.J., Wiedemann, P., Hinton, D.R., 2006. MMP-2 and MMP-9 secretion by rpe is stimulated by angiogenic molecules found in choroidal neovascular membranes. Retina 26, 454–461. https://doi.org/10.1097/01.iae.0000238549.74626.33

120. Hofmann, F., Loga, F., Domes, K., Patrucco, E., Wegener, J.W., 2013. cGMP kinase: past, presence and future. BMC Pharmacology and Toxicology 14, O11. https://doi.org/10.1186/2050-6511-14-S1-O11

121. Holliday, T.W., 1997. Postcranial evidence of cold adaptation in European Neandertals. American Journal of Physical Anthropology 104, 245–258. https://doi.org/10.1002/(SICI)1096-8644(199710)104:2

122. Hora, M., Pontzer, H., Wall-Scheffler, C.M., Sládek, V., 2020. Dehydration and persistence hunting in Homo erectus. Journal of Human Evolution 138, 102682. https://doi.org/10.1016/j.jhevol.2019.102682

123. Howells, W., 1973. Cranial Variation In Man: A Study By Multivariate Analysis Of Patterns Of Difference Among Recent Human Populations. Papers Of The Peabody Museum Of Archeology And Ethnology, (67), 1-259.

124. Hsieh, P., Hallmark, B., Watkins, J., Karafet, T.M., Osipova, L.P., Gutenkunst, R.N., Hammer, M.F., 2017. Exome Sequencing Provides Evidence of Polygenic Adaptation to a Fat-Rich Animal Diet in Indigenous Siberian Populations. Molecular Biology and Evolution 34, 2913–2926. https://doi.org/10.1093/molbev/msx226

125. Hu, H., Petousi, N., Glusman, G., Yu, Y., Bohlender, R., Tashi, T., Downie, J.M., Roach, J.C., Cole, A.M., Lorenzo, F.R., Rogers, A.R., Brunkow, M.E., Cavalleri, G., Hood, L., Alpatty, S.M., Prchal, J.T., Jorde, L.B., Robbins, P.A., Simonson, T.S., Huff, C.D., 2017. Evolutionary history of Tibetans inferred from whole-genome sequencing. PLOS Genetics 13, e1006675. https://doi.org/10.1371/journal.pgen.1006675

126. Hubbe, M., Hanihara, T., Harvati, K., 2009. Climate Signatures in the Morphological Differentiation of Worldwide Modern Human Populations. The Anatomical Record 292, 1720–1733. https://doi.org/10.1002/ar.20976

127. Hulur, I., Hermanns, P., Nestoris, C., Heger, S., Refetoff, S., Pohlenz, J., Grasberger, H., 2011. A Single Copy of the Recently Identified Dual Oxidase Maturation Factor (DUOXA) 1 Gene Produces Only Mild Transient Hypothyroidism in a Patient with a Novel Biallelic DUOXA2 Mutation and Monoallelic DUOXA1 Deletion. The Journal of Clinical Endocrinology & Metabolism 96, E841–E845. https://doi.org/10.1210/jc.2010-2321

128. Hung, T., Chen, G.M., Wang, C.G., Yao, H.L., Fang, Z.Y., Chao, T.X., Chou, Z.Y., Ye, W., Chang, X.J., Den, S.S., 1984. Waterborne outbreak of rotavirus diarrhoea in adults in China caused by a novel rotavirus. Lancet 1, 1139–1142.

129. Igoshin, A.V., Gunbin, K.V., Yudin, N.S., Voevoda, M.I., 2019. Searching for Signatures of Cold Climate Adaptation in TRPM8 Gene in Populations of East Asian Ancestry. Frontiers in Genetics 10, 759. https://doi.org/10.3389/fgene.2019.00759

130. Innes, A.M., Seshia, M.M., Prasad, C., Al Saif, S., Friesen, F.R., Chudley, A.E., Reed, M., Dilling, L.A., Haworth, J.C., Greenberg, C.R., 2002. Congenital rickets caused by maternal vitamin D deficiency. Paediatrics & Child Health 7, 455–458.

131. Jablonski, N.G., Chaplin, G., 2010. Human skin pigmentation as an adaptation to UV radiation. PNAS 107, 8962–8968. https://doi.org/10.1073/pnas.0914628107

132. Jablonski, N.G., Chaplin, G., 2017. The colours of humanity: the evolution of pigmentation in the human lineage. Philosophical Transactions of the Royal Society B: Biological Sciences 372, 20160349. https://doi.org/10.1098/rstb.2016.0349

133. Jacovas, V.C., Couto-Silva, C.M., Nunes, K., Lemes, R.B., de Oliveira, M.Z., Salzano, F.M., Bortolini, M.C., Hünemeier, T., 2018. Selection scan reveals three new loci related to high altitude adaptation in Native Andeans. Scientific Reports 8, 12733. https://doi.org/10.1038/s41598-018-31100-6

134. Jacovas, V.C., Rovaris, D.L., Peréz, O., Azevedo, S. de, Macedo, G.S., Sandoval, J.R., Salazar-Granara, A., Villena, M., Dugoujon, J.-M., Bisso-Machado, R., Petzl-Erler, M.L., Salzano, F.M., Ashton-Prolla, P., Ramallo, V., Bortolini, M.C., 2015. Genetic Variations in

the TP53 Pathway in Native Americans Strongly Suggest Adaptation to the High Altitudes of the Andes. PLOS ONE 10, e0137823. https://doi.org/10.1371/journal.pone.0137823

135. Jamal, M.H., Abu-Farha, M., Al-Khaledi, G., Al-Sabah, S., Ali, H., Cherian, P., Al-Khairi, I., AlOtaibi, F., Al-Ali, W., Bosso, M., Dsouza, C., Abubaker, J., Al-Mulla, F., 2020. Effect of sleeve gastrectomy on the expression of meteorin-like (METRNL) and Irisin (FNDC5) in muscle and brown adipose tissue and its impact on uncoupling proteins in diet-induced obesity rats. Surgery for Obesity and Related Diseases 16, 1910–1918. https://doi.org/10.1016/j.soard.2020.07.022

136. Jiménez, F.A., Gardner, S.L., Araújo, A., Fugassa, M., Brooks, R.H., Racz, E., Reinhard, K.J., 2012. Zoonotic and human parasites of inhabitants of Cueva de los Muertos Chiquitos, Rio Zape Valley, Durango, Mexico. Journal of Parasitology 98, 304–309. https://doi.org/10.1645/GE-2915.1

137. Johnson, N.A., Coram, M.A., Shriver, M.D., Romieu, I., Barsh, G.S., London, S.J., Tang, H., 2011. Ancestral Components of Admixed Genomes in a Mexican Cohort. PLoS Genetics 7, e1002410. https://doi.org/10.1371/journal.pgen.1002410

138. Johnston, C.E., White, M.D., Wu, M., Bristow, G.K., Giesbrecht, G.G., 1996. Eucapnic hypoxia lowers human cold thermoregulatory response thresholds and accelerates core cooling. Journal of Applied Physiology 80, 422–429. https://doi.org/10.1152/jappl.1996.80.2.422

139. Katzmarzyk, P.T., Leonard, W.R., 1998. Climatic influences on human body size and proportions: Ecological adaptations and secular trends. American Journal of Physical Anthropology 106, 483–503. https://doi.org/10.1002/(SICI)1096-8644(199808)106:4<483::AID-AJPA4>3.0.CO;2-K

140. Keatinge, W.R., Coleshaw, S.R.K., Easton, J.C., Cotter, F., Mattock, M.B., Chelliah, R., 1986. Increased platelet and red cell counts, blood viscosity, and plasma cholesterol levels during heat stress, and mortality from coronary and cerebral thrombosis. The American Journal of Medicine 81, 795–800. https://doi.org/10.1016/0002-9343(86)90348-7

141. Kern, A.D., Hahn, M.W., 2018. The Neutral Theory in Light of Natural Selection. Molecular Biology and Evolution 35, 1366–1371. https://doi.org/10.1093/molbev/msy092

142. Key, F.M., Abdul-Aziz, M.A., Mundry, R., Peter, B.M., Sekar, A., D'Amato, M., Dennis, M.Y., Schmidt, J.M., Andrés, A.M., 2018. Human local adaptation of the TRPM8 cold receptor along a latitudinal cline. PLOS Genetics 14, e1007298. https://doi.org/10.1371/journal.pgen.1007298

143. Khan, A., Dou, J., Wang, Y., Jiang, X., Khan, M.Z., Luo, H., Usman, T., Zhu, H., 2020. Evaluation of heat stress effects on cellular and transcriptional adaptation of bovine granulosa cells. Journal of Animal Science and Biotechnology 11, 25. https://doi.org/10.1186/s40104-019-0408-8

144. Kottke, F.J., Phalen, J.S., Taylor, C.B., Visscher, M.B., Evans, G.T., 1948. Effect of Hypoxia Upon Temperature Regulation of Mice, Dogs, and Men. American Journal of Physiology-Legacy Content 153, 10–15. https://doi.org/10.1152/ajplegacy.1948.153.1.10

145. Laitman, J.T., Reidenberg, J.S., Marquez, S., Gannon, P.J., 1996. What the Nose Knows: New Understandings of Neanderthal Upper Respiratory Tract Specializations. PNAS 93, 10543–10545.

146. Lans, A.A.J.J. van der, Hoeks, J., Brans, B., Vijgen, G.H.E.J., Visser, M.G.W., Vosselman, M.J., Hansen, J., Jorgensen, J.A., Wu, J., Mottaghy, F.M., Schrauwen, P., Lichtenbelt, W.D. van M., 2013. Cold acclimation recruits human brown fat and increases nonshivering thermogenesis. The Journal of Clinical Investigation https://doi.org/10.1172/JCI68993

147. Larsen, C.S., 2003. Equality for the sexes in human evolution? Early hominid sexual dimorphism and implications for mating systems and social behavior. PNAS 100, 9103–9104. https://doi.org/10.1073/pnas.1633678100

148. Lasisi, T., Shriver, M.D., 2018. Focus on African diversity confirms complexity of skin pigmentation genetics. Genome Biology 19, 13. https://doi.org/10.1186/s13059-018-1395-3

149. Law, J., Chalmers, J., Morris, D.E., Robinson, L., Budge, H., Symonds, M.E., 2018. The use of infrared thermography in the measurement and characterization of brown adipose tissue activation. Temperature (Austin) 5, 147–161. https://doi.org/10.1080/23328940.2017.1397085

150. Leakey, R.E.F., 1973. Evidence for an Advanced Plio-Pleistocene Hominid from East Rudolf, Kenya. Nature 242, 447–450. https://doi.org/10.1038/242447a0

151. Leonard, W.R., Sorensen, M.V., Galloway, V.A., Spencer, G.J., Mosher, M.J., Osipova, L., Spitsyn, V.A., 2002. Climatic influences on basal metabolic rates among circumpolar populations. American Journal of Human Biology 14, 609–620. https://doi.org/10.1002/ajhb.10072

152. Levy, S.B., Klimova, T.M., Zakharova, R.N., Federov, A.I., Fedorova, V.I., Baltakhinova, M.E., Leonard, W.R., 2018. Brown adipose tissue, energy expenditure, and biomarkers of cardio-metabolic health among the Yakut (Sakha) of northeastern Siberia. American Journal of Human Biology 30, e23175. https://doi.org/10.1002/ajhb.23175

153. Levy, S.B., Klimova, T.M., Zakharova, R.N., Fedorov, A.I., Fedorova, V.I., Baltakhinova, M.E., Leonard, W.R., 2021. Evidence for a sensitive period of plasticity in brown adipose tissue during early childhood among indigenous Siberians. American Journal of Physical Anthropology 175, 834–846. https://doi.org/10.1002/ajpa.24297

154. Li, L., Liu, Xinhua, He, L., Yang, J., Pei, F., Li, W., Liu, S., Chen, Z., Xie, G., Xu, B., Ting, X., Zhang, Z., Jin, T., Liu, Xujun, Zhang, W., Yuan, S., Yang, Z., Wu, C., Zhang, Y., Yang, X., Yi, X., Liang, J., Shang, Y., Sun, L., 2017. ZNF516 suppresses EGFR by targeting the CtBP/LSD1/CoREST complex to chromatin. Nature Communications 8, 691. https://doi.org/10.1038/s41467-017-00702-5

155. Lidell, M.E., Betz, M.J., Leinhard, O.D., Heglind, M., Elander, L., Slawik, M., Mussack, T., Nilsson, D., Romu, T., Nuutila, P., Virtanen, K.A., Beuschlein, F., Persson, A., Borga, M., Enerbäck, S., 2013. Evidence for two types of brown adipose tissue in humans. Nature Medicine 19, 631–634. https://doi.org/10.1038/nm.3017

156. Liu, Y., Hu, W., Murakawa, Y., Yin, J., Wang, G., Landthaler, M., Yan, J., 2013. Cold-induced RNA-binding proteins regulate circadian gene expression by controlling alternative polyadenylation. Scientific Reports 3, 2054. https://doi.org/10.1038/srep02054

157. Ma, Y., Olendzki, B.C., Li, W., Hafner, A.R., Chiriboga, D., Hebert, J.R., Campbell, M., Sarnie, M., Ockene, I.S., 2006. Seasonal variation in food intake, physical activity, and body weight in a predominantly overweight population. European Journal of Clinical Nutrition 60, 519–528. https://doi.org/10.1038/sj.ejcn.1602346

158. Mäkinen, T.M., Juvonen, R., Jokelainen, J., Harju, T.H., Peitso, A., Bloigu, A., Silvennoinen-Kassinen, S., Leinonen, M., Hassi, J., 2009. Cold temperature and low humidity are associated with increased occurrence of respiratory tract infections. Respiratory Medicine 103, 456–462. https://doi.org/10.1016/j.rmed.2008.09.011

159. Malaspinas, A.-S., Westaway, M.C., Muller, C., Sousa, V.C., Lao, O., Alves, I., Bergström, A., Athanasiadis, G., Cheng, J.Y., Crawford, J.E., Heupink, T.H., Macholdt, E., Peischl, S., Rasmussen, S., Schiffels, S., Subramanian, S., Wright, J.L., Albrechtsen, A., Barbieri, C., Dupanloup, I., Eriksson, A., Margaryan, A., Moltke, I., Pugach, I., Korneliussen, T.S., Levkivskyi, I.P., Moreno-Mayar, J.V., Ni, S., Racimo, F., Sikora, M., Xue, Y., Aghakhanian, F.A., Brucato, N., Brunak, S., Campos, P.F., Clark, W., Ellingvåg, S., Fourmile, G., Gerbault, P., Injie, D., Koki, G., Leavesley, M., Logan, B., Lynch, A., Matisoo-Smith, E.A., McAllister, P.J., Mentzer, A.J., Metspalu, M., Migliano, A.B., Murgha, L., Phipps, M.E., Pomat, W., Reynolds, D., Ricaut, F.-X., Siba, P., Thomas, M.G., Wales, T., Wall, C.M., Oppenheimer, S.J., Tyler-Smith, C., Durbin, R., Dortch, J., Manica, A., Schierup, M.H., Foley, R.A., Lahr, M.M., Bowern, C., Wall, J.D., Mailund, T., Stoneking, M., Nielsen, R., Sandhu, M.S., Excoffier, L., Lambert, D.M., Willerslev, E., 2016. A genomic history of Aboriginal Australia. Nature 538, 207–214. https://doi.org/10.1038/nature18299

160. Manichaikul, A., Mychaleckyj, J.C., Rich, S.S., Daly, K., Sale, M., Chen, W.-M., 2010. Robust relationship inference in genome-wide association studies. Bioinformatics 26, 2867–2873. https://doi.org/10.1093/bioinformatics/btq559

161. Marcus, J.H., Novembre, J., 2016. Visualizing the geography of genetic variants. Bioinformatics btw643. https://doi.org/10.1093/bioinformatics/btw643

162. Márquez, S., Pagano, A.S., Delson, E., Lawson, W., Laitman, J.T., 2014. The Nasal Complex of Neanderthals: An Entry Portal to their Place in Human Ancestry. The Anatomical Record 297, 2121–2137. https://doi.org/10.1002/ar.23040

163. Matthews, H., Penington, T., Saey, I., Halliday, J., Muggli, E., Claes, P., 2016. Spatially dense morphometrics of craniofacial sexual dimorphism in 1-year-olds. Journal of Anatomy 229, 549–559. https://doi.org/10.1111/joa.12507

164. Mattiangeli, V., Ryan, A.W., McManus, R., Bradley, D.G., 2006. A genome-wide approach to identify genetic loci with a signature of natural selection in the Irish population. Genome Biology 7, R74. https://doi.org/10.1186/gb-2006-7-8-r74

165. McDonald, J.H., Kreitman, M., 1991. Adaptive protein evolution at the Adh locus in Drosophila. Nature 351, 652–654. https://doi.org/10.1038/351652a0

166. McHenry, H.M., 1992. Body size and proportions in early hominids. American Journal of Physical Anthropology 87, 407–431. https://doi.org/10.1002/ajpa.1330870404

167. Miller, K., Duran-Pinales, C., Cruz-Lopez, A., Morales-Lechuga, L., Taren, D., Enriquez, F.J., 1994. Cryptosporidium Parvum in Children with Diarrhea in Mexico. The American Journal of Tropical Medicine and Hygiene 51, 322–325. https://doi.org/10.4269/ajtmh.1994.51.322

168. Miller, V., Bates, G., 2007. Hydration of outdoor workers in north-west Australia. Journal of Occupational Health and Safety, Australia 23, 79 - 87

169. Milunsky, A., Ulcickas, M., Rothman, K.J., Willett, W., Jick, S.S., Jick, H., 1992. Maternal Heat Exposure and Neural Tube Defects. JAMA 268, 882–885. https://doi.org/10.1001/jama.1992.03490070064043

170. Minder, J.R., Mote, P.W., Lundquist, J.D., 2010. Surface temperature lapse rates over complex terrain: Lessons from the Cascade Mountains. Journal of Geophysical Research: Atmospheres 115. https://doi.org/10.1029/2009JD013493

171. Morhenn, V.B., Nelson, T.E., Gruol, D.L., 2013. The rate of wound healing is increased in psoriasis. Journal of Dermatological Science 72, 87–92. https://doi.org/10.1016/j.jdermsci.2013.06.001

172. Müller, S., Perdikari, A., Dapito, D.H., Sun, W., Wollscheid, B., Balaz, M., Wolfrum, C., 2020. ESRRG and PERM1 Govern Mitochondrial Conversion in Brite/Beige Adipocyte Formation. Frontiers in Endocrinology 11, 387. https://doi.org/10.3389/fendo.2020.00387

173. Murdoch, D.R., 1995. Symptoms of infection and altitude illness among hikers in the Mount Everest region of Nepal. Aviation, Space, and Environmental Medicine 66, 148–151.

174. Murray, H.W., Berman, J.D., Davies, C.R., Saravia, N.G., 2005. Advances in leishmaniasis. The Lancet 366, 1561–1577. https://doi.org/10.1016/S0140-6736(05)67629-5

175. Muzik, O., Mangner, T.J., Leonard, W.R., Kumar, A., Janisse, J., Granneman, J.G., 2013. 15O PET Measurement of Blood Flow and Oxygen Consumption in Cold-Activated Human Brown Fat. Journal of Nuclear Medicine 54, 523–531. https://doi.org/10.2967/jnumed.112.111336

176. Nakajima, H., Nakagomi, T., Kamisawa, T., Sakaki, N., Muramoto, K., Mikami, T., Nara, H., Nakagomi, O., 2001. Winter seasonality and rotavirus diarrhoea in adults. The Lancet 357, 1950. https://doi.org/10.1016/S0140-6736(00)05086-8

177. Näyhä, S., Hassi, J., Jousilahti, P., Laatikainen, T., Ikäheimo, T.M., 2011. Cold-related symptoms among the healthy and sick of the general population: National FINRISK Study data, 2002. Public Health 125, 380–388. https://doi.org/10.1016/j.puhe.2011.02.014

178. Nedergaard, J., Bengtsson, T., Cannon, B., 2011. New Powers of Brown Fat: Fighting the Metabolic Syndrome. Cell Metabolism 13, 238–240. https://doi.org/10.1016/j.cmet.2011.02.009

179. Nedergaard, J., Cannon, B., 2018. Chapter 9 - Brown adipose tissue as a heat-producing thermoeffector, in: Romanovsky, A.A. (Ed.), Handbook of Clinical Neurology, Thermoregulation: From Basic Neuroscience to Clinical Neurology Part I. Elsevier, pp. 137–152. https://doi.org/10.1016/B978-0-444-63912-7.00009-6

180. Nepal, O., Pokhrel, B.R., Khanal, K., Gyawali, P., Malik, S.L., Koju, R., Kapoor, B.K., 2013. Thyroid hormone levels in highlanders- a comparison between residents of two altitudes in Nepal. Kathmandu University Medical Journal (KUMJ) 11, 18–21. https://doi.org/10.3126/kumj.v11i1.11017

181. Newman, M.T., 1953. The Application of Ecological Rules to the Racial Anthropology of the Aboriginal New World. American Anthropologist 55, 311–327.

182. Nichols, A.W., 2014. Heat-related illness in sports and exercise. Current Reviews in Musculoskeletal Medicine 7, 355–365. https://doi.org/10.1007/s12178-014-9240-0

183. Noback, M.L., Harvati, K., Spoor, F., 2011. Climate-related variation of the human nasal cavity. American Journal of Physical Anthropology 145, 599–614. https://doi.org/10.1002/ajpa.21523

184. Ocobock, C., 2016. Human energy expenditure, allocation, and interactions in natural temperate, hot, and cold environments. American Journal of Physical Anthropology 161, 667–675. https://doi.org/10.1002/ajpa.23071

185. Odonne, G., Bourdy, G., Castillo, D., Estevez, Y., Lancha-Tangoa, A., Alban-Castillo, J., Deharo, E., Rojas, R., Stien, D., Sauvain, M., 2009. Ta'ta', Huayani: Perception of leishmaniasis and evaluation of medicinal plants used by the Chayahuita in Peru. Part II. Journal of Ethnopharmacology 126, 149–158. https://doi.org/10.1016/j.jep.2009.07.015

186. Oelkrug, R., Polymeropoulos, E.T., Jastroch, M., 2015. Brown adipose tissue: physiological function and evolutionary significance. Journal of Compative Physiology B 185, 587–606. https://doi.org/10.1007/s00360-015-0907-7

187. Osorio, F.G., Soria-Valles, C., Santiago-Fernández, O., Bernal, T., Mittelbrunn, M., Colado, E., Rodríguez, F., Bonzon-Kulichenko, E., Vázquez, J., Porta-de-la-Riva, M., Cerón, J., Fueyo, A., Li, J., Green, A.R., Freije, J.M.P., López-Otín, C., 2016. Loss of the proteostasis factor AIRAPL causes myeloid transformation by deregulating IGF-1 signaling. Nature Medicine 22, 91–96. https://doi.org/10.1038/nm.4013

188. Ossendorf, G., Groos, A.R., Bromm, T., Tekelemariam, M.G., Glaser, B., Lesur, J., Schmidt, J., Akçar, N., Bekele, T., Beldados, A., Demissew, S., Kahsay, T.H., Nash, B.P.,

Nauss, T., Negash, A., Nemomissa, S., Veit, H., Vogelsang, R., Woldu, Z., Zech, W., Opgenoorth, L., Miehe, G., 2019. Middle Stone Age foragers resided in high elevations of the glaciated Bale Mountains, Ethiopia. Science 365, 583–587. https://doi.org/10.1126/science.aaw8942

189. Ouellet, V., Labbé, S.M., Blondin, D.P., Phoenix, S., Guérin, B., Haman, F., Turcotte, E.E., Richard, D., Carpentier, A.C., 2012. Brown adipose tissue oxidative metabolism contributes to energy expenditure during acute cold exposure in humans. Journal of Clinical Investigations 122, 545–552. https://doi.org/10.1172/JCI60433

190. Ozato, K., Shin, D.-M., Chang, T.-H., Morse, H.C., 2008. TRIM family proteins and their emerging roles in innate immunity. Nature Reviews in Immunology 8, 849–860. https://doi.org/10.1038/nri2413

191. Pagani, L., Ayub, Q., MacArthur, D.G., Xue, Y., Baillie, J.K., Chen, Y., Kozarewa, I., Turner, D.J., Tofanelli, S., Bulayeva, K., Kidd, K., Paoli, G., Tyler-Smith, C., 2012. High altitude adaptation in Daghestani populations from the Caucasus. Human Genetics 131, 423–433. https://doi.org/10.1007/s00439-011-1084-8

192. Palumbo, E., 2010. Treatment Strategies for Mucocutaneous Leishmaniasis. Journal of Global Infectious Diseases 2, 147–150. https://doi.org/10.4103/0974-777X.62879

193. Patterson, D.B., Braun, D.R., Behrensmeyer, A.K., Merritt, S., Zliobaite, I., Reeves, J.S., Wood, B.A., Fortelius, M., Bobe, R., 2017. Ecosystem evolution and hominin paleobiology at East Turkana, northern Kenya between 2.0 and 1.4Ma. Palaeogeography, Palaeoclimatology, Palaeoecology 481, 1–13. https://doi.org/10.1016/j.palaeo.2017.05.001

194. Pedersen, T.L., RStudio, 2021. ggforce: Accelerating “ggplot2.” R package version 0.3.3

195. Piazena, H., 1996. The effect of altitude upon the solar UV-B and UV-A irradiance in the tropical Chilean Andes. Solar Energy 57, 133–140. https://doi.org/10.1016/S0038-092X(96)00049-7

196. Pirinen, S., 1995. Endocrine regulation of craniofacial growth. Acta Odontologica Scandinavica 53, 179–185. https://doi.org/10.3109/00016359509005969

197. Pontzer, H., 2012. Ecological Energetics in Early Homo. Current Anthropology 53, S346–S358. https://doi.org/10.1086/667402

198. Pontzer, H., Brown, M.H., Wood, B.M., Raichlen, D.A., Mabulla, A.Z.P., Harris, J.A., Dunsworth, H., Hare, B., Walker, K., Luke, A., Dugas, L.R., Schoeller, D., Plange-Rhule, J., Bovet, P., Forrester, T.E., Thompson, M.E., Shumaker, R.W., Rothman, J.M., Vogel, E., Sulistyo, F., Alavi, S., Prasetyo, D., Urlacher, S.S., Ross, S.R., 2021. Evolution of water conservation in humans. Current Biology 31, 1804-1810.e5. https://doi.org/10.1016/j.cub.2021.02.045

199. Potts, R., 2012. Environmental and Behavioral Evidence Pertaining to the Evolution of Early Homo. Current Anthropology 53, S299–S317. https://doi.org/10.1086/667704

200. Poursharifi, P., Attané, C., Mugabo, Y., Al-Mass, A., Ghosh, A., Schmitt, C., Zhao, S., Guida, J., Lussier, R., Erb, H., Chenier, I., Peyot, M.-L., Joly, E., Noll, C., Carpentier, A.C., Madiraju, S.R.M., Prentki, M., 2020. Adipose ABHD6 regulates tolerance to cold and thermogenic programs. JCI Insights 5. https://doi.org/10.1172/jci.insight.140294

201. Profumo, E., Buttari, B., Tinaburri, L., D'Arcangelo, D., Sorice, M., Capozzi, A., Garofalo, T., Facchiano, A., Businaro, R., Kumar, P., Singh, B.K., Parmar, V.S., Saso, L., Riganò, R., 2018. Oxidative Stress Induces HSP90 Upregulation on the Surface of Primary Human Endothelial Cells: Role of the Antioxidant 7,8-Dihydroxy-4-methylcoumarin in Preventing HSP90 Exposure to the Immune System. Oxidative Medicine and Cellular Longevity 2018, e2373167. https://doi.org/10.1155/2018/2373167

202. Prufer, K.M., Alsgaard, A.V., Robinson, M., Meredith, C.R., Culleton, B.J., Dennehy, T., Magee, S., Huckell, B.B., Stemp, W.J., Awe, J.J., Capriles, J.M., Kennett, D.J., 2019. Linking late Paleoindian stone tool technologies and populations in North, Central and South America. PLoS One 14, e0219812. https://doi.org/10.1371/journal.pone.0219812

203. Prüss-Ustün, A., Bartram, J., Clasen, T., Colford, J.M., Cumming, O., Curtis, V., Bonjour, S., Dangour, A.D., De France, J., Fewtrell, L., Freeman, M.C., Gordon, B., Hunter, P.R., Johnston, R.B., Mathers, C., Mäusezahl, D., Medlicott, K., Neira, M., Stocks, M., Wolf, J., Cairncross, S., 2014. Burden of disease from inadequate water, sanitation and hygiene in low-and middle-income settings: a retrospective analysis of data from 145 countries. Tropical Medicine and International Health 19, 894–905. https://doi.org/10.1111/tmi.12329

204. Qi, X., Chan, W.L., Read, R.J., Zhou, A., Carrell, R.W., 2014. Temperature-responsive release of thyroxine and its environmental adaptation in Australians. Proceedings of the Royal Society B: Biological Sciences 281, 20132747. https://doi.org/10.1098/rspb.2013.2747

205. R Core Team (2021). R: A language and environment for statistical computing. R Foundation for Statistical Computing, Vienna, Austria. https://www.R-project.org/.

206. Raatikka, V.-P., Rytkönen, M., Näyhä, S., Hassi, J., 2007. Prevalence of cold-related complaints, symptoms and injuries in the general population: the FINRISK 2002 cold substudy. International Journal of Biometeorology 51, 441–448. https://doi.org/10.1007/s00484-006-0076-1

207. Racimo, F., 2016. Testing for Ancient Selection Using Cross-population Allele Frequency Differentiation. Genetics 202, 733–750. https://doi.org/10.1534/genetics.115.178095

208. Rademaker, K., Hodgins, G., Moore, K., Zarrillo, S., Miller, C., Bromley, G.R.M., Leach, P., Reid, D.A., Álvarez, W.Y., Sandweiss, D.H., 2014. Paleoindian settlement of the high-altitude Peruvian Andes. Science 346, 466–469. https://doi.org/10.1126/science.1258260

209. Rae, T.C., Koppe, T., Stringer, C.B., 2011. The Neanderthal face is not cold adapted. Journal of Human Evolution 60, 234–239. https://doi.org/10.1016/j.jhevol.2010.10.003

210. Rees, J.S., Castellano, S., Andrés, A.M., 2020. The Genomics of Human Local Adaptation. Trends in Genetics 36, 415–428. https://doi.org/10.1016/j.tig.2020.03.006

211. Reinhard, K.J., Araújo, A., 2016. Prehistoric Pathoecology as Represented by Parasites of a Mummy from the Peruaçu Valley, Brazil. Korean Journal of Parasitology 54, 585–590. https://doi.org/10.3347/kjp.2016.54.5.585

212. Reyes, L., Godfrey, D., Ming, L.-J., MacLean, C., Gonzalez, F.J., Madrigal, L., n.d. The distribution in native populations from Mexico and Central America of the C677T variant in the MTHFR gene. American Journal of Human Biology n/a, e23567. https://doi.org/10.1002/ajhb.23567

213. Reyes, L., Godfrey, D., Ming, L.-J., MacLean, C., Gonzalez, F.J., Madrigal, L., n.d. The distribution in native populations from Mexico and Central America of the C677T variant in the MTHFR gene. American Journal of Human Biology, e23567. https://doi.org/10.1002/ajhb.23567

214. Richardson, V., Hernandez-Pichardo, J., Quintanar-Solares, M., Esparza-Aguilar, M., Johnson, B., Gomez-Altamirano, C.M., Parashar, U., Patel, M., 2010. Effect of Rotavirus Vaccination on Death from Childhood Diarrhea in Mexico. New England Journal of Medicine 362, 299–305. https://doi.org/10.1056/NEJMoa0905211

215. Richmond, S., Howe, L.J., Lewis, S., Stergiakouli, E., Zhurov, A., 2018. Facial Genetics: A Brief Overview. Frontiers in Genetics 0. https://doi.org/10.3389/fgene.2018.00462

216. Rito, T., Vieira, D., Silva, M., Conde-Sousa, E., Pereira, L., Mellars, P., Richards, M.B., Soares, P., 2019. A dispersal of Homo sapiens from southern to eastern Africa immediately preceded the out-of-Africa migration. Scientific Reports 9, 4728. https://doi.org/10.1038/s41598-019-41176-3

217. Rosinger, A.Y., 2018. Household water insecurity after a historic flood: Diarrhea and dehydration in the Bolivian Amazon. Social Science & Medicine 197, 192–202. https://doi.org/10.1016/j.socscimed.2017.12.016

218. Ruff, C.B., 1993. Climatic adaptation and hominid evolution: The thermoregulatory imperative. Evolutionary Anthropology: Issues, News, and Reviews 2, 53–60. https://doi.org/10.1002/evan.1360020207

219. Ruxton, G.D., Wilkinson, D.M., 2011. Avoidance of overheating and selection for both hair loss and bipedality in hominins. PNAS 108, 20965–20969. https://doi.org/10.1073/pnas.1113915108

220. Salaman, R.N., 1939. Deformities and Mutilations of the Face as Depicted in the Chimu Pottery of Peru. The Journal of the Royal Anthropological Institute of Great Britain and Ireland 69, 109–122. https://doi.org/10.2307/2844233

221. Sample, A., He, Y.-Y., 2018. Mechanisms and prevention of UV-induced melanoma. Photodermatology, Photoimmunology, and Photomedicine 34, 13–24. https://doi.org/10.1111/phpp.12329

222. Santoro, C., Vinton, S.D., Reinhard, K.J., 2003. Inca expansion and parasitism in the Lluta Valley: preliminary data. Paleoparasitology in the Old and New World 98, 161–163. https://doi.org/10.1590/S0074-02762003000900024

223. Sarofim, M.C., Saha, S., Hawkins, M.D., Mills, D.M., Hess, J., Horton, R., Kinney, P., Schwartz, J., St. Juliana, A., 2016. Ch. 2: Temperature-Related Death and Illness. The Impacts of Climate Change on Human Health in the United States: A Scientific Assessment. U.S. Global Change Research Program. https://doi.org/10.7930/J0MG7MDX

224. Scheinfeldt, L.B., Tishkoff, S.A., 2013. Recent human adaptation: genomic approaches, interpretation and insights. Nature Reviews Genetocs 14, 692–702. https://doi.org/10.1038/nrg3604

225. Schifano, P., Asta, F., Dadvand, P., Davoli, M., Basagana, X., Michelozzi, P., 2016. Heat and air pollution exposure as triggers of delivery: A survival analysis of population-based pregnancy cohorts in Rome and Barcelona. Environment International 88, 153–159. https://doi.org/10.1016/j.envint.2015.12.013

226. Schlebusch, C.M., Gattepaille, L.M., Engström, K., Vahter, M., Jakobsson, M., Broberg, K., 2015. Human Adaptation to Arsenic-Rich Environments. Molecular Biology and Evolution 32, 1544–1555. https://doi.org/10.1093/molbev/msv046

227. Schlesinger, M.J., 1990. Heat shock proteins. Journal of Biological Chemistry 265, 12111–12114. https://doi.org/10.1016/S0021-9258(19)38314-0

228. Schön, M.P., 2019. Adaptive and Innate Immunity in Psoriasis and Other Inflammatory Disorders. Frontiers in Immunology 10. https://doi.org/10.3389/fimmu.2019.01764

229. Schrader, E.K., Harstad, K.G., Matouschek, A., 2009. Targeting proteins for degradation. Nature Chemical Biology 5, 815–822. https://doi.org/10.1038/nchembio.250

230. Schramm, W.M., Bartunek, A., Gilly, H., 1997. Effect of local limb temperature on pulse oximetry and the Plethysmographic pulse wave. International Journal of Clinical Monitoring and Computing 14, 17–22. https://doi.org/10.1007/BF03356574

231. Schreider, E., 1964. Ecological Rules, Body-Heat Regulation, and Human Evolution. Evolution 18, 1–9. https://doi.org/10.2307/2406414

232. Schwartz, J.H., Tattersall, I., 1996. Significance of some previously unrecognized apomorphies in the nasal region of Homo neanderthalensis. PNAS 93, 10852–10854.

233. Seersholm, F.V., Werndly, D.J., Grealy, A., Johnson, T., Keenan Early, E.M., Lundelius, E.L., Winsborough, B., Farr, G.E., Toomey, R., Hansen, A.J., Shapiro, B., Waters, M.R., McDonald, G., Linderholm, A., Stafford, T.W., Bunce, M., 2020. Rapid range shifts and megafaunal extinctions associated with late Pleistocene climate change. Nature Communications 11, 2770. https://doi.org/10.1038/s41467-020-16502-3

234. Sellayah, D., 2019. The Impact of Early Human Migration on Brown Adipose Tissue Evolution and Its Relevance to the Modern Obesity Pandemic. Journal of the Endocrine Society 3, 372–386. https://doi.org/10.1210/js.2018-00363

235. Sellayah, D., Cagampang, F.R., Cox, R.D., 2014. On the Evolutionary Origins of Obesity: A New Hypothesis. Endocrinology 155, 1573–1588. https://doi.org/10.1210/en.2013-2103

236. Shrine, N., Guyatt, A.L., Erzurumluoglu, A.M., Jackson, V.E., Hobbs, B.D., Melbourne, C.A., Batini, C., Fawcett, K.A., Song, K., Sakornsakolpat, P., Li, Xingnan, Boxall, R., Reeve, N.F., Obeidat, M., Zhao, J.H., Wielscher, M., Weiss, S., Kentistou, K.A., Cook, J.P., Sun, B.B., Zhou, J., Hui, J., Karrasch, S., Imboden, M., Harris, S.E., Marten, J., Enroth, S., Kerr, S.M., Surakka, I., Vitart, V., Lehtimäki, T., Allen, R.J., Bakke, P.S., Beaty, T.H., Bleecker, E.R., Bossé, Y., Brandsma, C.-A., Chen, Z., Crapo, J.D., Danesh, J., DeMeo, D.L., Dudbridge, F., Ewert, R., Gieger, C., Gulsvik, A., Hansell, A.L., Hao, K., Hoffman, J.D., Hokanson, J.E., Homuth, G., Joshi, P.K., Joubert, P., Langenberg, C., Li, Xuan, Li, L., Lin, K., Lind, L., Locantore, N., Luan, J., Mahajan, A., Maranville, J.C., Murray, A., Nickle, D.C., Packer, R., Parker, M.M., Paynton, M.L., Porteous, D.J., Prokopenko, D., Qiao, D., Rawal, R., Runz, H., Sayers, I., Sin, D.D., Smith, B.H., Soler Artigas, M., Sparrow, D., Tal-Singer, R., Timmers, P.R.H.J., Van den Berge, M., Whittaker, J.C., Woodruff, P.G., Yerges-Armstrong, L.M., Troyanskaya, O.G., Raitakari, O.T., Kähönen, M., Polašek, O., Gyllensten, U., Rudan, I., Deary, I.J., Probst-Hensch, N.M., Schulz, H., James, A.L., Wilson, J.F., Stubbe, B., Zeggini, E., Jarvelin, M.-R., Wareham, N., Silverman, E.K., Hayward, C., Morris, A.P., Butterworth, A.S., Scott, R.A., Walters, R.G., Meyers, D.A., Cho, M.H., Strachan, D.P., Hall, I.P., Tobin, M.D., Wain, L.V., 2019. New genetic signals for lung function highlight pathways and chronic obstructive pulmonary disease associations across multiple ancestries. Nature Genetics 51, 481–493. https://doi.org/10.1038/s41588-018-0321-7

237. Shriver, M.D., Kennedy, G.C., Parra, E.J., Lawson, H.A., Sonpar, V., Huang, J., Akey, J.M., Jones, K.W., 2004. The genomic distribution of population substructure in four populations using 8,525 autosomal SNPs. Human Genomics 1, 274–286. https://doi.org/10.1186/1479-7364-1-4-274

238. Silva, J.E., 1995. Thyroid Hormone Control of Thermogenesis and Energy Balance. Thyroid 5, 481–492. https://doi.org/10.1089/thy.1995.5.481

239. Slatkin, M., Racimo, F., 2016. Ancient DNA and human history. PNAS 113, 6380–6387. https://doi.org/10.1073/pnas.1524306113

240. Smith, G.D., Leary, S., Ness, S., Team, T.A.S., 2006. Could dehydration in infancy lead to high blood pressure? Journal of Epidemiology & Community Health 60, 142–143. https://doi.org/10.1136/jech.2005.040006

241. Solmonson, A., Mills, E.M., 2016. Uncoupling Proteins and the Molecular Mechanisms of Thyroid Thermogenesis. Endocrinology 157, 455–462. https://doi.org/10.1210/en.2015-1803

242. Steegmann, A.T., 2007. Human cold adaptation: An unfinished agenda. American Journal of Human Biology 19, 218–227. https://doi.org/10.1002/ajhb.20614

243. Steegmann, A.T., Cerny, F.J., Holliday, T.W., 2002. Neandertal cold adaptation: Physiological and energetic factors. American Journal of Human Biology 14, 566–583. https://doi.org/10.1002/ajhb.10070

244. Stinnesbeck, W., Rennie, S.R., Olguín, J.A., Stinnesbeck, S.R., Gonzalez, S., Frank, N., Warken, S., Schorndorf, N., Krengel, T., Morlet, A.V., González, A.G., 2020. New evidence for an early settlement of the Yucatán Peninsula, Mexico: The Chan Hol 3 woman and her meaning for the Peopling of the Americas. PLoS One 15, e0227984. https://doi.org/10.1371/journal.pone.0227984

245. Strand, L.B., Barnett, A.G., Tong, S., 2012. Maternal exposure to ambient temperature and the risks of preterm birth and stillbirth in Brisbane, Australia. American Journal of Epidemiology 175, 99–107. https://doi.org/10.1093/aje/kwr404

246. Suzuki, S.C., Takeichi, M., 2008. Cadherins in neuronal morphogenesis and function. Development, Growth & Differentiation 50, S119–S130. https://doi.org/10.1111/j.1440-169X.2008.01002.x

247. Szpiech, Z., Novak, T., Bailey, N., Stevison, L., 2021 Application of a novel haplotype-based scan for local adaptation to study high-altitude adaptation in rhesus macaques. Evolution Letters.

248. Szpiech, Z.A., Hernandez, R.D., 2014. Selscan: an efficient multi-threaded program to perform EHH-based scans for positive selection. Molecular Biology and Evolution 31, 2824–2827. https://doi.org/10.1093/molbev/msu211

249. Szpiech, Z.A., Novak, T.E., Bailey, N.P., Stevison, L.S., 2021. Application of a novel haplotype-based scan for local adaptation to study high-altitude adaptation in rhesus macaques. Evolution Letters 5, 401 - 421 https://doi.org/10.1002/evl3.232

250. Tabari, H., 2020. Climate change impact on flood and extreme precipitation increases with water availability. Scientific Reports 10, 13768. https://doi.org/10.1038/s41598-020-70816-2

251. Tafuri, M.A., Zangrando, A.F.J., Tessone, A., Kochi, S., Moggi Cecchi, J., Di Vincenzo, F., Profico, A., Manzi, G., 2017. Dietary resilience among hunter-gatherers of Tierra del Fuego: Isotopic evidence in a diachronic perspective. PLOS ONE 12, e0175594. https://doi.org/10.1371/journal.pone.0175594

252. Tajima, F., 1989. Statistical Method for Testing the Neutral Mutation Hypothesis by DNA Polymorphism. Genetics 123, 585–595.

253. Tanaka, H., Takahashi, T., Xie, Y., Minami, R., Yanagi, Y., Hayashishita, M., Suzuki, R., Yokota, N., Shimada, M., Mizushima, T., Kuwabara, N., Kato, R., Kawahara, H., 2016. A conserved island of BAG6/Scythe is related to ubiquitin domains and participates in short hydrophobicity recognition. The FEBS Journal 283, 662–677. https://doi.org/10.1111/febs.13618

254. Tansey, E.A., Johnson, C.D., 2015. Recent advances in thermoregulation. Advances in Physiology Education 39, 139–148. https://doi.org/10.1152/advan.00126.2014

255. Terjung, R. (Ed.), 2011. Comprehensive Physiology, 1st ed. Wiley. https://doi.org/10.1002/cphy

256. Thomas, G., Betters, J.L., Lord, C.C., Brown, A.L., Marshall, S., Ferguson, D., Sawyer, J., Davis, M.A., Melchior, J.T., Blume, L.C., Howlett, A.C., Ivanova, P.T., Milne, S.B., Myers, D.S., Mrak, I., Leber, V., Heier, C., Taschler, U., Blankman, J.L., Cravatt, B.F., Lee, R.G., Crooke, R.M., Graham, M.J., Zimmermann, R., Brown, H.A., Brown, J.M., 2013. The Serine Hydrolase ABHD6 Is a Critical Regulator of Metabolic Syndrome. Cell Reports 5, 508–520. https://doi.org/10.1016/j.celrep.2013.08.047

257. Tiffin, P., Ross-Ibarra, J., 2014. Advances and limits of using population genetics to understand local adaptation. Trends in Ecology & Evolution 29, 673–680. https://doi.org/10.1016/j.tree.2014.10.004

258. Tilkens, M.J., Wall-Scheffler, C., Weaver, T.D., Steudel-Numbers, K., 2007. The effects of body proportions on thermoregulation: an experimental assessment of Allen's rule. Journal of Human Evolution 53, 286–291. https://doi.org/10.1016/j.jhevol.2007.04.005

259. Tkachev, A.V., Ramenskaya, E.B., Bojko, J.R., 1991. Dynamics of hormone and metabolic state in polar inhabitants depend on daylight duration. Arctic Medical Research 50 Suppl 6, 152–155.

260. Tsuji, B., Hayashi, K., Kondo, N., Nishiyasu, T., 2016. Characteristics of hyperthermia-induced hyperventilation in humans. Temperature (Austin) 3, 146–160. https://doi.org/10.1080/23328940.2016.1143760

261. van der Lans, A.A.J.J., Hoeks, J., Brans, B., Vijgen, G.H.E.J., Visser, M.G.W., Vosselman, M.J., Hansen, J., Jörgensen, J.A., Wu, J., Mottaghy, F.M., Schrauwen, P., van Marken Lichtenbelt, W.D., 2013. Cold acclimation recruits human brown fat and increases nonshivering thermogenesis. Journal of Clinical Investigations 123, 3395–3403. https://doi.org/10.1172/JCI68993

262. van Marken Lichtenbelt, W.D., Vanhommerig, J.W., Smulders, N.M., Drossaerts, J.M.A.F.L., Kemerink, G.J., Bouvy, N.D., Schrauwen, P., Teule, G.J.J., 2009. Cold-activated brown adipose tissue in healthy men. New England Journal of Medicine 360, 1500–1508. https://doi.org/10.1056/NEJMoa0808718

263. Van Rossum, G. & Drake Jr, F.L., 1995. Python reference manual, Centrum voor Wiskunde en Informatica Amsterdam

264. Van Zutphen, A.R., Hsu, W.-H., Lin, S., 2014. Extreme winter temperature and birth defects: A population-based case-control study. Environmental Research 128, 1–8. https://doi.org/10.1016/j.envres.2013.11.006

265. von Cramon-Taubadel, N., Lycett, S. J. 2008. Brief Communication: Human Cranial Variation Fits Iterative Founder Effect Model With African Origin. American Journal of Physical Anthropology, 136, 108–113. https://doi.org/10.1002/ajpa.20775

266. Visscher, T.L.S., Seidell, J.C., 2004. Time trends (1993-1997) and seasonal variation in body mass index and waist circumference in the Netherlands. International Journal of Obesity Related Metabolic Disorders 28, 1309–1316. https://doi.org/10.1038/sj.ijo.0802761

267. Wang, Fengqi, Zang, Y., Li, M., Liu, W., Wang, Y., Yu, X., Li, H., Wang, Fang, Liu, S., 2020. DUOX2 and DUOXA2 Variants Confer Susceptibility to Thyroid Dysgenesis and Gland-in-situ With Congenital Hypothyroidism. Frontiers in Endocrinology 11, 237. https://doi.org/10.3389/fendo.2020.00237

268. Wang, Q., Liu, Y., Soetandyo, N., Baek, K., Hegde, R., Ye, Y., 2011. A ubiquitin ligase-associated chaperone holdase maintains polypeptides in soluble states for proteasome degradation. Molecular Cell 42, 758–770. https://doi.org/10.1016/j.molcel.2011.05.010

269. Wang, S., Zhang, Z., Peng, H., Zeng, K., 2019. Recent advances on the roles of epidermal growth factor receptor in psoriasis. American Journal of Translational Research 11, 520–528.

270. Warner, A., Rahman, A., Solsjö, P., Gottschling, K., Davis, B., Vennström, B., Arner, A., Mittag, J., 2013. Inappropriate heat dissipation ignites brown fat thermogenesis in mice with a mutant thyroid hormone receptor α1. Proceedings of the National Academy of Sciences 110, 16241–16246.

271. Weir, B.S., Cockerham, C.C., 1984. Estimating F-Statistics for the Analysis of Population Structure. Evolution 38, 1358–1370. https://doi.org/10.2307/2408641

272. Weiss, J.L., Overpeck, J.T., 2005. Is the Sonoran Desert losing its cool? Global Change Biology 11, 2065–2077. https://doi.org/10.1111/j.1365-2486.2005.01020.x

273. Wendt, D., van Loon, L.J.C., Marken Lichtenbelt, W.D., 2007. Thermoregulation during Exercise in the Heat. Sports Medicine 37, 669–682. https://doi.org/10.2165/00007256-200737080-00002

274. Wheeler, P.E., 1984. The evolution of bipedality and loss of functional body hair in hominids. Journal of Human Evolution 13, 91–98. https://doi.org/10.1016/S0047-2484(84)80079-2

275. Wheeler, P.E., 1991. The thermoregulatory advantages of hominid bipedalism in open equatorial environments: the contribution of increased convective heat loss and cutaneous evaporative cooling. Journal of Human Evolution 21, 107–115. https://doi.org/10.1016/0047-2484(91)90002-D

276. White, J.D., Ortega-Castrillón, A., Matthews, H., Zaidi, A.A., Ekrami, O., Snyders, J., Fan, Y., Penington, T., Van Dongen, S., Shriver, M.D., Claes, P., 2019. MeshMonk: Open-source large-scale intensive 3D phenotyping. Scientific Reports 9, 6085. https://doi.org/10.1038/s41598-019-42533-y

277. Whitehouse, A.J.O., Gilani, S.Z., Shafait, F., Mian, A., Tan, D.W., Maybery, M.T., Keelan, J.A., Hart, R., Handelsman, D.J., Goonawardene, M., Eastwood, P., 2015. Prenatal testosterone exposure is related to sexually dimorphic facial morphology in adulthood. Proceedings of the Royal Society B 282, 20151351. https://doi.org/10.1098/rspb.2015.1351

278. Wickens, C.D., Keller, J.W., Shaw, C., 2015. Human Factors in High-Altitude Mountaineering. Journal of Human Performance in Extreme Environments 12. https://doi.org/10.7771/2327-2937.1065

279. Wilkinson, P., Pattenden, S., Armstrong, B., Fletcher, A., Kovats, R.S., Mangtani, P., McMichael, A.J., 2004. Vulnerability to winter mortality in elderly people in Britain: population based study. BMJ 329, 647. https://doi.org/10.1136/bmj.38167.589907.55

280. Wilson, T.E., Sauder, C.L., Kearney, M.L., Kuipers, N.T., Leuenberger, U.A., Monahan, K.D., Ray, C.A., 2007. Skin-surface cooling elicits peripheral and visceral vasoconstriction in humans. Journal of Applied Physiology 103, 1257–1262. https://doi.org/10.1152/japplphysiol.00401.2007

281. Wolff, M. von, Nakas, C.T., Tobler, M., Merz, T.M., Hilty, M.P., Veldhuis, J.D., Huber, A.R., Hefti, J.P., 2018. Adrenal, thyroid and gonadal axes are affected at high altitude. Endocrine Connections 7, 1081–1089. https://doi.org/10.1530/EC-18-0242

282. Wollina, U., Bennewitz, A., Langner, D., 2014. Basal cell carcinoma of the outer nose: Overview on surgical techniques and analysis of 312 patients. Journal of Cutaneous and Aesthetic Surgery 7, 143. https://doi.org/10.4103/0974-2077.146660

283. Wolpoff, M.H., 1968. Climatic influence on the skeletal nasal aperture. American Journal of Physical Anthropology 29, 405–423. https://doi.org/10.1002/ajpa.1330290315

284. Wood, B., Collard, M., 1999. The Human Genus. Science 284, 65–71. https://doi.org/10.1126/science.284.5411.65

285. Wright, S., 1950. Genetical Structure of Populations. Nature 166, 247–249. https://doi.org/10.1038/166247a0

286. Wroe, S., Parr, W.C.H., Ledogar, J.A., Bourke, J., Evans, S.P., Fiorenza, L., Benazzi, S., Hublin, J.-J., Stringer, C., Kullmer, O., Curry, M., Rae, T.C., Yokley, T.R., 2018. Computer simulations show that Neanderthal facial morphology represents adaptation to cold and high energy demands, but not heavy biting. Proceedings of the Royal Society B: Biological Sciences 285, 20180085. https://doi.org/10.1098/rspb.2018.0085

287. Xing, J., Wuren, T., Simonson, T.S., Watkins, W.S., Witherspoon, D.J., Wu, W., Qin, G., Huff, C.D., Jorde, L.B., Ge, R.-L., 2013. Genomic analysis of natural selection and phenotypic variation in high-altitude mongolians. PLoS Genetics 9, e1003634. https://doi.org/10.1371/journal.pgen.1003634

288. Yan, D., Afifi, L., Jeon, C., Cordoro, K.M., Liao, W., 2018. A cross-sectional study of the distribution of psoriasis subtypes in different ethno-racial groups. Dermatology Online Journal 24. https://doi.org/10.5070/D3247040909

289. Yi, X., Liang, Y., Huerta-Sanchez, E., Jin, X., Cuo, Z.X.P., Pool, J.E., Xu, X., Jiang, H., Vinckenbosch, N., Korneliussen, T.S., Zheng, Hancheng, Liu, T., He, W., Li, K., Luo, R., Nie, X., Wu, H., Zhao, M., Cao, H., Zou, J., Shan, Y., Li, Shuzheng, Yang, Q., Asan, Ni, P., Tian, G., Xu, J., Liu, X., Jiang, T., Wu, R., Zhou, G., Tang, M., Qin, J., Wang, T., Feng, S., Li, G., Huasang, Luosang, J., Wang, W., Chen, F., Wang, Y., Zheng, X., Li, Z., Bianba, Z., Yang, G., Wang, X., Tang, S., Gao, G., Chen, Y., Luo, Z., Gusang, L., Cao, Z., Zhang, Q., Ouyang, W., Ren, X., Liang, H., Zheng, Huisong, Huang, Y., Li, J., Bolund, L., Kristiansen, K., Li, Y., Zhang, Y., Zhang, X., Li, R., Li, Songgang, Yang, H., Nielsen, R., Wang, Jun, Wang, Jian, 2010. Sequencing of 50 Human Exomes Reveals Adaptation to High Altitude. Science 329, 75–78. https://doi.org/10.1126/science.119037

290. Yokley, T.R., 2009. Ecogeographic variation in human nasal passages. American Journal of Physical Anthropology 138, 11–22. https://doi.org/10.1002/ajpa.20893

291. Zhang, Q., Gou, W., Wang, X., Zhang, Yawen, Ma, J., Zhang, Hongliang, Zhang, Ying, Zhang, Hao, 2016. Genome Resequencing Identifies Unique Adaptations of Tibetan Chickens to Hypoxia and High-Dose Ultraviolet Radiation in High-Altitude Environments. Genome Biology and Evolution 8, 765–776. https://doi.org/10.1093/gbe/evw032

292. Zhang, W., Han, Q., Liu, Z., Zhou, Wei, Cao, Q., Zhou, Weimin, 2018. Exome sequencing reveals a de novo PRKG1 mutation in a sporadic patient with aortic dissection. BMC Medical Genetics 19, 218. https://doi.org/10.1186/s12881-018-0735-1

293. Zhang, X., Chen, X., Qi, T., Kong, Q., Cheng, H., Cao, X., Li, Y., Li, C., Liu, L., Ding, Z., 2019. HSPA12A is required for adipocyte differentiation and diet-induced obesity through a positive feedback regulation with PPARγ. Cell Death and Differentiation 26, 2253–2267. https://doi.org/10.1038/s41418-019-0300-2

294. Zhang, Y.-H., Xing, Z., Liu, C., Wang, S., Huang, T., Cai, Y.-D., Kong, X., 2017. Identification of the core regulators of the HLA I-peptide binding process. Scientific Reports 7, 42768. https://doi.org/10.1038/srep42768

295. Zhou, D., Udpa, N., Ronen, R., Stobdan, T., Liang, J., Appenzeller, O., Zhao, H.W., Yin, Y., Du, Y., Guo, L., Cao, R., Wang, Y., Jin, X., Huang, C., Jia, W., Cao, D., Guo, G., Gamboa, J.L., Villafuerte, F., Callacondo, D., Xue, J., Liu, S., Frazer, K.A., Li, Y., Bafna, V., Haddad, G.G., 2013. Whole-Genome Sequencing Uncovers the Genetic Basis of Chronic Mountain Sickness in Andean Highlanders. The American Journal of Human Genetics 93, 452–462. https://doi.org/10.1016/j.ajhg.2013.07.011

296. Zhou, Q., Zhao, L., Guan, Y., 2016. Strong Selection at MHC in Mexicans since Admixture. PLoS Genetics 12, e1005847. https://doi.org/10.1371/journal.pgen.1005847

297. Zhou, S., Xie, P., Quoibion, A., Ambalavanan, A., Dionne-Laporte, A., Spiegelman, D., Bourassa, C.V., Xiong, L., Dion, P.A., Rouleau, G.A., 2019. Genetic architecture and adaptations of Nunavik Inuit. Proceedings of the National Academy of Sciences USA 116, 16012–16017. https://doi.org/10.1073/pnas.1810388116

298. Zihlman, A.L., Cohn, B.A., 1988. The adaptive response of human skin to the savanna. Human Evolution 3, 397–409. https://doi.org/10.1007/BF0244722